THEORETICAL INVESTIGATIONS OF HYDROGEN ON Si(111)

By

BETSY MAVITY RICE

Bachelor of Science

Cameron University

Lawton, Oklahoma

1984

Submitted to the Faculty of the
Graduate College of the
Oklahoma State University
in partial fulfillment of
the requirements for
the Degree of
DOCTOR OF PHILOSOPHY
December, 1987

THEORETICAL INVESTIGATIONS OF

HYDROGEN ON Si(111)

Thesis Approved:

Lionel M. Raff
Thesis Advisor

Paul Westhaus

Donald L. Thompson

Richard C. Powell

Norman N. Durham
Dean of the Graduate College

ACKNOWLEDGEMENTS

I would like to express my thanks to the following people who served as members of my advisory committee: Drs. L. M. Raff, D. L. Thompson, P. A. Westhaus, and R. C. Powell. I would like to thank my joint advisors, Donald L. Thompson and Lionel M. Raff, for their direction and help with the research problems. I especially want to extend my deepest gratitude to my dearest friend, Don Thompson, who tolerated me when I was insufferable, helped me through many crises, and shared his valuable insights and time in preparing me for a career in science. I also thank him for his gentle manner, kindness, and humor he shared with me during my graduate career.

I sincerely appreciate support from the Graduate College and from John W. Skinner in the form of scholarships and fellowships. I am grateful for the financial support provided by the U. S. Air Force Office of Scientic Research.

I would like to extend thanks to my friends during my stay in graduate school who provided many laughs and a great deal of company. I would particularly like to thank Dr. Bobby Sumpter for his help and friendship.

I express my deepest appreciation for the support and love of my dear parents, and for their help during difficult times.

I especially thank my husband, who willlingly and generously provided me with support, understanding, patience, and love.

TABLE OF CONTENTS

Chapter		Page
I.	INTRODUCTION	1
II.	POTENTIAL-ENERGY SURFACES	49
	Lattice Interaction Potential	49
	Adatom-Lattice and Adatom-Adatom Interaction Potential	50
III.	MODELS AND METHODS OF CALCULATIONS	86
	Hydrogen Atom Scattering/Chemisorption on Partially/Fully Covered Si(111)	88
	Model	88
	Initial Condition Selection . . .	91
	Trajectory Integration	95
	H_2 on Si(111)	95
	Model	95
	Initial Condition Selection . . .	96
	Trajectory Integration	98
	Hydrogen Atom Diffusion on Si(111) . .	101
	Model	106
	Initial Condition Selection . . .	106
	Monte Carlo Variational Phase-Space Theory (MCVPST) . .	107
	Thermal Diffusion Coefficient . .	112
	Tunneling	115
IV.	RESULTS	119
	Hydrogen Atom Scattering/Chemisorption on Partially/Fully Covered Si(111)	119
	Scattering and Adsorption Mechanisms	119
	Energy Transfer and Scattering Distributions	129
	Dissociative Chemisorption/Scattering of H_2 on Si(111)	154
	Hydrogen Atom Diffusion on Si(111) . .	167
	Classical Results	167
	Tunneling Calculations	175

Chapter Page

V. CONCLUSIONS 185

Hydrogen Atom Scattering/Chemisorption on Partially/Fully Covered Si(111) 185
Dissociative Chemisorption/Scattering of H_2 on Si(111) 191
Hydrogen Atom Diffusion on Si(111) 192
Suggestions for Future Work 195

BIBLIOGRAPHY 198

APPENDIX 204

LIST OF TABLES

Table		Page
I.	Experimental Data and Theoretical Information on H-Si(111) Interaction Potential	205
II.	Potential Energy Parameters	208
III.	Values of Parameters used in Metropolis Sampling and Trajectory Calculations . .	210
IV.	Features of Trajectories	212
V.	Final Average Energies for Hydrogen Scattering	213
VI.	Initial and Final Average Energies for H_2 Scattering	214
VII.	Dividing Surfaces and Variational Parameters used in MCVPST Calculation of Minimum Flux	215
VIII.	Top Site to Open Site Jump Frequencies . .	216
IX.	Open Site to Top Site Jump Frequencies . .	217

LIST OF FIGURES

Figure		Page
1.	Power Spectrum for Motion of a Si Atom in the Ideal Si(111) Lattice	51
2.	Top Site Si-H Stretching Potential	70
3.	Potential Energy Curves for Stretching Motion Perpendicular to Surface Plane for Hydrogen in Open Binding Site	73
4.	Power Spectrum of Hydrogen in Top Site . . .	74
5.	Power Spectrum of Hydrogen in Open Site . . .	75
6.	Potential Energy Surface of Hydrogen on Partially Covered Si(111) surface	77
7.	Contour Plot of Potential Energy Surface of Hydrogen on Fully Covered Si(111) . . .	79
8.	Contour Plot of Potential Energy Surface of Hydrogen on Si(111) with One Available Top Binding Site	80
9.	Contour Plot of Potential Energy Surface of Hydrogen on Si(111) with Three Available Top Binding Sites	81
10.	Contour Plot of Potential-Energy Surface of Hydrogen on Si(111) with Five Available Top Binding Sites	82
11.	Contour Plot of Potential-Energy Surface of Hydrogen on Si(111) with Seven Available Top Binding Sites	83
12.	Three-Dimension Contour Plot of Fig. 9 . . .	84
13.	Structural Models for the Si(111) (1 x 1) Crystal Lattice	89

Figure		Page
14.	Schematic Representation of Selection of Initial Conditions in Atomic Hydrogen Chemisorption/Scattering Study	94
15.	Schematic Representation of Selection of Initial Conditions in Molecular Hydrogen Chemisorption/Scattering Study	97
16.	Model of Si(111) Lattice used in H_2 Dissociative Chemisorption/Scattering Study	100
17.	Velocity Autocorrelation Function for Thermal Motion of Hydrogen Atom	103
18.	Schematic of Reactant and Product Space for Diffusing Hydrogen in MCVPST Study . .	110
19.	Phenomenological Model Used in Calculation of Thermal Diffusion Coefficient	113
20.	Schematic of Tunneling Paths	117
21.	Trajectory Resulting in Hydrogen Exchange Reaction on Si(111) Surface	125
22.	Trajectory Resulting in Scattering after Migration on Si(111)	128
23.	Trajectory Resulting in Migration after Chemisorption	130
24.	Trajectory Resulting in Migration after Deflection and Chemisorption	131
25.	Trajectory Resulting in Chemisorption after Deflection	132
26.	Product Translational Energy Distributions of Scattered Hydrogen Atoms	134
27.	Scattering Angle Distributions for Scattered Hydrogen Atoms	135
28.	Sticking Probabilities as Functions of Angle and Coverage	140

Figure		Page
29.	Sticking Probabilities as Function of Available Top Binding Sites	142
30.	Change in Energy of Hydrogen Atom and Si(111) Lattice upon Chemisorption	144
31.	Change in Energy of Incident Hydrogen Atom, Si(111) Lattice, and Ad-Hydrogen on Surface upon Chemisorption	145
32.	Average Energy in Top Site Si-H Bond as a Function of Time	148
33.	First-Order Decay Plot of Energy Transfer from Top-Site Si-H Bond	151
34.	Top Site Si-H Stretching Potential Curves . .	152
35.	Distributions of (a) Incident and (b) Scattering Angles of H_2	155
36.	Product Translation Energy Distribution of Scattered H_2 at 300 K	156
37.	Product Translation Energy Distribution of Scattered H_2 at 1500 K	157
38.	Product Vibrational Energy Distribution of Scattered H_2 at 300 K	158
39.	Product Vibrational Energy Distribution of Scattered H_2 at 1500 K	159
40.	Product Rotational Energy Distribution of Scattered H_2 at 300 K	161
41.	Product Rotational Energy Distribution of Scattered H_2 at 1500 K	162
42.	H-H Internuclear Distance as Function of Time for Trajectory Resulting in Dissociative Chemisorption	165
43.	Same as Figure 42, except for Si-H Internuclear Distance	165
44.	Instantaneous Hydrogen Atom Mobilities as Function of Residence Time on Si(111)	166

Figure		Page
45.	First-Order Decay Plot of Energy Transfer from Si-H Bond on Si(111) lattice at 300 K	168
46.	Same as Figure 45, except T = 1500 K	168
47.	Arrhenius Plot of Jump Frequencies for Top-to-Open Site Jumps	170
48.	Arrhenius Plot of Jump Frequencies for Open-to-Top Site Jumps	171
49.	Minimum Energy Path for Hydrogen Diffusion on Si(111)	174
50.	Frequency of Surface-Plane Vibrations of Hydrogen in Top Binding Site at Energies Above Tunneling Threshold	176
51.	Average Frequency of Surface-Plane Vibrations of Hydrogen in Top Binding Site at Energies Above Tunneling Threshold	178
52.	Tunneling Probabilities as a Function of Energies Above Tunneling Threshold . . .	179

CHAPTER I

INTRODUCTION

The electronic, structural, and chemical properties of semiconductor surfaces have been extensively studied. One of the most interesting and challenging problems in surface chemistry today is the determination of the structure of semiconductor surfaces. There is a strong tendency toward important structural changes, such as relaxation and reconstruction of semiconductor surfaces, due to unsaturated "dangling bonds" (orbitals containing unpaired electrons). The surface atoms with such unpaired electrons seek equilibrium positions to satisfy their valence and optimize their bonding interactions with the bulk. Relaxation occurs when the surface atoms seek new equilibrium positions that change the interlayer distance between the first and second layer of atoms. While expansion is theoretically possible, contraction is generally observed. The relaxation of the first layer atoms toward the second layer atoms affects the bond angles, but does not change the number of nearest neighbors or the rotational symmetry of the surface

atoms. Reconstruction of a surface takes place as the surface atoms seek new equilibrium positions that change not only the bond angles, but also the rotational symmetry and number of nearest neighbors.

Silicon is one of the most elemental semiconductors. It is well known that the atomic structure of a silicon surface differs from that of an ideal truncated lattice due to reconstruction of the surface. One of the more interesting silicon surfaces is the (111) plane, as three different phases of reconstruction have been observed for the clean Si(111) surface: (a) the vacuum-cleaved metastable (2 x 1) surface; (b) the annealed (7 x 7) surface which, near room temperature, is the thermodynamically most stable phase; and, (c) the (1 x 1) phase, stable only at temperatures higher than 1300 K. The (1 x 1) phase can be stabilized at room temperature by rapid cooling to give a metastable "quenched" (1 x 1) phase. It would seem that this (1 x 1) phase has reverted into an ideal Si(111) surface; however, experimental findings indicate that this surface is highly disordered (1). Although LEED measurements show the different reconstructions, the surface geometries of the various reconstructions have been a subject of controversy (2). In attempting to resolve the controversy, comparative studies have been done on clean surfaces and surfaces where the dangling bonds are saturated by adsorbed atoms (2a,3). One of the

most extensively studied adsorbate-Si(111) systems is hydrogen interacting with Si(111).

Hydrogen is the smallest and simplest adsorbate. Hydrogenation of silicon surfaces provides a certain means of investigating the various reconstructed surfaces. Comparison between spectra of hydrogenated surfaces and clean surfaces discriminates between bulk and surface states. Hydrogen is known to destroy certain silicon reconstructions completely, restoring the bulk geometry of the silicon surface (4). In addition to providing information about the different surface structures of single silicon crystals, studies showing the behavior and effects of the adsorbed hydrogen on the silicon surface are of interest. Each surface atom on the Si(111) surface has one unpaired electron, which would indicate a well-defined binding site for hydrogen adsorption. However, experimental studies (5-7) have indicated that more than one binding site exists on this surface. These binding sites undergo sequential filling and desorption. Additionally, there are questions of whether or not hydrogen provides a corrosive effect to the Si(111) surface. (8) Therefore, extensive experimental measurements (1-29) and theoretical calculations (30-49) directed toward elucidation of this fundamental, yet complex adsorbate-semiconductor system have been performed.

There is a two-fold interest in this system. One would like to understand the behavior and effects of the adsorption of hydrogen on the silicon surface; additionally, it is assumed that adsorption of hydrogen will provide information about the different surface structures of single silicon crystals. The work of this thesis is directed toward obtaining a thorough understanding of the important interactions of both molecular and atomic hydrogen with the Si(111) surface.

Early experimental studies of the chemisorption of hydrogen on surfaces of silicon crystals incited interest in the exact nature of hydrogen binding on a silicon surface. On chemical grounds, the simplest and most plausible model of hydrogen chemisorption on a Si(111) surface would be that in which a hydrogen atom sits atop a silicon atom in the ideal Si(111) surface to form a Si-H covalent bond directed normal to the surface, saturating the surface dangling bond. This type of hydrogen coverage on a Si(111) surface, described as monohydride coverage, and the experimental and theoretical findings will be discussed in detail in Chapter II.

Pandey, Sakurai and Hagstrum, in an ultraviolet photoemission spectroscopy (UPS) study, observed a new hydrogenated surface phase of Si(111) in addition to the phase characterized as the monohydride phase, represented as Si(111):H. (1(b)) The new hydrogenated surface phase

was interpreted as a trihydride phase, represented by $Si(111):SiH_3$, in which SiH_3 radicals are attached to the dangling orbitals of Si(111). Upon exposure of the silicon surface to hydrogen, UPS spectra show hydrogen-related structure similar to the UPS spectrum obtained by Sakurai and Hagstrum (6), with weaker and more broadened peaks. This was attributed to the monohydride phase. Continued hydrogen exposure changes the spectra dramatically with the disappearance of two peaks, designated C and D, and the appearance of two new peaks, designated as A and B. Peaks A and B are attributed to the trihydride phase. Subsequent thermal desorption experiments show a monotonic decrease of intensities of peaks A and B without the reappearance of peaks C and D. This indicates that the first stage of hydrogen exposure differs from the exposure which produces peaks A and B. A theoretical spectrum for $Si(111):SiH_3$ was calculated and is in good agreement with the observed UPS spectra. Pandey *et al.* suggest that eventual removal of the entire surface monolayer of silicon will permit the formation of the $Si(111):SiH_3$ phase by the adsorption of three hydrogen atoms per silicon atom in what was previously the second layer. The proposed mechanism will be discussed below. This model is used to explain the desorption spectra obtained from the thermal desorption experiments on $Si(111):SiH_3$, which showed a monotonic decrease of the spectral features of

Si(111):SiH_3 but no reappearance of the monohydride phase features as observed in the first stage of hydrogen exposure of the clean silicon crystal. The electronic energy levels of the trihydride phase are strikingly different from those of the monohydride phase, and the trihydride phase appears to be energetically more favorable.

Pandey (30) used a realistic tight-binding model to carry out further calculations of surface states, local densities of states, and theoretically simulated photoemission spectra for the two qualitatively distinct structural models, the monohydride and trihydride phases for chemisorption of hydrogen on Si(111). As seen in his previous study (31), the monohydride phase gave good quantitative agreement with the Appelbaum *et al.* (32) study. Pandey's study is more detailed than his previous one, and his calculations for both basic structural models explain the UPS spectra for low and high coverages of hydrogen. In the assumed trihydride phase, a single SiH_3 radical makes a covalent Si-Si bond with each surface Si atom, or it can be obtained by removing an entire layer of silicon atoms from the clean ideal surface and saturating each of the three dangling bonds on the second-layer silicon atoms with hydrogen atoms. Direct comparison between theoretically simulated spectra and experimental spectra (1(b),6) shows good agreement with this model.

In addition to the quantum mechanical calculations for the monohydride phase of hydrogen adsorption on Si(111), Ho *et al.* (34) present similar calculations for the trihydride phase. The calculations of the trihydride phase were done on the structural model proposed by Pandey, Sakurai and Hagstrum (1(b)). The outermost silicon layer is removed and replaced by one hydrogen layer. Thus, three hydrogen atoms are bound to each of the top silicon atoms. As found in the monohydride calculations, the adsorbed hydrogen interaction is localized and does not affect the bulk more than one or two atomic layers deep. Agreement with experiment for this phase is less quantitative, but it is suggested that minor changes in the structural model may improve it. The experimental spectrum shows two broad peaks, denoted as peaks A and B. The calculated local density of states for the trihydride phase gives good agreement with the experimental intensity for peak B, but the comparison is less satisfactory for peak A whose theoretically simulated spectrum shows four peaks rather than the one broad peak observed in experiment. The discrepancies between experimental observations and theory are due to strong hydrogen-hydrogen interactions of the dense hydrogen monolayer on the trihydride surface.

Butz, Memeo and Wagner (14) take issue with the results of Pandey *et al.* (1(b)) regarding the formation

of a stable SiH_3 phase. In the UPS and Auger electron spectroscopy (AES) investigation on the interaction of atomic hydrogen with Si(111) surfaces, they find that for high hydrogen exposures, oxygen impurities accumulate at the Si(111) surface and contribute to the UPS spectrum. In their experiment, they exposed the Si(111) surface to various oxygen exposures and observed the UPS and AES spectra. The oxygen contamination gives a spectrum which is virtually identical with the spectra attributed to a stable SiH_3 phase. 973 K is the temperature necessary to recover a clean surface from the Si(111):SiH_3 phase (1(b)). These authors suggest that SiH_3 is unlikely to be stable at this temperature. Furthermore, oxygen is known to desorb from silicon surfaces around 973 K, possibly as SiO, and could be the effect observed by Pandey *et al.* (1(b)). Therefore, the spectral features should be attributed to oxygen poisoning. However, these authors do not argue against the formation of SiH_3 units as intermediates for the formation of silane.

There is evidence that there are unconventional binding sites in addition to the monohydride and trihydride phases. The earliest studies of chemisorption of hydrogen on silicon crystals suggest that additional binding sites exist on the surface. Experimental findings and theoretical information regarding these unconventional binding sites are discussed in detail in Chapter II.

Formation of different silicon-hydrogen moieties on a Si(111) surface other than the monohydride and trihydride phases is further evidence of unconventional bond sites. The early study of Becker and Gobeli (9) suggests this when they attribute the broadening of the IR signal to a variety of silicon hydrides present on the surface. Shi, Sahu and Corbett (37) attribute shifts in the IR signal observed by Becker and Gobeli (9) to three different IR peaks, rather than one broad one. In an earlier study, they proposed a model for Si-H vibration centers in crystalline silicon (50) based on the chemical effect of nearest neighbor atoms on the bond character and on the IR vibrational frequency of the Si-H bond (51). The model explained various discrete resolved IR bands observed for Si-H complexes in crystalline silicon. Comparison of the Becker and Gobeli results with this model indicates existence of silicon hydride species in addition to the expected monohydrides on the silicon surface.

In an attempt to experimentally determine the trihydride phase, Sakurai, Muller, Culbertson, and Melmed (17) used field-ion microscopy (FIM) to study formation of hydrides at the silicon surface upon exposure to hydrogen. The results show that in addition to formation of the monohydride on Si(111), silicon dihydride is formed as well. They suggest that some kink-site silicon atoms of the (111) plane have two

dangling orbitals which can bond to hydrogen atoms and form silicon dihydrides. Additionally, they detected silane desorption from the disordered (311) surface area. They propose that the disordered (311) surface has surface vacancies similar to the disordered Si(111) (1 x 1) surface upon which Pandey *et al.* (1(b)) believed trihydride formation began. Observation of silane desorption from the (311) surface is taken as evidence of the existence of the SiH_3 surface phase.

It was, however, the surprising findings of Wagner, Butz, Backes and Bruchmann (8) which ignited the controversy over formation of different silicon-hydrogen complexes. This group performed a study of hydrogen adsorption on the Si(111) (7 x 7) surface using high resolution electron energy loss spectroscopy (HREELS). Their results indicate that right from the beginning of hydrogen adsorption, silicon dihydride and silicon trihydride are formed. They based this conclusion on three loss peaks on the electron energy loss spectrum centered at 630, 900 and 2100 cm^{-1}, respectively. Assignment of the peaks was accomplished by comparing the values to infrared absoption spectra of gaseous silanes and of hydrogenated amorphous silicon films (52-54). The band at 2100 cm^{-1} was assigned to the stretching mode of the Si-H bonds. The bands at 900 and 630 cm^{-1} are connected with bending modes of the silicon hydrides. The 900 cm^{-1} band can be assigned to bond angle changes

in SiH_2 (scissor mode) or SiH_3 (symmetric and asymmetric deformation) complexes. The 630 cm^{-1} regime was assigned to the bending mode in SiH and wagging and rocking modes in SiH_2 and SiH_3 complexes. Because of these unexpected results, the authors exposed the silicon surface simultaneously to hydrogen and deuterium, with the idea that if dihydride species were formed, then such an exposure would yield a loss peak due to the SiHD scissor mode. Loss spectra yielded the following four loss intensities in the bending mode regime: Losses at 900 and 640 cm^{-1} are attributed to hydrogen vibrations. Losses at 640 and 460 cm^{-1} were due to pure deuterium exposures. There was an additional loss peak at 790 cm^{-1}. A loss frequency of 780 cm^{-1} is expected for the SiHD scissor mode. This calculated value is remarkably close to the observed frequency of 790 cm^{-1}. This confirms the FIM experiments of Sakurai *et al.* (17) which showed formation of multihydrides at the silicon surface upon exposure to hydrogen.

The Wagner findings spurred several groups to investigate this interesting chemical phenomena, and to attempt to explain how hydrogen can bind to a surface forming multihydride complexes, whereas the ideal structure formally provides one unpaired electron per surface atom to share in bonding with one hydrogen atom. Disputes are currently active over whether hydrogen is bound to silicon via unconventional bonds, causes

roughening or corrosion of the surface by breaking Si-Si bonds in forming Si-H bonds, or is simply bound in multihydride form on steps and kinks inherent on a silicon surface.

Fujiwara (18) performed a UPS study of hydrogen interactions with thermally cleaned Si(111) surfaces in the temperature range of 300-650 K. The findings in this study show that in addition to the conventional tetrahedral Si-H bonds, hydrogen atoms are also weakly adsorbed on Si(111) forming unconventional bonds. The UPS for hydrogen adsorption around 500 K is in agreement with previously reported results (6). However, the UPS spectra of room-temperature hydrogen adsorption on the clean Si(111) (7 x 7) surface agrees with Ibach and Rowe (4) but disagrees with Sakurai and Hagstrum (6) by the observation of a single broad peak rather than two sharp peaks. This spectral feature is attributed to hydrogen adsorption states other than the monohydride. The line shape of the peak is asymmetric which is a distinction from the symmetric line shape of the peak of the trihydride phase reported by Pandey *et al.* (1(b)) These authors conclude that the line shape cannot be explained by a mixture model of various SiH_x (x = 1,2,3) moieties on the surface and instead feel the line shape implies the presence of weakly bound hydrogen atoms.

Using mass spectroscopy, Schulze and Henzler (7) detected SiH_3 and SiH_4 during exposure of the surface to

atomic hydrogen. Roughening of the surface and silane desorption are observed only at high coverages, disagreeing with Wagner *et al.* (8) However, at coverages too low for roughening or filling of the Beta 2 site (described in detail in Chapter II), SiH_2 and SiH_3 formation is observed and must be explained without silane desorption. The trihydride phase observed by Pandey *et al.* (1(b)) may originate from the state Beta 2 (and Beta 3) and may be involved as a precursor to the SiH_3 phase and silane production.

A new vibrational mode of hydrogen adsorbed on a Si(111) (2 x 1) surface was found by Froitzheim, Lammering and Gunter (20) using energy-loss spectroscopy. Its intensity is dependent on the surface step density, indicating that this mode is related to adsorption sites near or on step atoms. Although Froitzheim *et al.* (10) had performed an earlier study of hydrogen chemisorption on the surface, they reexamined this system upon the findings of SiH_2 formation and erosion of the silicon surface. (8) High-resolution ELS was used to study room-temperature adsorption of hydrogen on Si(111) (2 x 1) and to compare the results with the former experiment (10). The ELS spectra after hydrogen exposure show a loss at 806 cm^{-1} which is attributed to hydrogen adsorption onto step edges or onto sites in the vicinity of steps. Intensity of this peak is dependent on step density. Upon exposure to atomic hydrogen or

heating the surface, the 806 cm^{-1} peak decreases and an increase in the 621 and 2073 cm^{-1} loss peaks occurs. The authors suggest that molecular hydrogen adsorbs on step positions and that adsorption of atomic hydrogen predominately occurs on the terraces. Because loss spectra do not show any structure due to H_2 stretching or bending, it was suggested that adsorption is either dissociative or that the perpendicular component of the dynamic dipole giving rise to a loss is very small. The authors expect under these conditions that a bending or stretching vibration of the whole molecule about the step edge or a vibration of the whole molecule against the substrate would be observed. It is possible that a hydrogen atom is bonded in a widely straddled bridgelike conformation between two silicon step edge atoms giving the 806 cm^{-1} peak. This suggests that such a nonconventional bond of hydrogen would, upon heating, cause the hydrogen to change into a conventionally bonded mode. Annealing of the surface changes the spectrum in that two new loss peaks appear, at 968 and 2258 cm^{-1} in addition to a decrease of the 806 cm^{-1} peak. The effect of heating could cause dissociation of the H_2 molecule adsorbed on a step, whereby each hydrogen atom will be bonded to one dangling bond of the edge atom, forming a SiH_2 complex. The observed modes at 968 and 2258 cm^{-1} could then be explained as a bending and a stretching mode, respectively. Assignment of the two other loss

peaks, one at 621 cm^{-1} and a broad one at 2073 cm^{-1} was done. The peak at 2073 cm^{-1} could not be resolved among the Si-H stretching modes of SiH, SiH_2, and SiH_3 which are 2016, 2105 and 2157 cm^{-1}, respectively. At high exposure, the 2073 cm^{-1} loss broadened even more, possibly representing a superposition of losses with different frequencies. A similar statement can be made about the 621 cm^{-1} loss, as it can be assigned to the wagging modes of the SiH_2 and SiH_3 complexes, definitely indicating that at this adsorption stage such complexes already exist. This statement is supported by the structure of the spectrum after coadsorption of hydrogen and deuterium. A loss of 782 cm^{-1} is observed, which does not scale directly with the square root of the mass ratio of deuterium and hydrogen. Assuming, however, a SiH_2 configuration which has a symmetric scissor mode with a frequency of 887 cm^{-1}, the corresponding SiHD mode has a frequency of 768 cm^{-1} which agrees almost quantitatively with the measured values and is identical to the result found by Wagner *et al.* (8)

Seel and Bagus (39) comment on the ELS study by Froitzheim, Lammering and Gunter regarding the observed vibrational mode at 806 cm^{-1} (20). Seel and Bagus had previously done *ab initio* cluster-model calculations (35) (described in Chapter II), finding stable adsorption sites at the open site of the silicon surface both above and below the surface. They had predicted a frequency

for the normal vibration of a hydrogen atom either above or below the Si(111) surface at the open site to be 806 cm^{-1}. In this study, no relaxation or reconstruction effects were taken into account. They postulate that changing the geometry of the cluster used in the calculation to a reconstructed (2 x 1) surface using Haneman's model (55) would not affect the results appreciably. They conclude that the new vibrational loss intensity is attributed to the vibration of a hydrogen atom adsorbed above or below the center of this adsorption site, and that this study, as well as the Froitzheim study, supports the theory that adsorption at this site provides an intermediate step in the production of gaseous silane and subsequent adsorption of various hydrides on the surface.

A comparative study of hydrogen vibrations on the Si(111) (7 x 7) and the laser-annealed (1 x 1) surfaces has been carried out by Chabal, Higashi and Christman (21) using high-resolution infrared spectroscopy. A sensitive way to compare these two similar surfaces is to monitor the properties of chemisorbed species. They attempted to find the subtle differences in local chemical bonding between the two surfaces. The two surfaces have broad distributions of chemisorption sites. However, there are two distinct adsorption sites on the (7 x 7) surface while only one well-defined site is present on the laser-annealed

surface. Both low- and high-coverage regimes were studied, and the (7 x 7) surface gives two absorption lines polarized perpendicular to the surface. One is at 2073 cm^{-1}, and has been attributed to saturation of the silicon surface dangling bond by one hydrogen atom. This line is absent on the laser-annealed surface at any coverage and has been attributed to the long-range nature of the (7 x 7) reconstruction, and is possibly located in the corner of the (7 x 7) unit cell (15). A line is found at 2077 cm^{-1} on both surfaces, and is thought to be associated with a well-defined local structure. It is determined that at low coverage, adsorption takes place on sites polarized purely perpendicular to the surface, forming a monohydride. At higher coverages, the dominant features in the spectra for both surfaces is the presence of a broad background centered around 2100 cm^{-1}, exhibiting an absorption component parallel to the surface whose relative importance increases up to saturation. The broadness and lack of features indicate that the hydrogen is chemisorbed in an inhomogeneous distribution of sites. Etching of the surface and intrinsic roughness of both surfaces would provide a variety of chemisorption sites. Based on previous experimental evidence by Wagner *et al.* (8), and on infrared work on the Si(100) surface where the dihydride mode SiH_2 is observed with components perpendicular and parallel to the surface around 2100 cm^{-1}, the authors

attribute the background to a presence of SiH_2 on a distribution of sites. The presence of steps with dangling bonds at some angle from the normal (56) or the formation of a trihydride could also account for part of the observed background. There is a broad band centered at 1970 cm^{-1} which appears on the (7 x 7) surface only, which is assigned to vibrations of Si-H inside the bulk. This would indicate that the (7 x 7) unit cell is an open structure which makes diffusion of hydrogen into subsurface layers possible.

Both He I and He II UPS was used by Ciraci, Butz, Oellig and Wagner (22) to study the occurrence of the dihydride phase on several surfaces of silicon, including the Si(111) (3 x 3) and (1 x 1) surfaces. They suggest that the intermediate phase forming on the (7 x 7) surface at room temperature has a connection with the dihydride phase, but that at higher hydrogen exposures, the monohydride phase prevails over the dihydride phase.

Adsorbed states of atomic hydrogen on the Si(111) (7 x 7) surface at 300 K have been studied by EELS and LEED measurements by Kobayashi, Edamoto, Onchi and Nishijima (13). At low exposures, only a single loss peak at 2057 cm^{-1} is observed, which has been attributed to the stretching vibrational energy of SiH for hydrogen atoms positioned on top of the silicon atoms, pointing in the surface-normal direction (denoted as n-SiH). They do not observe the bending vibration of the n-SiH species.

Upon higher exposure, the 2057 cm^{-1} peak is shifted toward higher loss energy of 2080 cm^{-1}, accompanied by the appearance of two new peaks at 637 and 879 cm^{-1}. The 637 cm^{-1} is assigned to the bending vibration of the t-SiH species (whose Si-H bond axes are tilted from the surface-normal direction) and the wagging vibration of the SiH_2 species. The 879 cm^{-1} is assigned to the scissor mode of the SiH_2 species and the symmetric deformation mode of the SiH_3 species. The shift of the 2057 cm^{-1} peak is due to adsorbate-adsorbate interaction of the SiH species and to the formation of SiH_2 and SiH_3 species. At higher hydrogen exposures, the intensities of the 637 and 879 cm^{-1} peaks are increased while the intensity of the Si-H symmetric stretching mode is reduced and shifted to 2100 cm^{-1}. This indicates that more t-SiH, SiH_2 and SiH_3 species are formed. Heating of the surface causes some changes in the loss spectrum, such as a downward shift of the 2100 cm^{-1} peak and decrease in the 879 cm^{-1} peak intensity. This would suggest decomposition of some SiH_2 and SiH_3 species with the formation of the n- and t-SiH species and from complete dehydrogenation of some SiH_2 and SiH_3 species. However, they do not exclude the possibility that the amount of SiH_2 or SiH_3 species is negligibly small. They suggest a further analysis of the vibrational loss spectra is needed for more precise interpretation.

In following up the Kobayashi study, Nishijima, Edamoto, Kubota, Kobayashi and Onchi (23) studied the interaction of hydrogen with Si(111) (7 x 7) surfaces using HREELS, AES, and LEED techniques. At 300 K, atomic hydrogen produces the SiH, SiH_2 and SiH_3 species on the Si(111) surfaces, depending on exposure to hydrogen. At low coverage, a single loss peak at 2057 cm^{-1} is observed and attributed to the stretching vibrational excitation of the SiH species formed on the Si(111) surface. Absence of a loss peak attributed to the bending vibration indicates that in the initial state, hydrogen atoms react with silicon atoms in the first layer to saturate the dangling bonds forming the SiH species directed along the surface normal (denoted by n-SiH). Defects in the surface may have dangling bonds pointing to a direction away from the surface normal; SiH species formed on these defects are denoted as t-SiH, as defined in the Kobayashi *et al.* study (13). The bending vibration is expected to be observed for t-SiH, but is believed to exist only in small amounts, which would explain non-observation of this mode. Upon higher exposure, the 2057 cm^{-1} loss is shifted to 2081 cm^{-1}, and 637 and 879 cm^{-1} losses appear. By referring to IR and Raman-scattering studies of hydrogenated a-Si:H (57,58), the 637 cm^{-1} loss can be attributed to the bending vibration of the t-SiH species and to the wagging vibration of the SiH_2 species. The 879 cm^{-1} loss is

attributed to the scissors mode of the SiH_2 species and to the symmetric deformation mode of the SiH_3 species. The 2081 cm^{-1} loss is attributed to stretching vibrations of all species, with the shift being attributed to the formation of SiH_2 and SiH_3 species, and the possibility of adsorbate-adsorbate interactions. Upon increasing the hydrogen exposure, the intensities of the 637 and 879 cm^{-1} losses are increased, while the intensity of the SiH symmetric stretching mode is reduced. The energy of the SiH symmetric stretching mode is shifted toward higher energy (2097 cm^{-1}). All of these are attributed to the increase in the amount of SiH_2, SiH_3 and t-SiH being formed. The reduction in intensity of the SiH symmetric stretching mode indicates that the amount of n-SiH species is decreased. After heating of the Si(111) surface, changes occur in the loss spectrum: The 2097 cm^{-1} loss is shifted to lower energy and its intensity is increased; the 879 cm^{-1} loss intensity is decreased, and the 637 cm^{-1} loss is nearly unchanged. The decrease in the 879 cm^{-1} peak results from decomposition of SiH_3 and SiH_2 species with the formation of n- and t-SiH species and from complete dehydrogenation of SiH_2 and SiH_3 species. The dehydrogenation is accompanied by desorption of H_2 from the surface. The increase in intensity of the shifted 2097 cm^{-1} loss indicates the amount of n-SiH species increases, while the shift occurs due to amounts of SiH_2 and SiH_3 species decreasing. The

637 cm^{-1} loss intensity remains unchanged due to two competing effects; (1) Decomposition of SiH_3 species forms t-SiH and SiH_2 species, causing an increase in the 637 cm^{-1} loss intensity; and, (2) complete dehydrogenation of some SiH_2 species decreases the 637 cm^{-1} loss intensity. Formation of both SiH_2 and SiH_3 species must be invoked to explain these effects. Further heating causes a reduction of the shifted 2097 cm^{-1} intensity as well as a large decrease in the 879 cm^{-1} peak. The 637 cm^{-1} loss remains the same. The large decrease in the 879 cm^{-1} loss is attributed to the decomposition of some SiH_2 and SiH_3 species with the formation of t-SiH species, and to the complete dehydrogenation of some SiH_2 and SiH_3 species. Because the large decrease in the 879 cm^{-1} loss is not accompanied by an equally large decrease in the shifted 2097 cm^{-1} loss, it is suggested that the amount of SiH_2 and SiH_3 species formed on the surface is small. Observation of a peak at 637 cm^{-1} is considered evidence that t-SiH species exist. At 900 K, all peaks completely disappear with the desorption of molecular hydrogen.

HREELS and LEED studies in comparison with TDS data are reported by Froitzheim, Kohler and Lammering (24) for atomic hydrogen adsorbed on Si(111) surfaces. They claim the only two configurations formed are SiH and SiH_2. The spectra show a bending mode (637 cm^{-1}) and a stretching mode (2089 cm^{-1}) of a SiH configuration

respectively and the scissor mode (887 cm^{-1}) of a SiH_2 configuration. Upon heating of this surface to approximately 650 K, the SiH_2 configuration is desorbed, indicated by a decrease in loss intensity at 887 cm^{-1}. In TDS, the maximum desorption rate of this state occurs at 693 K. At sample adsorption temperatures above 623 K, this state will not be occupied at all. The present results do not show a measurable indication of a stretching mode of the SiH_2 configuration and conclude that the contribution of SiH_2 is very small, if any. The existence of a SiH_2 configuration demands a site with formally two dangling bonds. These sites are provided at certain reconstructions of a Si(111) surface, and on those surfaces with kinks and other defects. On the Si(111) (2 x 1) surface, sites with two dangling bonds may be provided by edge atoms of the cleavage steps. This is supported by the observation that the intensity in the peak at 887 cm^{-1} loss was proportional to the step density. On the Si(111) (7 x 7) surface, those sites may be provided by adatoms or island structures. They claim that adsorption sites with two dangling bonds occupied with only one hydrogen cannot be distinguished from those occupied sites with only one dangling bond. This gives rise to the appearance of a stretching mode around 2089 cm^{-1} whose adsorption kinetics will be described by the same parameters. Double sites can be occupied by a second hydrogen only if there is no empty site in the

immediate neighborhood. Adsorption can take place only if an atom hits an empty dangling bond. If it hits an already occupied site, then there is a given probability to empty this site. This model neglects a possible preference for a single hydrogen to occupy either an empty single site or an empty double site when both types are present. The following experimental results support the model: Only one stretching mode (2089 cm^{-1}) has been observed. The second site is occupied after the first one is nearly filled. Atomic deuterium is able to replace adsorbed hydrogen. However, it is not understood why there is no stretching mode observed from the SiH_2 configuration and why the intensity of the 637 cm^{-1} loss is so strong in EELS.

The unexpected findings of various hydride species on the Si(111) surfaces points raises many questions as to how bonding could occur. In addition to effects due to the atomic geometries of the various reconstructed surfaces, the effect of surface irregularies and possibilities of corrosion of the surface by the hydrogen are considered to play a part in forming these species.

The Wagner *et al.* group (8), upon finding evidence of existence of multihydride complexes on the silicon surface, suggest that either a sufficient number of silicon atoms with more than one dangling bond is present on the surface, or that atomic hydrogen is

capable of breaking Si-Si bonds. In examining the latter proposal, they followed an experiment wherein the same total exposure of H_2 and D_2 were applied to a silicon surface, but not simultaneously. The surface was first exposed to deuterium, and a loss spectrum was taken. Subsequently, the surface was exposed to atomic hydrogen and the spectrum changed drastically to a pure hydrogen spectrum, with only one small loss feature attributed to deuterium. They conclude that corrosion by hydrogen had occurred, with the deuterium atoms being removed from the surface by silane formation and desorption during the hydrogen atom exposure. The authors did not perform an experiment in which the surface was first exposed to hydrogen and then to deuterium to determine if deuterium would also cause erosion of the surface. While concluding that corrosion of the silicon surface by hydrogen interactions was the cause of the multihydride complex formations, they do not rule out the possibility of kinks and steps on the silicon surface which could have more than one dangling bond and subsequently form the multihydride complexes.

Pandey *et al.* (1(b)) suggested a mechanism for formation of the trihydride phase using a vacancy model for Si(111) (7 x 7) and (1 x 1) surfaces. In this model, approximately 27% of the surface atoms are missing in the outermost silicon layer. There will be vacancy clusters within which some hydrogen adsorption to the three

dangling orbitals of the silicon atoms in the second layer can occur. The release of the energy in formation of these bonds can contribute to the removal of silicon atoms at the edges of the vacancy cluster which can, with further bonding to incident hydrogen, be desorbed as silane and disilane.

In studying surface states and reactivity of hydrogen chemisorption on thermally cleaned Si(111) surfaces, Fujiwara (28) supports rough-surface models to describe the adsorption of hydrogen onto the Si(111) surfaces. He performed adsorption experiments using three surfaces which were thermally cleaned in different ways. He shows that depending on surface preparation, the spectral intensities for intrinsic surface states are discernably different among thermally cleaned Si(111) surfaces. He interprets the differences as arising from microscopic changes of the surface atomic arrangements upon thermal agitation or annealing. He observes significant differences in reactivity and bond character of adsorbates and attributes these to changes in the surface caused by creation of surface atomic imperfections such as vacancies, adatoms, or bilayer atomic microdomains. He agrees with the mechanism for formation of the trihydride phase proposed by Pandey *et al.* (1(b)) and concludes that the present experimental results give support for the vacancy models.

In examining LEED patterns of hydrogenated Si(111) surfaces, Schulze and Henzler (7) found oscillations of broadened spots in the patterns. Oscillations with electron energy coincide with a series of characteristic voltages due to silicon steps. Because this was observed for both surfaces upon hydrogenation, these authors believe there is strong roughening of the surface due to interactions with hydrogen. To distinguish between roughening by surface diffusion or by desorption of some compound, a preliminary mass spectrometric study was made. Because SiH_3 and SiH_4 were detected during exposure to atomic hydrogen, it was believed that roughening due to etching by formation of volatile silane is established. Because roughening and silane desorption are observed only at high exposures in their experiments, the model proposed by Wagner *et al.* (8), which assumes silane formation and desorption at low exposures explains the existence of SiH_2 complexes, is not confirmed.

Verwoerd (38) explains the observed roughening of the surface in terms of his model giving further support for the existence of two subsurface interstitial sites (see discussion in Chapter II). The sites are labelled sites A and B. He proposes that Site A exists directly above the fourth-layer silicon crystal between the second and third crystal layers. Site B is located directly below a first-layer silicon atom. The repulsive force

exerted by hydrogen atoms in the type A site is insufficient to break the Si-Si bonds between the second and third crystal layers, but becomes strong enough when augmented by that of additional atoms in the type B positions. This is in accord with the previous quantum mechanical calculations that a hydrogen atom on its own is unable to break a chemically unstrained Si-Si bond (59).

Froitzheim *et al.* (20) support the assumption that because SiH_2 complexes are observed, hydrogen is able to break Si-Si bonds from the uppermost layer of the Si(111) surface to create enough asymmetric sites with two or three dangling bonds. This erosive process takes place by a production and desorption of silane observed in TDS measurements. Roughening of the surface is assumed to take place. In a later study, however, Froitzheim *et al.* (24) claim that the adsorption sites for the SiH_2 species are not produced by corrosion because the relative intensities of loss peaks are always the same, independent of the history of the surface. Even repeated desorption of the SiH_2 state and saturation adsorption will not change the relative saturation intensities of the losses at 887, 2073 and 673 cm^{-1}, no matter how often this is done. Also, no SiH_x ($x > 1$) configuration could be observed in the mass spectra during adsorption or desorption even at elevated surface temperatures. They assume that if there is any

production of silane or other SiH_x complexes, then it is much too small to produce the number of sites with two dangling bonds necessary for the relatively high intensity of the 887 cm^{-1} loss. Loss spectra of a Si(111) (7 x 7) surface saturated with hydrogen and subsequent exposure to deuterium provides identical spectra with all peaks shifted by about a factor of 1.4 (according to the square root of the mass ratio of hydrogen and deuterium), indicating replacement of the hydrogen by deuterium. In previous studies, (8,20) the appearance of a loss peak associated with a HD scissor mode besides a HH and a DD loss when the surface was exposed to atomic hydrogen up to half saturation and then saturated with deuterium was considered confirmation of corrosion of the surface. However, this may not be the case, because it is indicated that desorption of hydrogen does not destroy the (7 x 7) periodicity. The appearance of the HD scissor mode is explained in terms of their proposed model of double sites. They suggest that atomic detuerium or hydrogen is able to empty a site doubly occupied by hydrogen or deuterium atoms whenever it hits such a site and so creates the possibility to occupation afterwards with a different atom.

Chabal *et al.* (21) attribute the broadness and lack of features of spectral peaks to an inhomogeneous distribution of adsorption sites, and state that the

broadening is a result of etching as was observed on the Si(111) surface for large exposures (25).

Ciraci (40) proposes a mechanism of deconstruction which explains the observed structural change from the (2 x 1) surface to the (1 x 1) surface at low coverages of hydrogen. Assuming Pandey's pi-bonded chain model (60) for the (2 x 1) reconstruction for the Si(111) surface, he suggests that subsequent to the saturation of some dangling bonds, this chain is broken. If this is true, the formation of di- and trihydrides follows naturally. He proposes a simple mechanism which converts the chain surface to the (1 x 1) form. The model assumes that incident hydrogen atoms are likely to interact with the atoms forming the five-fold rings proposed in the pi-chain model. Upon the binding of hydrogen, a Si-Si bond in the five-fold ring is broken, and the surface unreconstructs to the monohydride phase. Hydrogen chemisorbed at the distorted regions of silicon, such as five-fold rings, can be precursor states responsible for the breaking of the surrounding bonds, such as chain bonds.

Webb and Veprek (26) studied the reactivity of solid silicon with a hydrogen plasma, and examined the erosion of the surface with plasma flow. Miller, Luz, Wiesmann, Rock, Ghosh, Ramamoorthy and Stronging (61) show that atomic hydrogen breaks Si-Si bonds and leads to the production of silane.

The Seel and Bagus calculation of hydrogen in the open site (35) suggests corrosion of the outer layer of the silicon surface and subsequent formation of the trihydride phase observed by Pandey *et al.* (1(b)) by the following mechanism: Upon adsorption of hydrogen to a head-on site, enough energy is released to contribute to the penetration of hydrogen atoms at three adjacent open sites. If another hydrogen atom adsorbs (or has already been adsorbed) directly over the central silicon in between the three open sites, then an SiH_4 complex is formed which can be easily desorbed as SiH_4. This mechanism can lead to the eventual removal of the entire surface monolayer of Si(111). Adsorption to the three dangling bonds of the silicon atoms in the second layer can then occur, thus leading to the formation of the Si(111):SiH_3 phase as described by Pandey *et al.* (1(b))

Fujuiwara (18), in concluding hydrogen is weakly bound in unconventional sites on the Si(111) surface, supports corrosion of the surface by hydrogen. He postulates that the weakly adsorbed hydrogens atoms are involved in a precursor state which is important to break Si-Si bonds and to form the tetrahedral SiH_3 configurations on the surface. Additionally, he states that in order to initiate SiH_3 unit formation, it is inevitably necessary to postulate the existence of surface atomic imperfections such as vacancies, adatoms, and bilayer microdomains.

Kobayashi *et al.* (13) suggest that the n- and t-SiH, SiH_2 and SiH_3 species are formed by corrosive action of atomic hydrogen as follows: Reaction of atomic hydrogen with the Si(111) surface is accompanied with the Si-Si bond breaking and desorption of silane and possibly SiH_3 during hydrogen exposure. Some of the Si atoms are removed from the outermost layer of the Si(111) surface and silicon atoms with one, two or three dangling bonds are formed. Further hydrogen exposure results in the formation of n- and t-SiH, SiH_2 and SiH_3 species. The SiH_4 (SiH_3) complexes are produced at the portions of the Si(111) surface with high local density of hydrogen. They confirm desorption of silane in this experiment.

Nishijima *et al.* (23) attribute formation of the SiH_x species to the corrosive action of atomic hydrogen (Si-Si bond breaking and SiH_4 desorption and bonding at defects such as vacancies, adatoms, etc.) (13). The adsorbates break the Si-Si bonds due to a strong Si-adsorbate interaction which surpasses the effect of surface silicon dangling bonds.

Chadi (62) proposes a new adatom model for Si(111) (7 x 7) and (5 x 5) reconstructed surfaces which is consistent with structural information from vacuum tunneling microscopy. Using this model, Chadi explains the occurrence of formation of SiH_2 and SiH_3 complexes in the early stages of hydrogen chemisorption and also explains the unique chemisorption site found by

Chabal (15). He proposes that his model has sites at the position of the second-layer atoms which are under high stress, and that upon hydrogen approach, these stress points will undergo bond rupture, leading to dangling bonds. Chemisorption of one hydrogen atom to each of the resulting dangling bonds should lead to a large decrease in energy of the system.

Changes in bulk bond strengths upon adsorption of hydrogen would contribute to roughening or corrosion. Katterle and Lorenz (41) performed a quantum chemical study of chemisorption of hydrogen on a Si(111) surface with steps and kinks sites in order to study the influence of crystal surface imperfections. The study was limited to the ideal or relaxed (1 x 1) surface structure. They report that the density of states of a dangling bond near the step does not differ much from that of a perfect surface. The Si-Si back-bonds (bonds between first-layer silicon and second-layer silicon) near the step differ in some details from that of a perfect surface, but are relatively small. Local densities of the dangling bonds are strongly altered near a kink site, because of first-neighbor interactions between the two dangling bonds at the kink site, or of second neighbor interaction of the dangling bonds from the kink with the dangling bonds on the nearby terrace atoms. Also, the densities of back-bonds near a kink site are significantly altered relative to back-bonds at

the perfect surface or the step, again due to the interaction with an enlarged number of dangling bonds. These obviously play a role in chemisorption.

The Appelbaum *et al.* (36) calculation shows a marked weakening of the Si-Si bond between the surface and subsurface silicon atoms upon chemisorption of atomic hydrogen to the unconventional subsurface site. The study supports corrosive modification of the surface by hydrogen.

Understanding the character of the hydrogen-Si(111) surface bond can clarify the nature of the various reconstructions of the surfaces. While the (2 x 1) reconstructed surface is generally explained in terms of a buckling model (55), the reconstruction of the (7 x 7) and high-temperature (1 x 1) phase still remains a challenging problem. These reconstructions have been described by different structural models, all of which can be categorized two ways: Models in which the surface atoms are strongly perturbed from the ideally truncated bulk (111) plane of silicon due to missing or added surface atoms (defect or rough surface models), and models which assume a small perturbation in the smooth (111) plane which causes the surface atoms to buckle or ripple (smooth models). Several models have been proposed explaining the various reconstructions (2(b)). Adsorption of hydrogen onto the (2 x 1) superlattice appears to destroy the reconstruction, converting the

surface to its bulk positions. Haneman's buckling model (55) suitably describes the Si(111) (2 x 1) metastable surface which reverts to the ideal (1 x 1) surface upon hydrogenation. According to this model at the (111) surface, the sp^3 hybridization of the orbitals will be partially reversed due to the half-filled dangling-bond orbitals. This leads to a buckling of the surface, where half of the surface atoms are raised above their average position on the surface, and the other half are depressed because of more *s*-like or *p*-like bonds, respectively. Adsorbed hydrogen would restore the sp^3 hybridization of the surface atoms and the structure would revert to the (1 x 1) ideal surface. The best model for the thermodynamically stable Si(111) (7 x 7) surface still remains a challenging problem. Adsorption of hydrogen onto the (7 x 7) superlattice does not completely destroy the superstructure as evidenced by the persistence of seventh-order diffraction spots upon hydrogen chemisorption. This indicates more complex rearrangements must occur on the Si(111) (7 x 7) surface or its subsurface atomic layers. The special influence of the hydrogen to remove a reconstruction of silicon is important in determining the electronic and structural properties of silicon crystals.

Ibach and Rowe (4) show different influences on hydrogen adsorption for cleaved and clean surfaces. On the (111) (7 x 7) surface, no changes are observed in the

LEED pattern, while the half-order spots are completely extinguished upon hydrogen saturation coverage on the (2 x 1) surface. This indicates that the (7 x 7) reconstruction is not just due to the presence of dangling bonds. They suggest that vacancies exist on this surface. The metastable (2 x 1) surface can be described by up and down displacement of every second surface atom. This study suggests that the different surface structures are not caused by a single reconstruction mechanism.

Contrary to the findings of Ibach and Rowe (4), Sakurai and Hagstrum (6) observed a change in the LEED pattern for the (7 x 7) lattice upon hydrogen exposure. Past half saturation exposure, the nonintegral spots become weak and finally disappear, except for certain spots near the integral spots. They conclude that Ibach and Rowe performed their study at less than one-half monolayer coverage.

Appelbaum and Hamann (42) propose that the charge density from the unpaired electron in the dangling bond is distributed to the back bonds of the surface atoms. This strengthens these back bonds and reduces the lattice spacings between the first and second layer, giving rise to deep lying surface states at the bottom of the *s*- and *p*-like valence bands. Upon adsorption of hydrogen to the surface silicon atoms, the charge density is redistributed toward a distribution similar to that of bulk

silicon. Surface relaxation and the corresponding surface states disappear. However, influence of the hydrogen adsorption on the LEED pattern is very different for the (111) (7 x 7) surface compared to that of the (111) (2 x 1) cleaved surface (32). At saturation, the (111) (2 x 1) reconstruction is destroyed, suggesting that the adsorbed hydrogen has restored the bulk geometry of the silicon surface atoms. The (111) (7 x 7) surface is more stable to the hydrogen adsorption because at saturation coverage, the LEED pattern for the (7 x 7) surface is somewhat intact. These authors suggest that because of these discrepancies, the different surface superstructures are not caused by a single reconstruction mechanism.

In proposing a unique chemisorption site, Chabal (15) shows a decrease in the 3/7 and 4/7 fractional-order spots in the LEED pattern upon increasing hydrogen exposure to the (7 x 7) reconstructed surface. He states that the exposure induces the atoms to rearrange in an inhomogeneous way. Chabal *et al.* (21), in a comparative study of hydrogen chemisorption on the (7 x 7) and the laser-annealed (1 x 1) surface, conclude that since the unique site discussed in Ref. 21 appears only on the (7 x 7) surface, the (7 x 7) reconstruction has an open structure involving several layers and hydrogen diffuses and binds at this deep-lying adsorption site. Absence of this site

on the (1 x 1) indicates that this surface is "smooth" and that diffusion below the top layer does not take place.

Nishijima *et al.* (23) report that hydrogen forms disordered structures on the Si(111) (7 x 7) surface at 300 K. They found that adsorbate-adsorbate interactions on the Si(111) surface are small and that the long-range structure of the (7 x 7) surface has little effect on the adsorbed states.

Kobayashi *et al.* (13) observe persistence of fractional order spots in LEED patterns at high hydrogen exposures to the Si(111) surface. This is interpreted as due to corrosion-induced patches of the n- and t-SiH, SiH_2 and SiH_3 species forming. The patch formation may be related to surface defects.

Froitzheim *et al.* (24) also show that hydrogen has a small effect on the (7 x 7) superstructure, but that complete desorption of hydrogen from the surface leaves behind a strongly disturbed surface.

Harrison (3), in examining surface reconstruction of semiconductors, considers the effects of adsorption on silicon. As found in Ibach and Rowe (4), saturation of the dangling bonds by hydrogen eliminates the (2 x 1) reconstruction on the Si(111) surfaces but does not eliminate the (7 x 7) reconstruction for the annealed Si(111) surface. They conclude that since adsorbed hydrogen did not destroy the

(7 x 7) pattern, this surface is not simply a distortion of the ideal surface (as in the (2 x 1) surface), but that there are either extra atoms above the nominal surface plane or vacancies below, or both.

McRae and Caldwell (43) examined LEED patterns of hydrogen-covered Si(111) (7 x 7) surfaces to see the effect of adsorption on the reconstruction of this annealed surface. Hydrogen atom adsorption on the surface simplifies the LEED pattern from a (7 x 7) superstructure to one which has patterns of local (1 x 1) periodicity. They explain unreconstruction of the Si(111) (2 x 1) superstructure upon chemisorption of hydrogen as due to satisfying silicon valancies which, when unsatisfied, causes buckling of the surface. Buckling strain is removed upon chemisorption and the structure reverts to the (1 x 1) periodicity. Similarly, on the Si(111) (7 x 7) surface there are islands and troughs of locally buckled structures that revert to islands of (1 x 1) periodicity as shown in the LEED patterns. The (7 x 7) reconstruction is not completely destroyed.

Fujiwara (28) finds retention of 7th-order diffraction spots for the Si(111) (7 x 7) surface upon hydrogen chemisorption. This indicates the effect of hydrogen atoms on LEED patterns should be small as long as the original (7 x 7) atomic structures are preserved. Because the trihydride phase was observed, he supports

the rough-surface models as a structural model for the Si(111) (7 x 7) surface.

DV (Discrete Variational)-Xα cluster calculations were performed by Tsukada and Hoshino (44) on the electronic structure of the hydrogen-silicon chemisorptive bond on the Si(111) surface. The calculations used a vacancy cluster and an ideal cluster. It was found that chemisorption of hydrogen is best explained using a vacancy model, rather than an ideal one. In a further study, Hoshino and Tsukada (46) investigate hydrogen chemisorption for two reconstruction models of the Si(111) (7 x 7) surface using the same techniques in the previously mentioned study. The models used were the vacancy model and the buckled model to complement the preliminary results reported above. The authors believed this model explains the observed peaks in the UPS of Si(111) (7 x 7) by Sakurai and Hagstrum (6). Features in the density of states figures caused by the buckled model do not correspond to the experimental results. Because their studies support the vacancy model, they question whether vacancies on the surface are stable. Preliminary calculations show that energy loss in forming a single vacancy is not large if the displacement around the vacancy is taken into account.

Schulze and Henzler (7) find that after cleavage, the (2 x 1) LEED pattern appeared as usual, but the half order spots weakened and were completely extinguished

upon exposure and coverage of one-half monolayer. The (7 x 7) superstructure is less affected by hydrogen adsorption. Even close to saturation coverage of Site Beta 1, fractional order spots can still be observed. By increasing the exposure, all of the extra spots finally vanish. In both cases, broadening of the spots and background increases in the LEED patterns.

Selioni and Bertoni (45) compared the change in state density induced by chemisorption of hydrogen on different surface geoemetries in an attempt to explain the reconstruction of the Si(111) surface. The two models compared are the buckling surface and the pi-bonded chain model proposed by Pandey (60). They compute the densities of states using the empirical tight-binding method. Comparison of these theoretically simulated spectra with experimental spectra lead them to support the chain model.

The broad background in spectral features at fairly low coverages led Chabal *et al.* (21) to conclude that the (7 x 7) and (1 x 1) surfaces are rough and have a variety of chemisorption sites. They also conclude that the (1 x 1) surface is not unreconstructed and is highly disordered. Nishijima *et al.* (23) also found that hydrogen forms disordered structures on the Si(111) (7 x 7) surface.

Other aspects of chemisorption of hydrogen are sticking probabilities of atomic and molecular hydrogen

on Si(111). Adsorption of molecular hydrogen is negligible (4,5,7,11,18), and the H_2 adsorption that is seen is attributed to adsorption at defects sites on the Si(111) surface.

Law (63) reported the variation in sticking probability as a function of θ, the hydrogen coverage on the surface. For $\theta < 0.15$, the sticking probability is constant and approximately unity. The sticking probability then decreases by two orders of magnitude in going to $\theta = 0.4$, after which the sticking probability remains constant until the effect of monolayer coverage sets in. At that point, the sticking probability rapidly drops another two orders of magnitude. The decrease in the sticking probability at intermediate coverages of the surface by hydrogen is attributed to adsorption in the beta site in his proposed model (5) discussed in Chapter II.

Auger Electron Spectroscopy (AES) techniques were used to study hydrogen adsorption on a Si(111) surface by Thanailakis, Ioannou and Reed (27). Hydrogen and helium cannot be studied in a straighforward manner by this method because they do not emit Auger electrons. The study was done by measuring the decrease in the principal silicon Auger peak when the Si(111) surface is exposed to hydrogen. The calculated sticking coefficient for atomic hydrogen on silicon is 0.0003; however, they report large experimental errors, particularly at high coverages.

Schulze and Henzler (7) calculate a sticking probability of unity for hydrogen atom chemisorption on Si(111) (7 x 7) in the primary binding site; the sticking probability at the secondary binding site is negligible except at high coverages in the primary binding site. Molecular hydrogen does not affect the surface. Brzoska and Kleint (11) measured a sticking probability of 10^{-5} for H_2 and approximately unity for hydrogen atoms on Si(111). Froitzheim (10) found adsorption of molecular hydrogen on steps of cleaved faces. Joyce and Neave (16) observe a large sticking coefficient of molecular hydrogen, but state the possibility that some adsorption of atomic hydrogen had occurred, because of the operation of hot filaments in the system which would cause some dissociation of H_2.

The recombination and desorption of molecular hydrogen on Si(111) surfaces has been studied both experimentally and theoretically. Experimentally, adsorption of hydrogen on Si(111) has been found only for hydrogen atoms (4,5,7,11,18) and only H_2 is found to desorb from Si(111) surfaces covered with hydrogen atoms (7,11). At low coverages, desorption is governed by a second-order process, whereas at higher coverages, the reaction follows first-order kinetics.

Brzoska and Kleint (11) show three desorption peaks, and find that the main H_2 desorption peak follows

second-order kinetics. They calculate a desorption energy for this primary desorption as 42 ± 1.5 kcal/mol.

Schulze and Henzler (7) show two desorption peaks, the primary peak and a secondary peak (described as an unresolved double peak). Its desorption is second order with the activation energy of desorption varying from 2.5 to 3.5 eV with increasing coverage. Additionally, at high hydrogen coverages, a shift to first-order desorption kinetics is suggested with an estimated desorption energy of 2.1 ± 0.1 eV, and pre-exponential factor of $9.7 \times 10^{(12\pm0.1)}$ cm^2/s. Desorption from the secondary site is expected to be first order. Using this data, Verwoerd (38) estimates a desorption energy and frequency factor from this site of 1.13 eV and 3.1×10^7 s^{-1}, respectively.

Verwoerd (38) also discusses thermal desorption of hydrogen from the interstitial site. Using his model of adsorption sites, he explains why the desorption peak for the secondary site shows a first-order kinetic behavior in contrast to the primary peak. This happens because the hydrogen atoms are not chemically bound and can be dislodged by comparatively low thermal energies. Also, when the hydrogen escapes from this site, it will, for geometric reasons, not have the appropriate momentum to enter a neighboring site and thus its escape

probability is independent of whether these sites are occupied. He estimates an activation energy of desorption of 0.7 eV and a frequency factor of 10^4 s^{-1}.

The interest of Joyce and Neave (16) was in finding complicating effects introduced by the interaction of adsorbed species with electron beams in experiments which would affect adsorption and desorption. They found that beam stimulated desorption of H_2 from silicon occurs which is first order with respect to beam current. Spectra recording thermal desorption of H_2 gives desorption energies for the three observed binding sites of hydrogen (discussed in Chapter II).

Froitzheim *et al.* (24) observed two desorption states and propose two desorption models as follow: (1) The desorption takes place first by removing one hydrogen atom out of each doubly occupied site. This results in a desorption peak at 693 K. Next, at 793 K, the second peak appears due to emptying all sites completely; or, (2) The desorption takes place first by emptying all doubly occupied sites completely (first peak) and then emptying all singly occupied double sites together with the occupied single sites if both types are present.

Raff, NoorBatcha and Thompson (48) performed a variational transition-state theory study of the recombination/desorption rate of H_2 from an ideal Si(111) surface using a Monte Carlo procedure. A semi-empirical

potential-energy surface was used which described the lattice-adatom interaction, adatom-adatom interaction, and lattice potential. The parameters of the potential were fitted to the results of the hydrogen atom-silicon cluster calculations by Hermann and Bagus (33), the experimental and theoretical results for the H_2 insertion barrier into silicon and SiH_2, and the measured $H_2(g)$ bond dissociation energy, fundamental frequency, and equilibrium bond distance. A Monte Carlo random walk procedure with importance sampling was used to find the minimum energy path for H_2 recombination/desorption. They calculate a recombination/desorption barrier of 2.52 eV with a back-reaction barrier of 0.182 eV. Variational rate calculations were carried out by minimizing the calculated flux across a dividing surface. Activation parameters were obtained from an Arrhenius plot of the minimized flux giving an activation energy and frequency factor of 2.41 eV and 0.202 cm^2/s.

A series of studies were carried out to investigate elementary reactions involving hydrogen and a Si(111) surface. We examined the dynamics of H_2 scattering and dissociative chemisorption on a clean, ideal Si(111) surface. The potential-energy surface used is the one developed by Raff *et al.* (48). The energy and spatial distributions for H_2 scattered from the surface are calculated and sticking probabilities are determined as a function of temperature. We have examined the

mechanism of energy transfer from the newly chemisorbed hydrogen atom to the lattice phonon modes and determined the transfer rates as a function of surface temperature. The variation of H atom mobility has been computed as a function of residence time on the surface and surface temperature.

Next, we studied the dynamics of hydrogen atom scattering and chemisorption on a Si(111) surface with partial or full hydrogen atom coverage. A potential-energy surface has been developed using available experimental data and theoretical information which describes two types of binding sites for hydrogen. The energy and spatial distributions of hydrogen atoms scattered from the surface are calculated as functions of incident azimuthal angle and hydrogen coverage on the Si(111) crystal face. Sticking probabilities and the mechanism of adsorption are also studied as functions of initial angle and surface coverage. The mechanisms of adsorption and scattering, and the effect of the heterogeneity of the binding sites are examined. The mechanisms of energy transfer from adsorbed atom to the lattice are examined and discussed, and the rate of energy transfer to the lattice from a hydrogen atom in a highly excited vibrational mode is calculated.

We studied thermal diffusion of hydrogen on a Si(111) surface. The potential-energy surface used in the study is the one used in the H-atom scattering and

chemisorption study on partially covered Si(111) surfaces, and which describes two different binding sites. We have computed the classical jump frequencies of hydrogen on a partially H-covered Si(111) surface using Monte Carlo Variational Phase-Space Theory (MCVPST) methods. Jump frequencies are calculated for adsorbate hops from two different binding sites. A lower bound and an estimated upper bound for the classical diffusion coefficient was calculated using a method developed by NoorBatcha *et al.* (64) We also used a Monte Carlo method to extract the minimum-energy reaction path in this system.

Additionally, we report a method to obtain an approximate rate of tunneling using Metropolis Monte Carlo methods with the WKB approximation. We calculated a rate of diffusion due to tunneling of a hydrogen atom on this surface at T=300 K. We describe a method to obtain tunneling rates at higher temperatures using the calculated tunneling probabilities at T=300 K. Using these data, we calculated a lower bound and estimated upper bound for the diffusion coefficient with the tunneling correction.

CHAPTER II

POTENTIAL-ENERGY SURFACES

In all calculations, we assume the potential energy for the Si(111)-Hydrogen systems can be written in the separable form:

$$V_{Total} = V_l + V_g + V_{gs} \tag{1}$$

where V_l is the interaction between the lattice atoms in the Si(111) crystal, V_g is the potential between gaseous adatoms, and V_{gs} is the adatom-lattice interaction potential.

Lattice Interaction Potential

For all calculations, we have used Keating's formulation (65) as modified by Weber (66) to describe the potential energy for the silicon crystal. Weber's form of the Keating potential is given by

$$V_l = \sum_{ij} \frac{f_a(r_{ij}^2 - R_{ij}^2)^2}{2R_{ij}^2} - \sum_{ijk} \frac{f_b(r_{ij}\cdot r_{ik} - R_{ij}\cdot R_{ik})^2}{8R_{ij}\cdot R_{ik}} \tag{2}$$

where f_a and f_b are bond stretching and bond bending force constants, respectively. R_{ij} is the equilibrium vector between lattice atoms i and j, and r_{ij} is the instantaneous vector between these atoms. The first

summation in Eq. 2 corresponds to bond-stretching interactions between nearest neighbors and the second summation corresponds to the bond bending interactions between the second nearest neighbors. We found it necessary to use a potential with second nearest neighbor terms for the following reason: Due to the tetrahedral arrangement of the silicon atoms for the geometry corresponding to the (111) plane, there are no silicon atoms directly below the atoms in the top layer in either the second, third, or fourth layers. Consequently, the formulation of nearest-neighbor pairwise interactions alone will result in a lattice that exhibits an exceptionally large, aphysical freedom of motion in the direction of the surface normal. This problem is resolved by use of the Keating potential, which includes the second nearest neighbor bending interactions. This potential-energy function has been found to reproduce the experimental elasticity constants and distortion energy of silicon. Figure 1 is a power spectrum of the motion of a surface silicon atom and gives lattice phonon frequencies of 256, 262, 412, 419, and 436 cm^{-1} (resolution = 1.6 cm^{-1}).

Adatom-Lattice Atom and Adatom-Adatom Interaction Potential

In one of the earliest studies of hydrogen chemisorption on Si(111), Becker and Gobeli (9) used

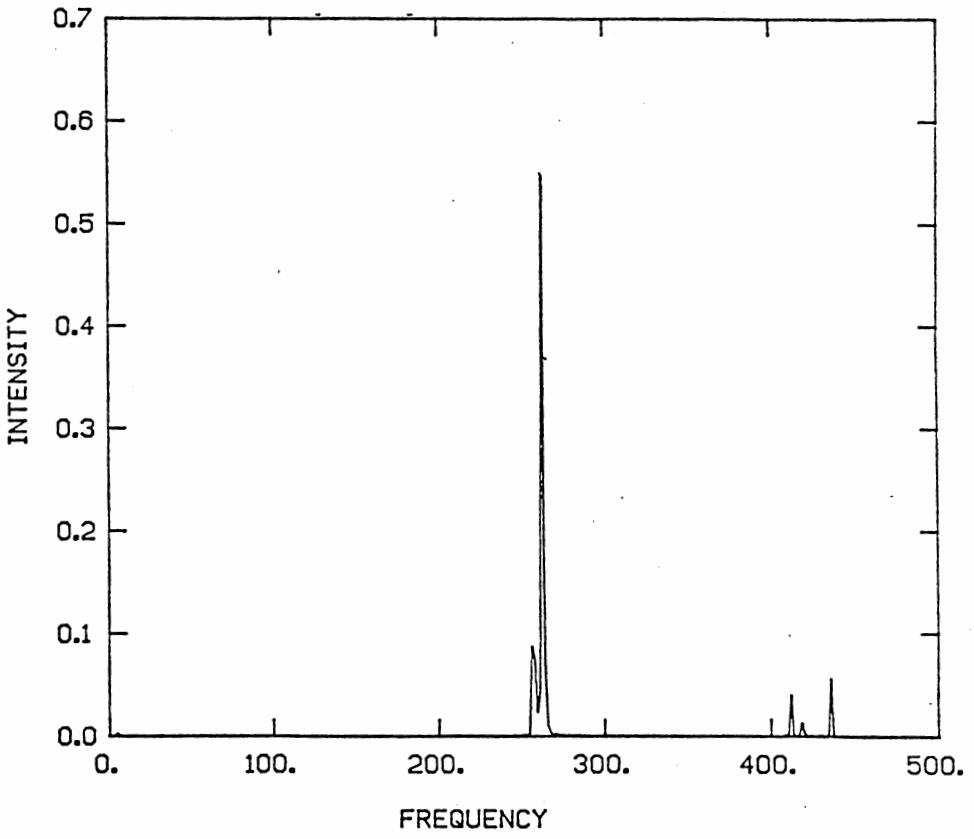

Figure 1. Power spectrum for motion of a silicon atom in the ideal Si(111) surface

infrared spectroscopy to investigate this process. This resulted in the direct observation of a broad absorption line centered at 2062 cm^{-1}, which was ascribed to the Si-H bond. After reaching maximum intensity, the absorption line was removed by sputtering the sample with argon ions. The total number of ions used to remove the adsorbed hydrogen was approximately the same as the number of surface atoms per cm^2. This observation, coupled with the fact that the experiments were done on the (111) face of a silicon crystal, led the authors to suggest that a single hydrogen atom is adsorbed on top of each silicon atom in the surface, saturating the dangling bond of the surface atom. Evidence of any other adsorption site was not observed. They suggest, due to the circumstantial evidence of saturation of the absorption peak, that monohydride coverage had occurred. Their observations did not agree with earlier experiments by Law (5,63) (discussed below), which suggested that more than one type of binding site exists on the surface.

Several other groups (1-29) have observed adsorption of hydrogen in the top site, by using a variety of experimental methods; these include low energy electron diffraction (LEED) (4,6,7,13,23,24), electron energy loss spectroscopy (ELS) (4,8,10,13,20,23,24), ultraviolet photoemission spectroscopy (UPS) (1,4,6,12,14,18,28,29), Auger electron spectroscopy (AES) (14,16,23,27), thermal desorption spectroscopy (TDS)

(7,16,19,24), infrared spectroscopy (IR) (9,15,21), and ion neutralization spectroscopy (INS) (6). Additionally, several detailed and realistic theoretical treatments of hydrogen chemisorbed on a Si(111) surface have been reported (30-49) which are in good agreement with experiments.

Froitzheim, Ibach and Lehwald (10) detected a localized surface vibration of atomic hydrogen chemisorbed on a cleaved clean Si(111) surface using high resolution electron energy loss spectroscopy (HREELS) and attributed it to the saturation of the silicon surface dangling bonds by hydrogen. Brzoska and Kleint (11) in their study of adsorption and desorption properties of hydrogen on silicon films, favor binding to the dangling bond site. Pandey (31) presents a realistic tight-binding model for chemisorption of hydrogen on silicon, which assumes that the local bond (chemisorption bond) at the surface is similar to the corresponding bond in the molecule silane. The chemisorptive bond at the on-top site is clearly reflected in the calculated local density of states for the surface silicon atoms and is in good agreement with experiment (6).

Adsorption of atomic hydrogen on Si(111) (2 x 1) and (7 x 7) surfaces was studied by Ibach and Rowe (4) using ELS and UPS. Photoemission spectra of surfaces with adsorbed hydrogen were compared with spectra of clean surfaces. A clean surface has structure in the spectra

corresponding to "dangling bond" surface states (as opposed to surface states associated with back bonds). After hydrogen adsorption, the "dangling bond" surface state structure has completely disappeared, and a new broad peak is observed in the photoemission spectrum. Additionally, electron energy loss spectra of both clean and hydrogen-covered surfaces were examined. Transitions from surface states apparent in the spectrum of the clean surface disappear upon exposure of the surface to hydrogen. These show that the adsorbed atomic hydrogen remove the "dangling bond" surface states, and the new peak appearing in the spectra is attributed to the Si-H bond, assumed to be bonded by the "dangling bond" surface state. On both surfaces, a dangling bond surface state at approximately the same energy is found.

Appelbaum and Hamann (32) report results of a detailed and realistic theoretical treatment of a chemisorbed monolayer of hydrogen on an ideal Si(111) (1 x 1) surface. A plot of the calculated local density of states on the chemisorbed hydrogen atoms shows a structure with two distinct peaks. This is in contrast to the findings of Ibach and Rowe (4), who had observed one broad peak in the UPS spectrum rather than the two sharp peaks predicted by Appelbaum and Hamann. This calculation is limited to the monohydride phase only.

Sakurai and Hagstrum (6) used INS to resolve the differences between theory and experiment. They found

that both INS and UPS show two peaks in agreement with the theoretical calculations of Appelbaum and Hamann (32), but contrary to observations of Ibach and Rowe (4). These authors suggest that in the earlier work of Ibach and Rowe (4), the hydrogen coverage of the Si(111) surface was less than one-half monolayer, giving rise to the discrepancy. Additionally, they measured the change in work function with hydrogen exposure. The observed behavior suggests that atomic hydrogen can occupy more than one adsorption site on the Si(111) surface, as predicted by Law (5) and discussed below.

UPS measurements and theoretical model calculations on the electron density of states were reported for partial monolayers of hydrogen on Si(111) by Appelbaum, Hagstrum, Hamann and Sakurai (29). Clean, well-annealed Si(111) surfaces were exposed to hydrogen at both room temperature and 423 K. Two peaks are observed in the UPS spectra, corresponding with the detailed theoretical calculation for hydrogen chemisorbed on Si(111) as an ordered monolayer. However, at fractional coverage significant differences develop between the room temperature and the 423 K sequences in that the room temperature sequence never develops one of the peaks unless further hydrogen exposure is allowed. Upon further hydrogen exposure, the peak begins to develop and is fully formed upon saturation of the surface. This is interpreted in terms of the mobility of

the hydrogen atoms. At the higher temperature, the hydrogen atoms are mobile and tend to cluster into islands whose spectrum resembles that of the saturated monolayer. At room temperature, however, the hydrogen atoms are not particularly mobile on the silicon surface so that they chemisorb in a disordered homogeneous monolayer at low coverage. Thus, for room temperature sequences at low coverage, the isolated Si-H bond spectrum is observed, whereas upon saturation the ordered monolayer spectrum has developed. Intermediate coverages should show a broad spectrum suggesting a strongly disordered hydrogen overlayer.

Hermann and Bagus (33) examined chemisorptive hydrogen-silicon interactions in *ab initio* cluster model calculations using three different clusters. The smallest cluster was the diatom SiH, the next larger was the cluster $(SiH_3)H$ and the largest cluster was $(Si_4H_9)H$. The calculation was done assuming that atomic hydrogen stabilizes on the Si(111) surface directly above a silicon atom of the first layer. The calculated results for the largest clusters agree with the calculated values of (32) and with the experimental measurements of (10). Differences in results between the diatom and the larger clusters indicate that the nearest neighbor environment of the silicon surface atom is important for the adsorbate-substrate interaction. While acknowledging a study on a larger cluster including several adsorbate

atoms is needed to account for the direct and indirect adsorbate-adsorbate interactions, they believe the present investigation shows the hydrogen adsorption process on the Si(111) dangling bond site is governed by a strongly localized adsorbate-substrate interaction.

Schulze and Henzler (7) performed extensive experiments on hydrogen adsorption onto Si(111) surfaces using LEED and thermal desorption techniques in an attempt to provide quantitative structural, binding, and electronic information for hydrogen on clean cleaved Si(111). At small coverages ($\theta < 0.3$), a state defined as Beta 1 is observed in desorption spectra. By evaluating the area below the desorption peak, coverage in the binding state is obtained. State Beta 1 is saturated at exactly the density of the silicon surface atoms. Therefore, the authors interpret this state as associated with the adsorption site for the dangling bond of each silicon surface atom.

Ho, Cohen and Schluter (34) report self-consistent quantum mechanical calculations for a monohydride structural model of hydrogen adsorption on a Si(111) surface. It was found that the adsorbed hydrogen presents a relatively localized surface disturbance affecting mainly the surface dangling bonds and only weakly affecting the silicon backbonds. It is also found that the Si-H bond potential is about 50% stronger than the Si-Si bond potential. Calculated local

density of states for hydrogen chemisorption forming the monohydride phase produces two main structures in the spectrum, in agreement with (32). They interpret these peaks to correspond to hydrogen orbitals of mostly *s*-like character coupling to Si *s*-like orbitals and Si *p*-like orbitals.

Photoelectron spectra of hydrogen adsorption on Si(111) is presented by Rowe (12). Three UPS peaks are observed and attributed to the chemisorbed hydrogen on surface dangling bonds. Appearance of the peaks is interpreted as arising from hydrogen-induced surface states.

Binding energies, Si-H bond lengths, vibrational energies, and force constants for the monolayer adsorption have been calculated. Appelbaum and Hamann (32) calculated a bond length of the Si-H bond to be 2.73 a.u. and the Si-H bond force constant to be 4.762 $eV/a.u.^2$. Froitzheim *et al.* (10) found the energy of the Si-H vibration to be 2073 cm^{-1}, comparable to the 2062 cm^{-1} found in the infrared absorption spectrum of Becker and Gobeli (9). However, the signal observed in this experiment did not have the broadened structure as in the Becker and Gobeli experiment. The Froitzheim group attributed the broadness of the infrared signal to the contribution of different surface vibrations for hydrogen adsorbed on different sites. From the observations, this group calculated a bond force constant of 4.3 $eV/a.u.^2$.

Kobayashi, Edamoto, Onchi, and Nishijima (13) estimate a force constant for this bond at 4.245 eV/a.u.^{2} In their *ab initio* cluster calculation, Hermann and Bagus (33) calculate a binding energy of 3.29 and 3.02 eV for the clusters $(SiH_3)H$ and $(Si_4H_9)H$, respectively. They also calculated a vibrational energy of approximately 2274 cm^{-1} for hydrogen vibrations perpendicular to the surface. The calculated equilibrium bond distance is 2.8 a.u. Schulze and Henzler (7) calculate a binding energy of 3.5 eV for this site. The self-consistent quantum-mechanical calculations of Ho *et al.* (34) give 2.93 a.u. as the equilibrium Si-H bond distance, and a force constant of 6.803 eV/a.u.^{2}. Brzoska and Kleint (11) measured the binding energy of this site as 3.19 eV. The relevant information regarding hydrogen binding in the top site is summarized in Table I, Appendix.

In addition to the top binding site, there is evidence that other types of binding states exist on this surface.

By measuring surface electrical changes caused by the adsorption of hydrogen on silicon, Law (5) proposed a model for adsorption which involves two adsorption sites, both of which are accompanied by electron transfer in such a way as to produce protons. The model was constructed according to observed changes in the work function upon hydrogenation. The two proposed adsorption

sites for hydrogen atoms are alpha sites, located on top of the surface silicon atoms, and deep-lying beta sites, located below the surface silicon atoms. A proton adsorbed in the alpha site would explain the observed decrease in the work function, while a proton adsorbed in the beta site explains the increase in the work function at higher hydrogen exposures. The model supports the interpretation that the adsorption process involves filling of the alpha sites at low hydrogen exposures and subsequent adsorption in the beta sites at higher hydrogen coverage.

Seel and Bagus (35) used *ab initio* Hartree-Fock LCAO calculations to study the interaction of a hydrogen atom with a Si(111) surface at the surface open site, located directly over the fourth-layer silicon atom. This study complements the *ab initio* study (33) for hydrogen adsorbed at the head-on site directly over a silicon surface atom. A cluster of ten silicon atoms represented the first four layers of the silicon crystal. A hydrogen atom was added at the central symmetry position in the open site. The calculation of the interaction potential curve as a function of the hydrogen atom distance normal to the open site shows two corresponding binding sites. At 1.4 Å above the surface, there is a well with a depth of 1 eV, and a second well of 0.3 eV is located at 1.2 Å below the surface. This suggests that atomic hydrogen can stabilize above and

below the open threefold site. Barrier height for penetration of the surface is 1.8 eV. From the binding curves, this group calculated parameters for the hydrogen vibrations perpendicular to the surface. They calculate a vibrational energy in this threefold site of approximately 823 and 1044 cm^{-1} for the outer and inner wells, respectively, and force constants of 0.696 and 1.121 $eV/a.u.^2$ for the outer and inner wells, respectively. They caution that this calculation has extreme limitations and is not of high quantitative accuracy. They suggest that hydrogen adsorption in this site aids the formation of the SiH_3 surface species as discussed in Chapter I.

The interactions which occur between electron beams and various adsorbates, including molecular hydrogen, on silicon surfaces have been investigated by Joyce and Neave (16) using AES, TDS and mass spectroscopy. It was found that hydrogen is adsorbed into three energetically distinct binding sites. They do not, however, discuss the nature of these binding sites.

In a theoretical study of the bonding of atomic hydrogen to Si(100), Appelbaum, Hamann and Tasso (36) propose a strong but unconventional covalent bond between a hydrogen atom and a silicon atom in the second layer whose conventional tetatrahedral bonds are already saturated. They admit that the detailed results pertain to one particular surface geometry, but suggest parallel

results for any relaxed or reconstructed silicon surface with approximately tetrahedrally coordinated subsurface silicon open to the vacuum. They performed self-consistent calculations which show that atomic hydrogen is capable of forming a strong chemical bond to subsurface (second layer) silicon atoms in spite of the completely saturated chemical environment of these atoms. The chemisorptive bond is not activated, and is thought to have a bonding energy of approximately one eV less than to surface silicon atoms. The bonds are not attributed to weakly bound hydrogen complexes formed on the surface, but rather are precursor states responsible for corrosive modification of silicon surfaces in the formation of the trihydride phase.

As in the study by Law (5), Schulze and Henzler (7) found a second, and possibly a third, binding site in addition to the obvious one attributed to the silicon surface dangling bond. Increasing the hydrogen exposure above $\theta > 0.3$ causes a new peak in the desorption spectrum to evolve, and is attributed to the surface state defined as Beta 2. The Beta 2 state may be resolved into two peaks, but since they are close together, they are treated as a single peak. In evaluating the area below the desorption peak, it is found that additional hydrogen is bound in the Beta 2 state with a steep increase vs. hydrogen exposure up to a maximum coverage in the range 0.4 to 0.6. Only at higher

coverages of hydrogen on the surface will state Beta 2 be filled to a measurable extent. The state Beta 2 is described as a binding site with a lower binding energy than that of state Beta 1 discussed above, and which may be filled only if three neighboring sites of state Beta 1 are already filled with hydrogen atoms. Various models of adsorption in the Beta 2 state proposed are: (a) Hydrogen may be adsorbed on top of the surface as single atoms located directly above either 2nd or 4th layer silicon atoms and within triangles of three hydrogen atoms bound in the surrounding top sites; (b) the hydrogen atoms may be adsorbed in hollow (interstitial) sites between the 2nd and 3rd layer silicon atoms; or, (3) a model described by Wagner *et al.* (8) where SiH_2 complexes reside on the surface. For all three models, the adsorption in Beta 2 requires pre-adsorption in site Beta 1. The evaluation of the binding energy of state Beta 2 is estimated as 1.9 eV, although it is difficult to determine due to the overlapping with a possible state Beta 3.

A futher study done by Klimesch, Meyer and Henzler (19) on the adsorption and desorption of hydrogen on the clean Si(111) surface using TDS, AES, and measurements of workfunction, surface conductivity and field effect mobilities confirms occupation of the Beta 2 state. They conclude that at small coverages, hydrogen randomly adsorbs in the Beta 1 state, causing the

workfunction decrease as shown by Law (5). Annealing to 700 K leads to an increase in workfunction, but no hydrogen desorbs from the Beta 1 state. Higher mobility observed at elevated temperatures may enable surface diffusion to occur, allowing formation of islands of ordered hydrogen atoms to take place. When the coverage increases, the initially unordered hydrogen layer becomes ordered because the empty states are filled up, leading to an increase in workfunction, as during heating. The final decrease in workfunction at coverages higher than one monolayer is correlated with the occupation of the Beta 2 state.

In studying diffusion effects on thermal desorption spectra, Verwoerd (38) presents a model of hydrogen adsorption on the Si(111) surface which explains several features of the experimental results of Schulze and Henzler (7). A preliminary quantum chemical cluster calculation suggests that the adsorption site associated with the secondary peak (state Beta 2) may not be on top of the crystal but instead at an interstitial position between the 2nd and 3rd crystal layers, open to the surface along a line through the 4th layer silicon atom. Additionally, he suggests that the hydrogen, once adsorbed to this site, may diffuse into the crystal rather than escape on heating, which could explain the lack of observation of this peak at low coverages. He suggests two adsorption sites in the open site of the

silicon crystal: One described as above the 4th layer atom (type A) between the 2nd and 3rd crystal layers, and a second site (type B) located directly below a 1st layer atom, and between the 2nd and 3rd crystal layers. The following model of the secondary peak adsorption of hydrogen on Si(111) is proposed. When a hydrogen atom approaches a surface on which the dangling bonds are already saturated, it experience a repulsive force. If its speed and line of approach is appropriate, it can penetrate this barrier and reach the subsurface interstitial site (Site A). This is a physical trap by the cage of silicon atoms that surround it. With continued exposure to atomic hydrogen, all of the sites eventually become filled, and in the meantime, deeper interstitial sites (Site B) become filled. This explains the experimental results of Schulze and Henzler (7) which show that occupancy of the interstitial sites will not occur unless the primary sites are filled, due to the fact that as a hydrogen atom approaches this interstitial site, it will be deflected to a bond-saturating site unless all three binding sites surrounding the interstitial site are filled.

Using the available data, we have developed a potential-energy surface which describes two types of binding sites for hydrogen on a Si(111) surface. This potential-energy surface was used in the studies of scattering and chemisorption of atomic hydrogen on a

Si(111) with various degrees of hydrogen coverage and in the Monte Carlo variational phase-space theory calculation of hydrogen atom diffusion on a Si(111) surface.

The two binding sites described by this surface are defined as the top site, located directly above each surface silicon atom, and the open site, located in the threefold interstitial site on the surface. Due to the lack of knowledge of the detailed nature of the forces, several aspects of this potential are arbitrary. We have based the potential to the extent possible on experimental and theoretical information, particularly with regard to the binding sites. We have developed a reasonably accurate description of the adsorbate-substrate interactions for the two binding sites and the migration barrier between them. Because of lack of knowledge, the adsorbate-adsorbate interaction as well as some of the other features of the hypersurface may not be as accurately represented. Since the adsorbate-substrate attractions are very strong for the top and open site (on the order of 3 eV and 1 eV, respectively), accurate modelling of the other features should not be required for the surface to yield meaningful dynamical results.

The interaction potential describing the two binding sites on the Si(111) surface has the following functional form:

$$V_{gs} = \sum_{j=1}^{N} \sum_{i=1}^{19} \begin{cases} V_{T_{ji}} + V_{O_{ji}} + V_{2_{ji}}; & r_{ji(xy)} \leq 8 \text{ a.u.} \\ 0.0; & r_{ji(xy)} > 8 \text{ a.u.} \end{cases} \qquad (3)$$

Because of the complex nature of the potential and the large number of equations of motion which were integrated in the trajectory study, we used a cutoff of the gas-surface interaction potential when a hydrogen atom was more than 8.0 a.u. away from a surface silicon atom in the surface plane direction. This cutoff did not include distance in the surface normal direction. The value of the cutoff was chosen to minimize effects of discontinuities. The attenuation functions described below cause the binding terms of the gas-surface interaction potential to approach zero when the hydrogen is a distance of approximately 7.5 a.u. away from a surface silicon atom in the surface plane direction. The effects of this discontinuity in our calculations were minimal.

Throughout Eqs. 3-17, the index variable j denotes a hydrogen atom, index variable i denotes a first-layer silicon atom, and index variable l denotes one of three nearest-neighbor second-layer silicon atoms for a given first-layer silicon atom i. Our model used a Cartesian coordinate system, with the x-y plane in the plane of the surface, and the z axis in the direction normal to the surface.

The functional form of the potential describing the top binding site is:

$$V_{T_{ji}} = \left[V_{Top_{ji}} + \sum_{l=1}^{3} V_{Bend_l} \right] S_{Top} \, S'_{Top} \qquad (4)$$

$V_{Top_{ji}}$ is the top site bonding function of the surface silicon atoms and the hydrogen atoms. It is a function of the z-component only of the surface silicon atoms and the hydrogen atoms, and its form is:

$$V_{Top_{ji}} = D\{1-\exp(-\alpha[r_{z_{ji}}-z_e])\}^2 - D \tag{5}$$

where

$$r_{z_{ji}} = [(z_j-z_i)^2]^{1/2} \tag{6}$$

V_{Bend_1} is the top site bending potential with a functional form of:

$$V_{Bend_1} = [0.5k_\theta(\theta_{jil}-\theta_{eq})^2]\exp[-\beta(r_{ji}-r_e)^2] \tag{7}$$

where θ_{jil} is the Si-Si-H angle and r_{ji} is the interatomic distance between hydrogen atom j and first-layer silicon atom i.

Two switching functions are used with the top site binding and bending potentials. S_{Top} attenuates the top binding site interaction potential as a hydrogen moves away from the site in the surface plane direction. Accordingly, it is a function of the surface plane direction (x-ȳ in our model) and its form is:

$$S_{Top} = 1-\mathrm{Tanh}^4(A_{Top}r^2_{xy_{ji}}) \tag{8}$$

where

$$r_{xy_{ji}} = [(x_j-x_i)^2+(y_j-y_i)^2]^{1/2} \tag{9}$$

S'_{Top} attenuates the top binding site completely if that site is already occupied by a hydrogen atom. Its form is:

$$S'_{Top} = \frac{\prod_{k=1}^{M}\mathrm{Tanh}[\rho(r_{ki}-r_e)^2]}{\mathrm{Tanh}[\rho(r_{ji}-r_e)^2]} \tag{10}$$

where r_{ki} is the interatomic distance between hydrogen atom k and silicon atom i. M is the total number of hydrogen atoms in the system.

The parameters in Eqs. 4-10 were fitted to the available experimental data. Figure 2 is a potential curve for a hydrogen in the top binding site interacting with a surface silicon atom as a function of the distance in the surface normal direction.

$V_{2_{ji}}$ is a repulsive potential between one of three second-layer silicon atoms which are nearest neighbors to silicon atom i and hydrogen atom j. Its form is:

$$V_{2_{ji}} = \sum_{l=1}^{3} B_{H\text{-}Si}\, r_{jl}^{-9} \qquad (11)$$

where r_{jl} is the interatomic distance between hydrogen atom j and second-layer silicon atom l.

The open site interaction potential has the following form:

$$V_{O_{ji}} = 1/3\; V_{Open} S_{Open} \prod_{l=1}^{3} S_{Repul_l} \qquad (12)$$

Using the information given by Seel and Bagus (35,39) in their *ab initio* calculation of this site, we developed the following functional form for the bonding potential at the open site. This is also a function of the surface-normal component of the hydrogen atoms and the surface silicon atoms (z component in our model). It has the following form:

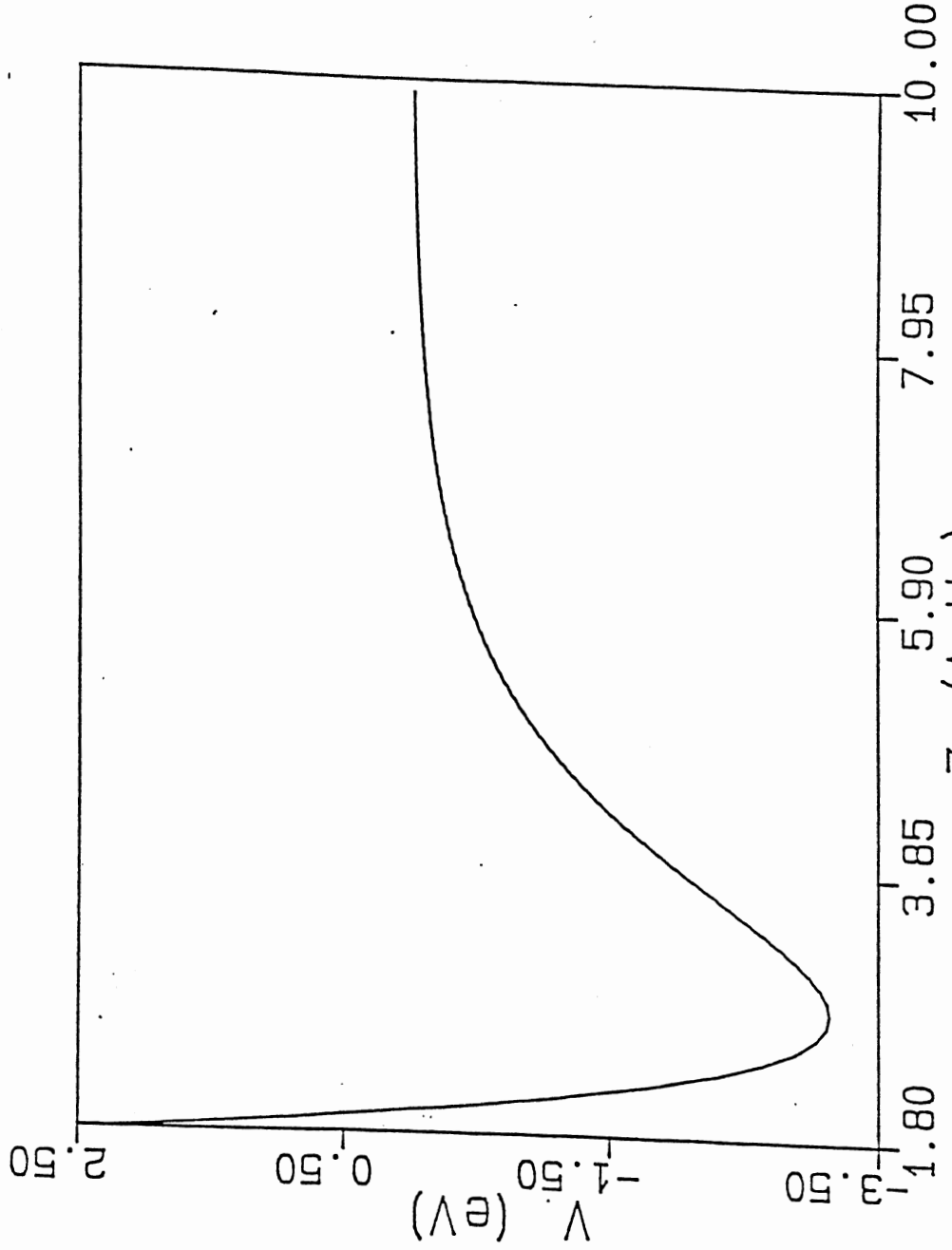

Figure 2. Top Site Si-H stretching potential

$$V_{Open} = \begin{cases} 0.5\, k_{in}\,(z_{ji}-ze_{in})^2 - D_{in}; & z_{ji} < -1.08 \text{ a.u.} \\ E_{pb} - k'_{in}\, z_{ji}^2; & -1.08 \leq z_{ji} \leq 0.00 \text{ a.u.} \\ E_{pb} - k_{out}\, z_{ji}^2; & 0.00 \leq z_{ji} \leq 1.45 \text{ a.u.} \\ D_0\{1-\exp[-\gamma(z_{ji}-ze_0)]\}^2 - D_0; & z_{ji} > 1.45 \text{ a.u.} \end{cases} \quad (13)$$

where

$$z_{ji} = z_j - z_i \quad (14)$$

Care was taken to ensure that the discontinuities in this function were minimal. However, the calculations reported in this thesis did not involve interaction in the energy regions of the discontinuities.

Switching functions were also used with this binding site. S_{Open} attenuates the open binding site potential as the hydrogen atom moves away from it in the surface-plane direction (x-y in our system). Its form is:

$$S_{Open} = 1-\text{Tanh}[A_{Open}(r^2_{xy_{ji}} - r^2_{e_{xy}})^2] \quad (15)$$

where $r_{xy_{ji}}$ is defined in Eq. (9).

Because the second-layer silicon atoms are located at the same distance in the surface plane from a first-layer silicon atom as the open site is, S_{Repul_1} attenuates the open site interaction as a hydrogen atom moves across the second-layer silicon atom. Its form is:

$$S_{Repul_1} = \text{Tanh}[C(r^2_{xy_{j1}})] \quad (16)$$

where

$$r_{xy_{j1}} = [(x_j-x_1)^2+(y_j-y_1)^2]^{1/2} \quad (17)$$

The parameters in Eqs. (12)-(17) were fitted to the information given by Seel and Bagus (35,39) and are given

in Table II, Appendix. Figure 3 shows potential curves for a hydrogen interacting with the open binding site as a function of the distance in the surface normal direction from the site. Figure 3(a) is the curve calculated by Seel and Bagus (35); Fig. 3(b) is the curve calculated using the potential function in this study. As is illustrated, there exist two binding states at this site, one located 2.646 a.u. above the surface (outer well) and the other located 2.268 a.u. below the surface (inner well). The penetration barrier at the surface plane is 1.6 eV, and the well depths for the outer and inner well are 1.01 and 0.3 eV, respectively.

Power spectrum analyses of Si-H motion when hydrogen is adsorbed in both the top and open sites yield the frequencies given in Table I, Appendix. Figure 4 is the power spectrum of the motion of a hydrogen atom adsorbed in the top binding site. The peak at 2115 cm^{-1} is assigned to the Si-H stretch, and the peak at 642 cm^{-1} is assigned to the Si-H bending vibration for hydrogen adsorbed in this site. Figure 5 is the power spectrum of the motion of a hydrogen atom adsorbed in the open binding site. The peak at 846 cm^{-1} is assigned to the hydrogen atom vibration perpendicular to the surface plane. The peak at 1027 cm^{-1} corresponds to vibration of the hydrogen atom in the surface plane. In both spectra, the lower frequencies correspond to the lattice phonon modes (see Fig. 1). Hydrogen occupying the inner well of

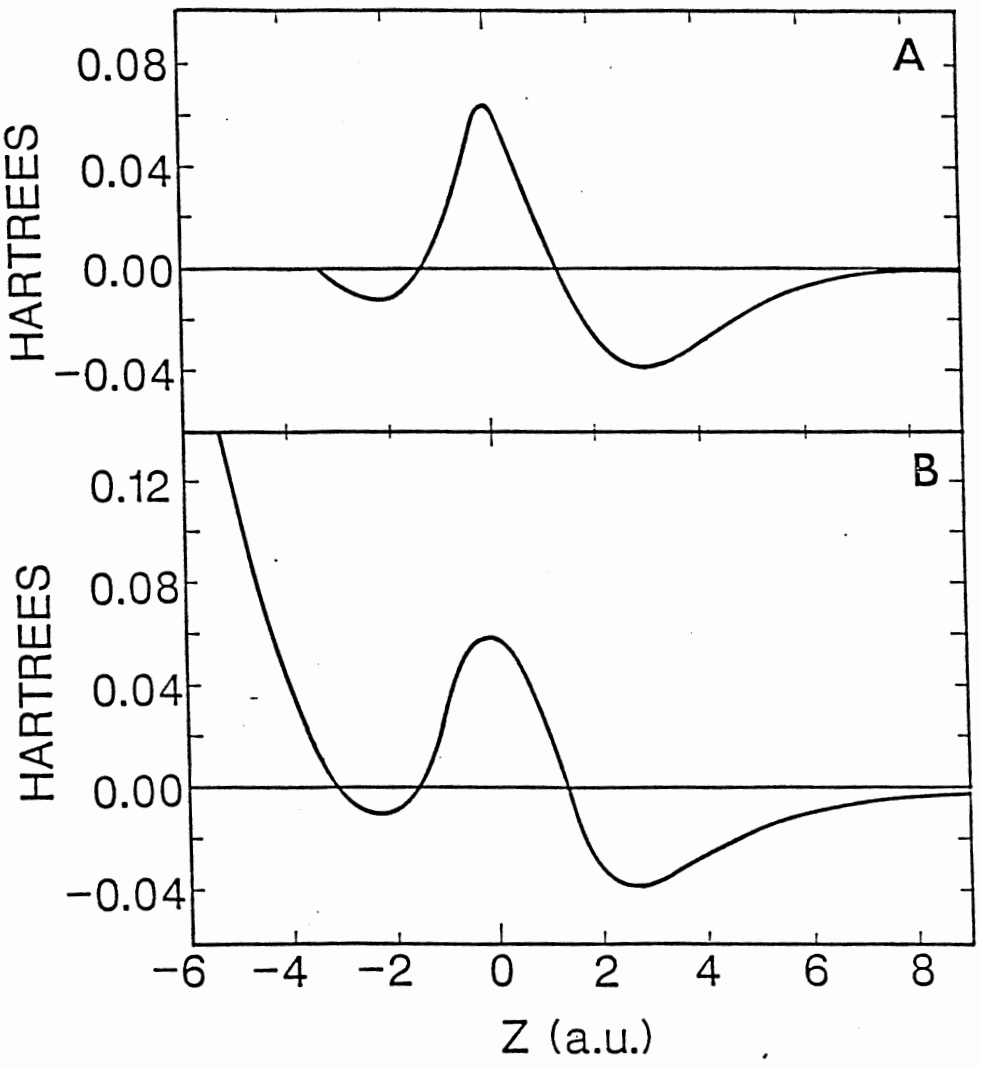

Figure 3. Potential energy curves for stretching motion perpendicular to the surface plane for a hydrogen atom in the open site. (a) Potential energy curve calculated by Seel and Bagus (Ref. 35); (b) Potential energy curve calculated from analytic function (Eq. 1)

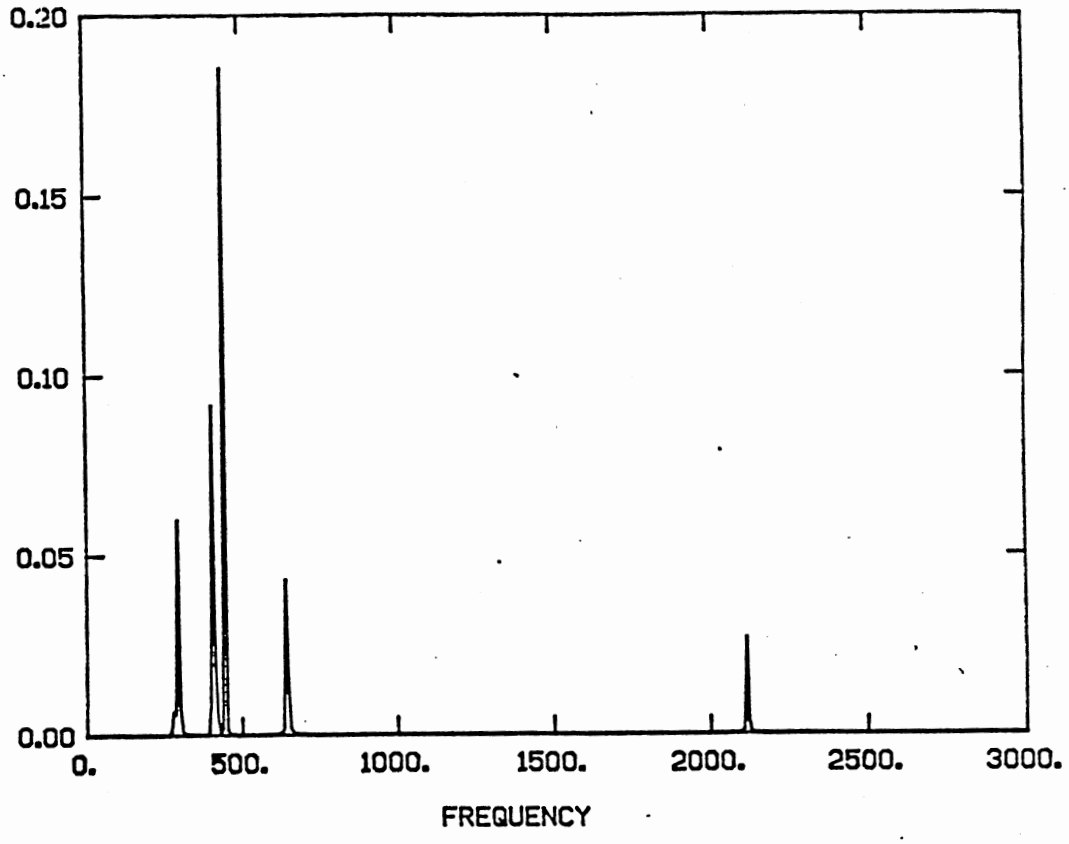

Figure 4. Power spectrum of motion of a hydrogen atom in the top binding site on a Si(111) surface. Frequencies are given in units of 1/cm.

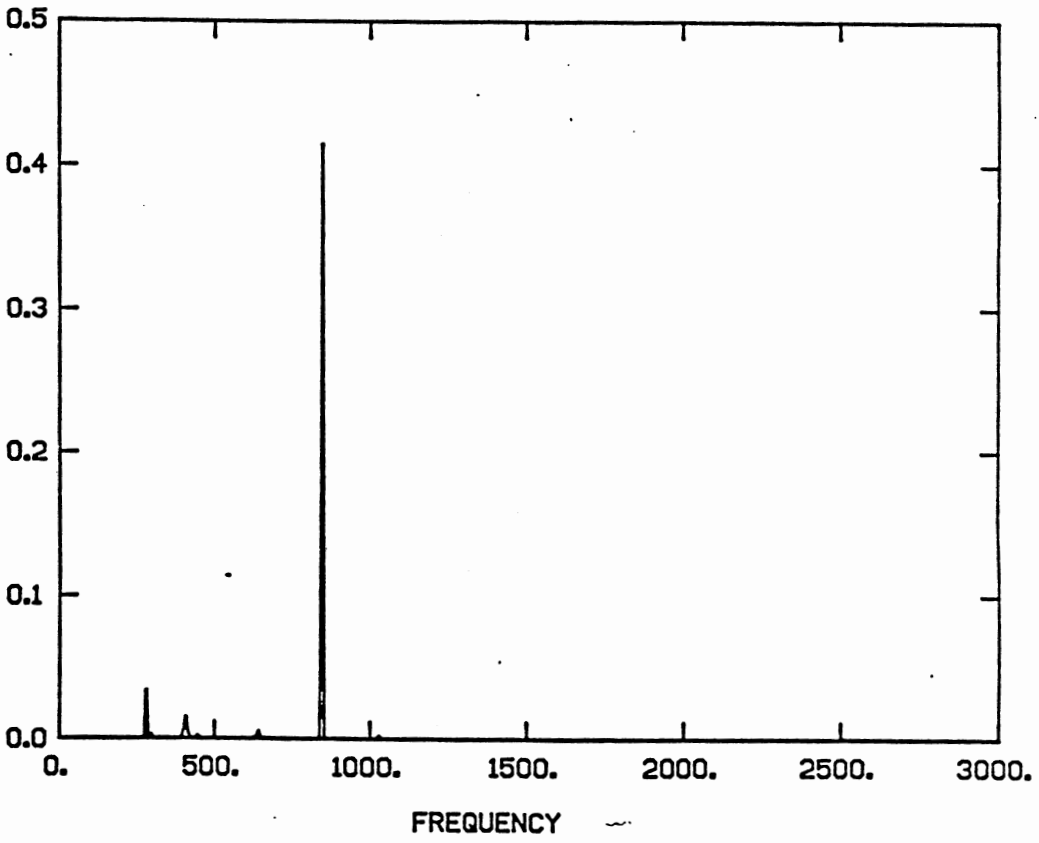

Figure 5. Power spectrum of motion of a hydrogen atom in the open binding site on a Si(111) surface. Frequencies are given in units of 1/cm.

the open site was not analyzed in this manner, because in the current study, we will not examine situations in which migration into the surface is energetically possible. As can be seen, the potential accurately reproduces the available experimental frequencies. Furthermore, the migration barrier from the open site directly to the top site is 0.65 eV. The migration barrier from the open site over a second-layer silicon atom to the top site is 1.0 eV. While there is no experimental or theoretical information available concerning the barriers to diffusion for hydrogen on this surface, we have used results for hydrogen atom diffusion in single crystal silicon reported by van Wieringen and Warmoltz (67) and by Ichimiya and Furuichi (68). van Wieringen and Warmoltz report an activation energy for diffusion of 0.48 eV for experiments carried out at temperatures between 1240 and 1480 K. (67) Ichimiya and Furuichi esimtate an activation energy for diffusion of 0.56 eV. (68) Using these data, we fitted the parameters of our function so that the migration barrier from the open site directly to the top site would roughly correspond to the reported activation energies. Figure 6 illustrates the potential experienced by a hydrogen atom as it is moved across the equilibrium Si(111) surface a distance of 2.79 a.u. above the surface plane. The surface has all but one top site occupied with a hydrogen atom. No open site is occupied. From left to right on

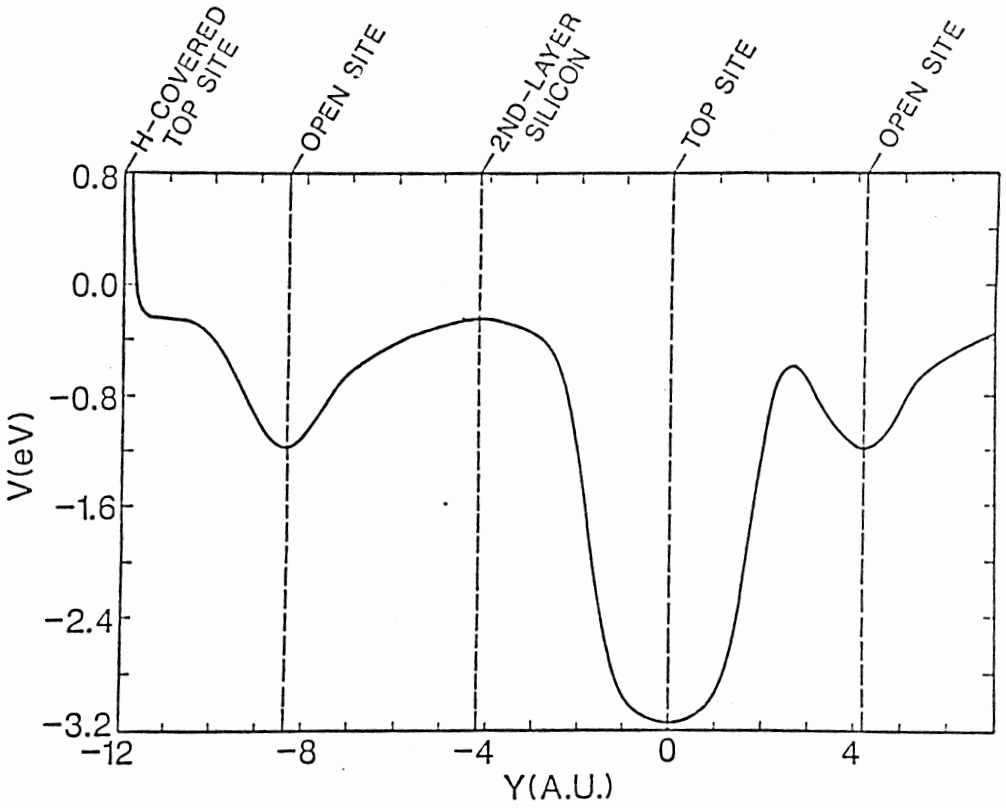

Figure 6. Potential energy experienced by a hydrogen atom as it is moved across a partially covered Si(111) surface. Its distance above the surface plane is 2.79 a.u.

Fig. 6, the hydrogen is moved across a top site occupied by a hydrogen atom, an open site, over a second-layer silicon atom, over an unoccupied top site, to another open site. Figs. 7-11 are projections of three-dimensional contour maps showing the potential experienced by a hydrogen as it is moved across a Si(111) surface with different coverages of hydrogen occupying top sites. The hydrogen is 2.79 a.u. above the surface plane. Figure 12 is a three-dimensional contour map of Fig. 9. This surface has three available top binding sites.

The interaction potential for the hydrogen-hydrogen interactions was assumed to be a repulsive potential, since no evidence indicates that weak attractions exist between hydrogen atoms bound on a Si(111) surface. Its functional form is:

$$V_g = \sum_{i=1}^{N} \sum_{j>i}^{M} A_{HH} r_{ij}^{-9} \qquad (18)$$

where r_{ij} is the interatomic distance between hydrogen atom i and hydrogen atom j. N is the total number of moving hydrogen atoms in the system and M is the total number of hydrogen atoms in the system. The parameters for this function are also given in Table II, Appendix.

The calculations for scattering and dissociative chemisorption of H_2 on Si(111) employed the potential developed by Raff *et al.* (48). It is described in detail in Ref. 48. Briefly, the adatom-lattice term is written as a pairwise sum of Morse potentials each multiplied by

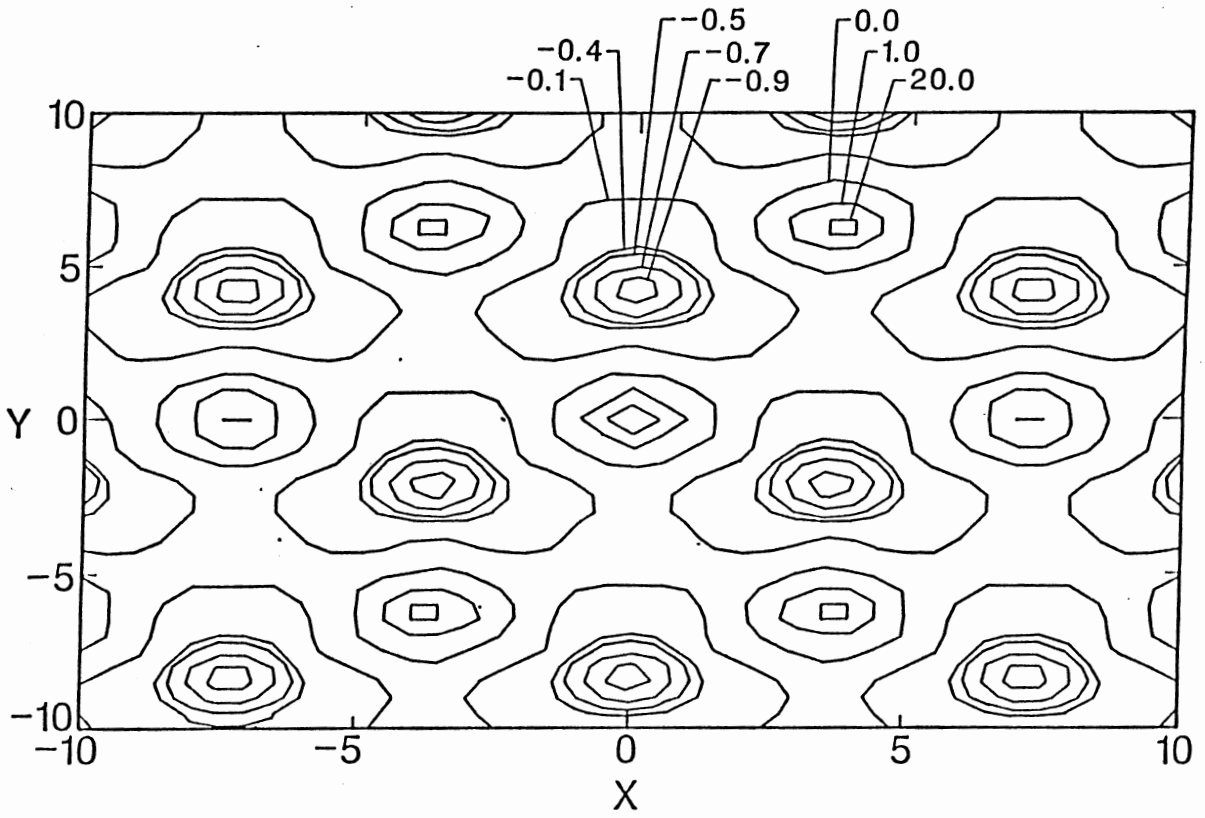

Figure 7. Potential-energy surface for the interaction of a hydrogen atom with a Si(111) surface which has every top site occupied by a hydrogen atom. Contour levels are given in eV relative to the hydrogen atom at infinity. The contours are shown for a cut parallel to and 2.79 a.u. above the Si(111) surface plane. Distances along axes are given in a.u.

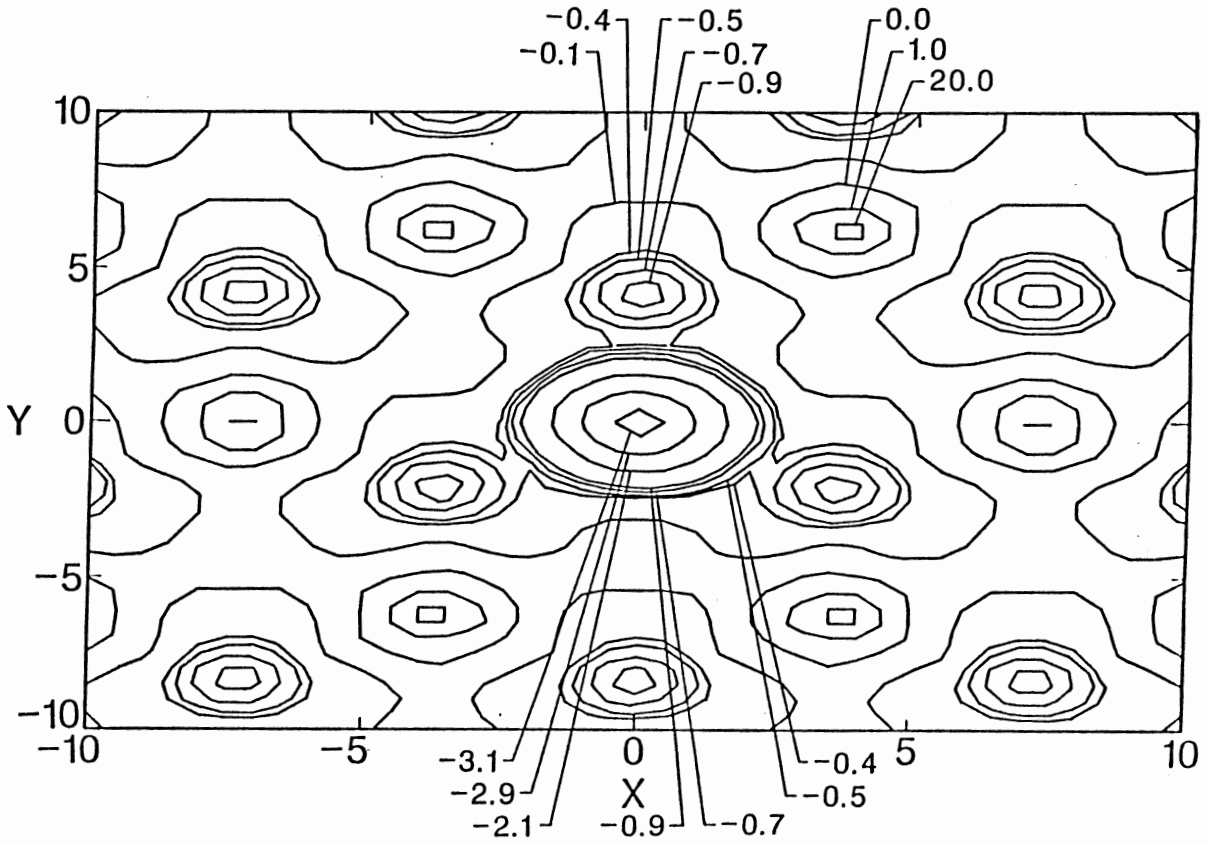

Figure 8. Same as Figure 7, except for a Si(111) surface with one available top binding site.

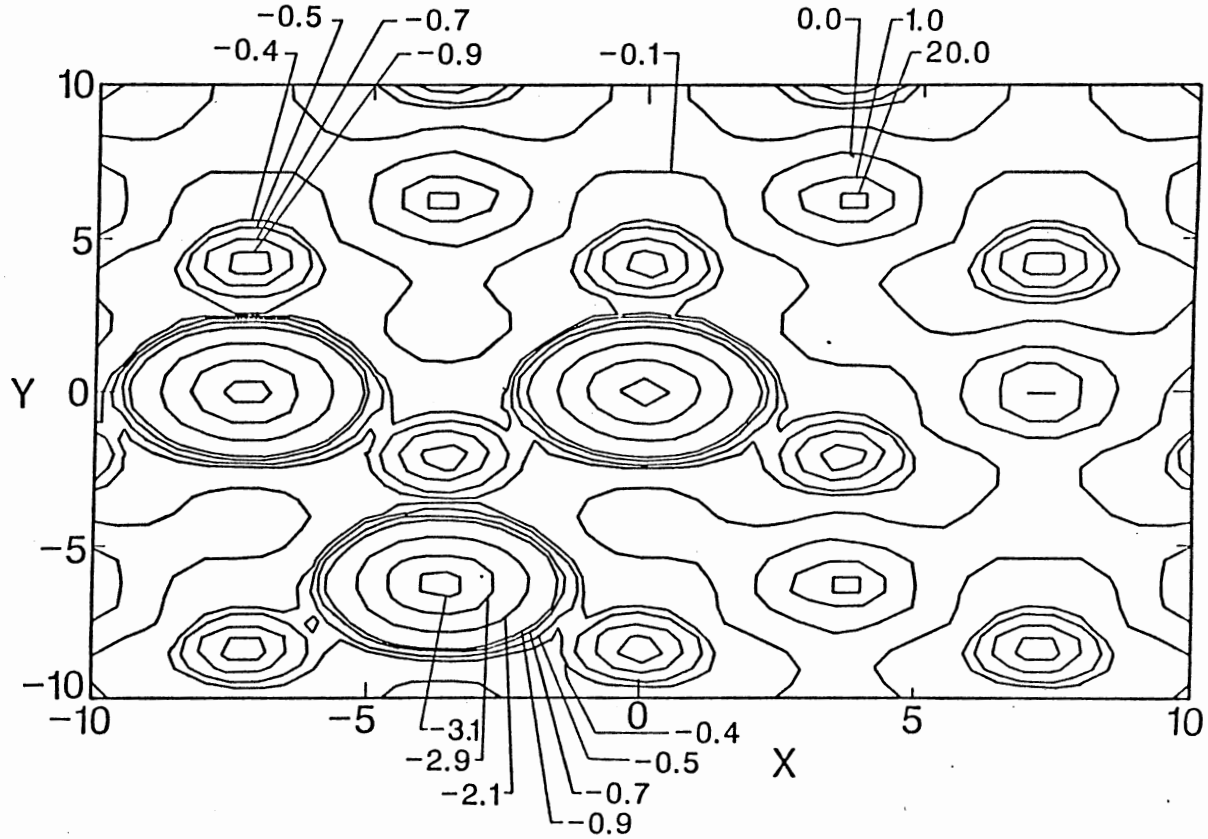

Figure 9. Same as Figure 7, except for a Si(111) surface with three available top binding sites.

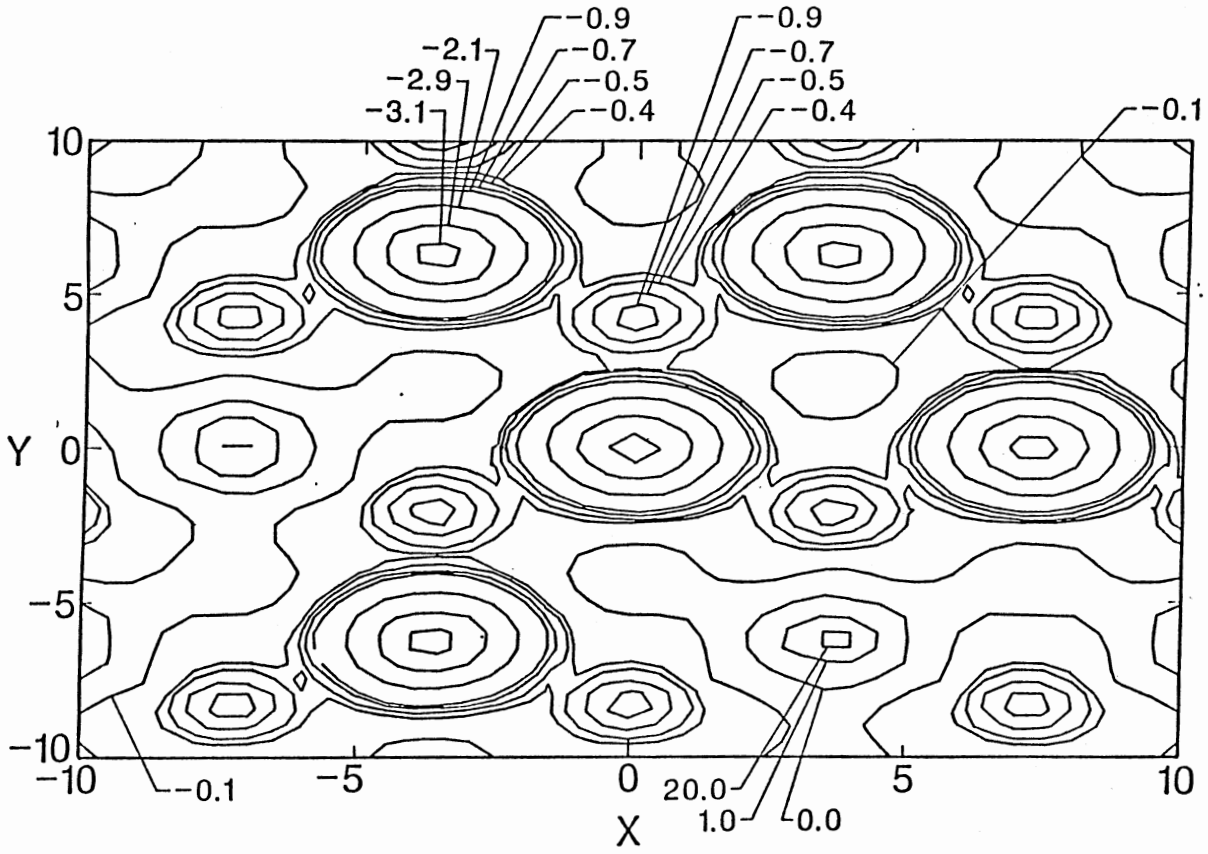

Figure 10. Same as Figure 7, except for a Si(111) surface with five available top binding sites.

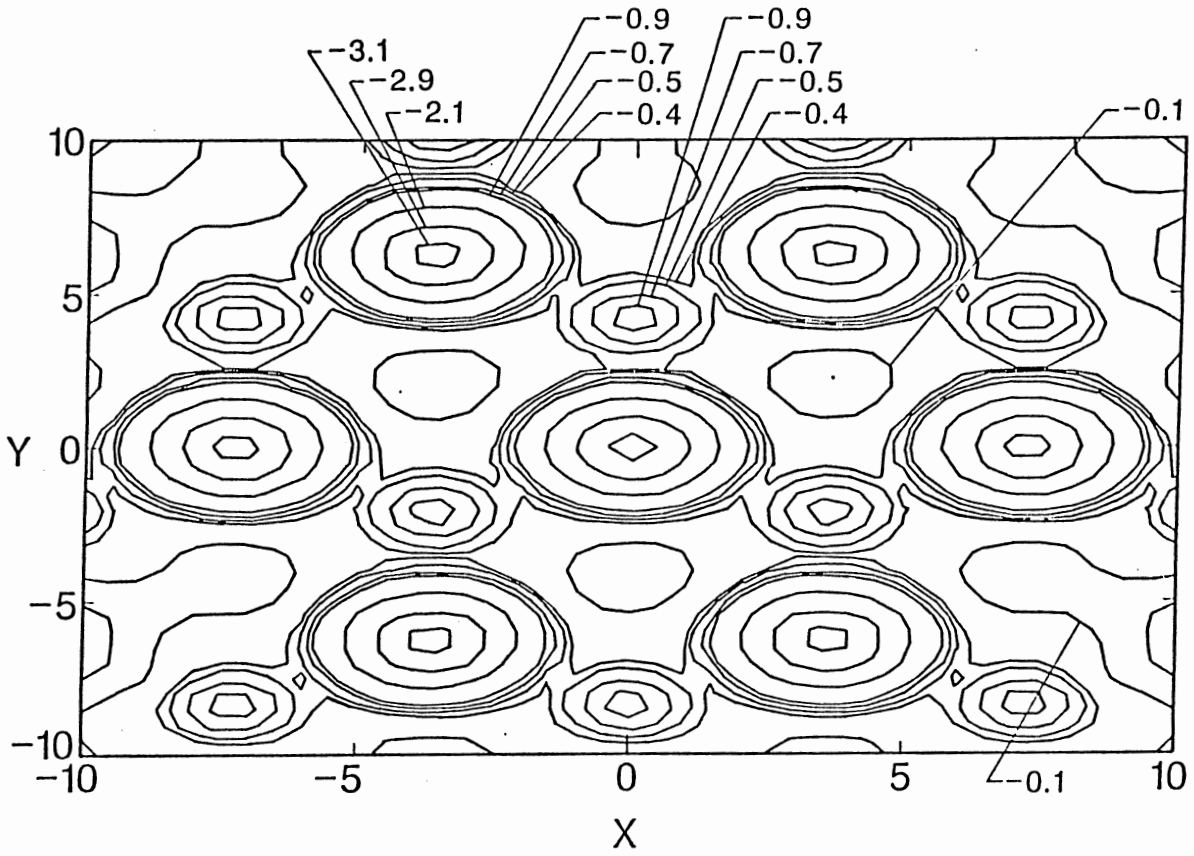

Figure 11. Same as Figure 7, except for a Si(111) surface with all top binding sites unoccupied.

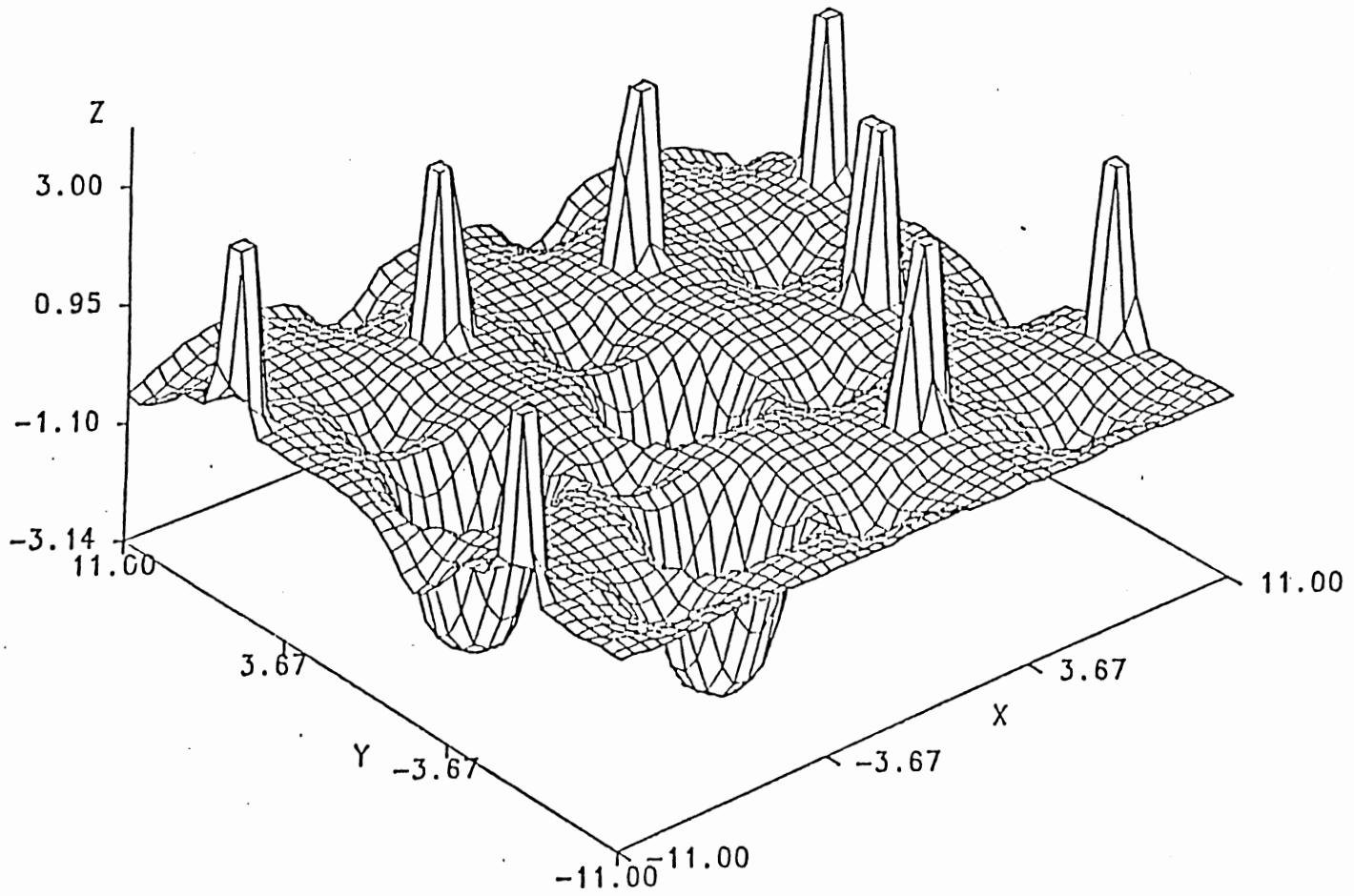

Figure 12. Three-dimensional contour plot of Figure 9. The large peaks designate where hydrogen atoms occupy top binding sites. The Z-axis has units of energy in eV. The X and Y axes are distances given in a.u.

a hyperbolic switching function that limits each adsorption site to one bond. The adatom-adatom interaction is the product of an H_2 Morse potential and a switching function that attenuates the H-H interaction as the Si-H bonds form. The parameters of the potential were adjusted to fit the results of hydrogen atom-silicon cluster calculations, the experimental and theoretical results for the H_2 insertion barrier into Si and SiH_2, and the measured $H_2(g)$ bond dissociation energy, fundamental frequency, and equilibrium bond distance. The potential surface predicts a 0.182 eV barrier to dissociative chemisorption.

CHAPTER III

MODELS AND METHODS OF CALCULATIONS

A chemical reaction on a surface is usually comprised of several elementary steps. These steps include adsorption on the surface, diffusion of adsorbates between binding sites, bond-breaking, insertion of atoms or molecular rearrangements, and desorption of product molecules. This thesis has focused on realistic simulation of some of these elementary processes: scattering and chemisorption of atomic and molecular hydrogen, and diffusion of hydrogen atoms on Si(111).

Dynamical information has been obtained for hydrogen interactions on Si(111) surfaces which were clean or partially covered with hydrogen using classical trajectory techniques or Monte Carlo methods. The studies have given sticking probabilities, scattering distributions, rates of diffusion, and rates of energy transfer, as well as providing insight into the behavior of hydrogen atoms adsorbed on a Si(111) surface with different degrees of hydrogen coverage. This chapter contains a discussion of the methods used in our calculations and the models of the systems studied.

Integration of classical trajectories was done in two of the calculations described in this thesis. The calculation of classical trajectories involves the numerical solution of Hamilton's equations of motion for an ensemble of particles in each system. The classical Hamiltonian is defined by:

$$H = \tfrac{1}{2} \sum P_i/m_i + V_{Total} \tag{19}$$

where m_i is the mass of particle i, and p_i are the momenta conjugate to the coordinates q_i. Hamilton's equations of motion are:

$$\dot{x}_i = \partial H/\partial p_{x_i} = p_{x_i}/m_i \tag{20}$$

$$\dot{y}_i = \partial H/\partial p_{y_i} = p_{y_i}/m_i \tag{21}$$

$$\dot{z}_i = \partial H/\partial p_{z_i} = p_{z_i}/m_i \tag{22}$$

$$\dot{p}_{x_i} = - \partial V/\partial x_i \tag{23}$$

$$\dot{p}_{y_i} = - \partial V/\partial y_i \tag{24}$$

$$\dot{p}_{z_i} = - \partial V/\partial z_i \tag{25}$$

for i = 1, 2, 3, . . . , N.

The position and momenta of each particle in the system at every time step in a trajectory is determined by solving the 6N-coupled first-order differential equations. For all trajectory calculations described in this thesis, a fourth-order Runge-Kutta method (69,70) was used to solve the equations of motion. Integration accuracy was checked by energy conservation and back integration.

Hydrogen Atom Scattering/Chemisorption on Partially/Fully Covered Si(111)

Model

The model used in this calculation consists of 73 lattice atoms, positioned in three layers. The first layer contains 19 atoms, and the second and third layers each contain 27 atoms. Seven of the first-layer atoms are allowed to move; the region which contains these atoms is termed the reaction zone. This is the area within the dashed line in Fig. 13. All other silicon atoms remain fixed during the initial condition sampling procedure and the trajectory integration. Each surface silicon atom has a binding site located directly above it in the surface normal direction. Each top binding site in the reaction zone is numbered as illustrated in Fig. 13. Effects on the dynamics due to hydrogen coverage on the surface are examined. The different coverages are:

a. No available top site (all top sites are occupied by a hydrogen atom;

b. One available top site (the central top site, 1, is unoccupied; all other top sites are occupied by hydrogen atoms);

c. Three available top sites (the central top site and two other sites are unoccupied. These sites are numbered 1, 2, and 3. All other top sites are occupied by hydrogen atoms);

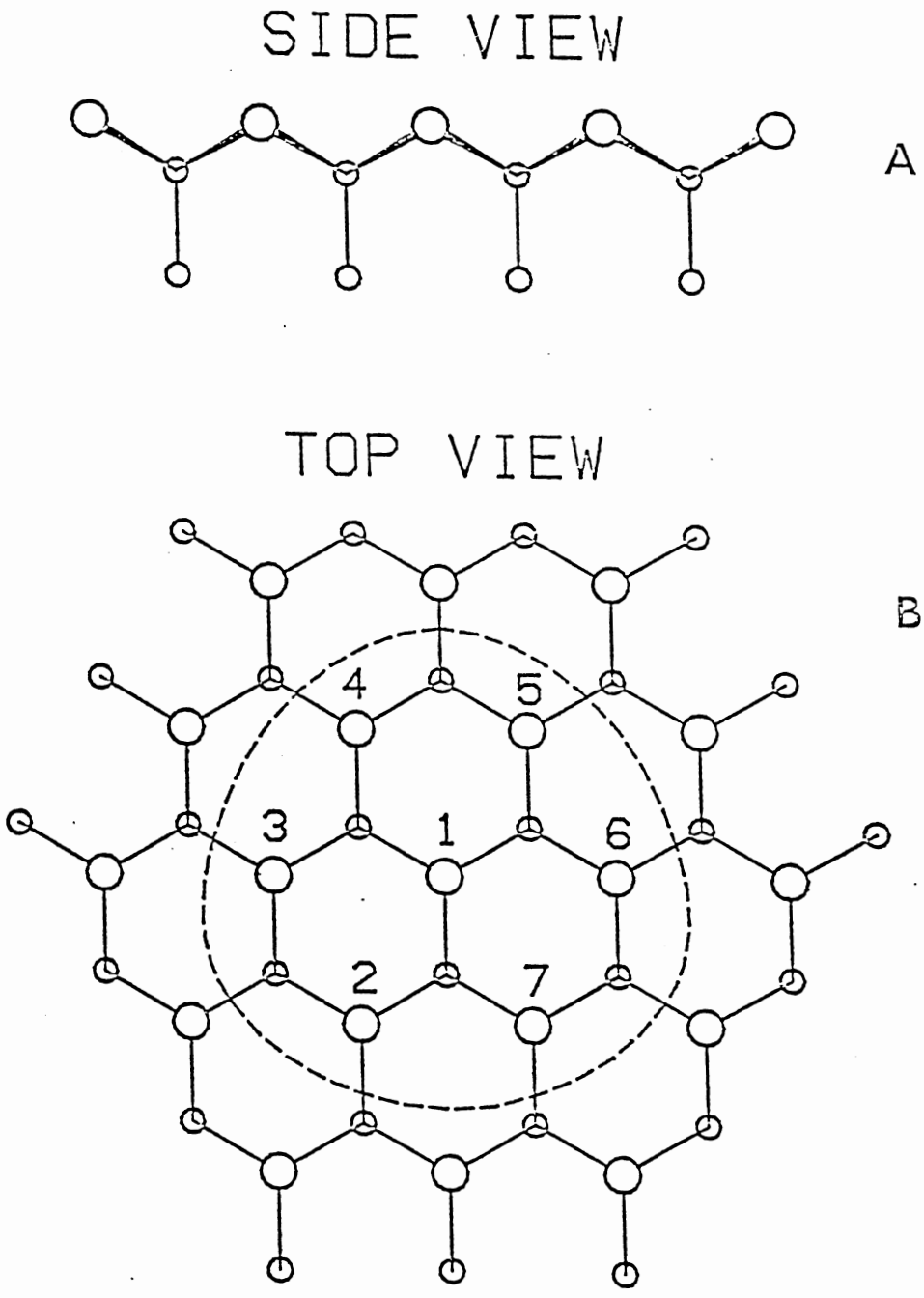

Figure 13. Structural models for the Si(111) (1 x 1) crystal lattice.

d. Five available top sites (the central top site and four other sites are unoccupied. These sites are numbered 1, 2, 4, 5, and 6. All other sites are occupied by hydrogen atoms); and

e. Seven available top sites (all top sites in the reaction zone are unoccupied).

In all calculations, the top binding sites for the silicon atoms outside the reaction zone are occupied by hydrogen atoms which also remain fixed during initial condition sampling and integration of trajectories. Additionally, every open site on this surface is initially unoccupied. There are 12 open binding sites on this model surface, three of which are in the reaction zone. Trajectories which result in adsorption in, migration to, or scattering off of an open site outside of the reaction zone are not considered in the results, because the silicon atoms surrounding the outer edges of these open sites are not moving, while the silicon atoms surrounding the inner edges of the outer open sites are moving. Therefore, these outer open sites cannot be considered as directly equivalent to those completely within the reaction zone. A few trajectories migrated outside of the reaction zone and were discarded. In the most extreme case, this resulted in the elimination of 12% of the trajectories. We do not believe this affects any of our conclusions. Langevin friction and random forces on subsurface atoms and surface atoms outside the

reaction zone were not included in this study based on the results of a study reported by Agrawal *et al.* (71) on the effect of the lattice model on the dynamics of dissociative chemisorption of molecular hydrogen on Si(111). In that study, the results indicate that surface relaxation to the bulk is not an important factor for the properties studied, which include sticking probabilities, energy transfer and mobility of the hydrogen atom on the surface.

Initial Condition Selection

Initial conditions for the first-layer silicon atoms and adsorbed hydrogen atoms located within the reaction zone were selected by canonical Metropolis-Monte Carlo sampling (72). This is described as follows: At the beginning of each ensemble of trajectories, all of the lattice atoms and adsorbed hydrogen atoms are placed in their equilibrium positions. In this configuration, the potential energy of the lattice and adsorbed atoms is zero. The total energy of each atom is taken to be 3kT where k is the Boltzmann constant and T is the desired surface temperature for the ensemble. The energy is equipartitioned into the x, y and z momentum components of each atom. The signs of the individual momentum components are assigned randomly. The system undergoes a succession of 1000 Markov moves. One Markov move is a step defined as:

$$q_i = q_i + (0.5 - \zeta_2) \quad \Delta q_i \tag{26}$$

$$p_i = p_i + (0.5 - \zeta_3) \quad \Delta p_i \tag{27}$$

which is taken by each of two first-layer silicon atoms and two adsorbed hydrogen atoms in the reaction zone (Note that only silicon atoms participate in this Markov succession when there are seven available top sites.) ζ_i (i = 1,2,. . . n) are random numbers uniformly distributed over the interal [0,1]. If a move lowers the energy of the lattice, it is accepted. If a move raises the system energy, the move is accepted with a probability of exp $(-\Delta E/kt)$, where ΔE is the change in the energy caused by the move and T is the temperature of the lattice. In other words, a random number ζ_4 is selected and if $\zeta_4 < \exp(-\Delta E/kt)$, the move is accepted. If it is not accepted, another attempt to move it from the original configuration is made. The magnitude of Δp_i and Δq_i are selected such that approximately 50% of the moves are accepted. One thousand Markov moves are made between every third trajectory, and 50 Markov moves are made between all other trajectories. Table III, Appendix gives the Metropolis parameters used in this sampling procedure.

Initial conditions for the incident hydrogen atom were selected as follows: The atom was placed 13 a.u. above the Si(111) surface. Because we simulated beam experiments, initial energy and azimuthal angle were fixed. Three sets of 200 trajectories were calculated

for each surface coverage. The initial energy of the incident hydrogen atoms in all studies was 0.126 eV. The three sets of trajectories at each coverage consisted of ensembles of trajectories whose initial azimuthal angles were 0°, 15°, or 30°. The initial hydrogen velocity vector is chosen so as to aim the hydrogen atom at a square area about the central lattice atom (see Fig. 14). The side length of this square area is 1.1 a.u. Experimentally, impact points would be averaged over several unit cells on the surface. However, the size of our model precludes averaging over a unit cell, because by enlarging the area of impact points, many more trajectories must be thrown out due to migration to, chemisorption in, or scattering from the region outside the reaction zone. While this condition introduces bias in our calculations, we were able to obtain meaningful dynamical information of a hydrogen interacting with a top site, and the effect of open sites on that interaction.

Orientation angles of the incident hydrogen are:

$$\Theta = 0°,\ 15°,\ \text{or}\ 30° \qquad (28)$$

$$\Phi = 2\pi\zeta_5 \qquad (29)$$

In order to ensure that the hydrogen atom would always start its trajectory from a position above the lattice surface, the initial azimuthal angle had a maximum limit. Because our model size is so small, coupled with the requirement that the initial hydrogen must be located

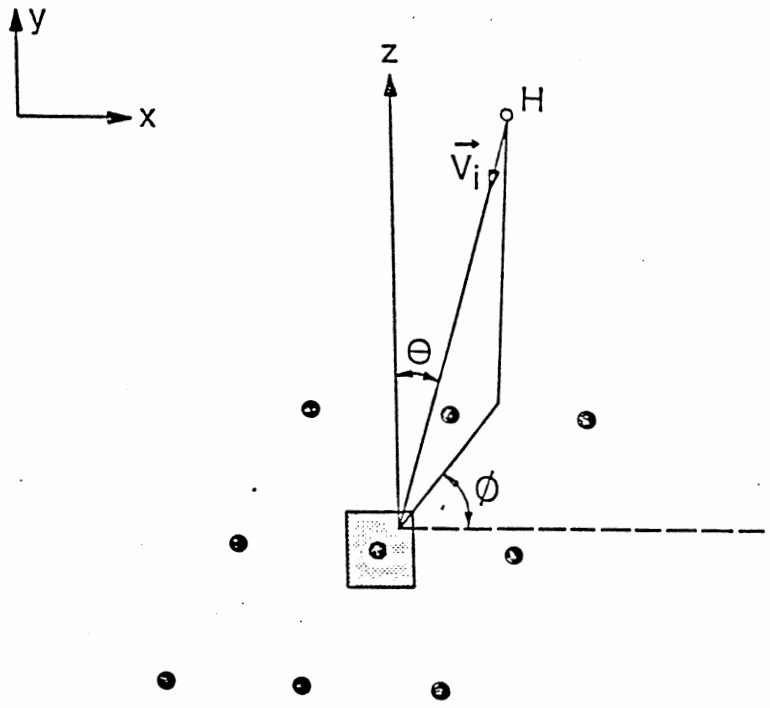

Figure 14. Schematic representation of the selection of initial conditions for hydrogen atom scattering/chemisorption on Si(111) study. The "aiming point" is selected randomly within the shaded area, defined as a square with side length of 1.1 a.u. The Si(111) surface lies in the X-Y plane and the Z axis is normal to the surface

13 a.u. above the surface, we were unable to study the scattering or chemisorption of hydrogen on Si(111) surfaces at larger incidence angles.

Trajectory Integration

Instantaneous sticking probabilities were calculated from the results of 200 trajectories for the systems at the various initial conditions. Chemisorption in this system is considered to have occurred if the adsorbed atom undergoes five inner turning points with respect to motion in the surface normal direction. Because of the large number of equations of motion which are integrated and the complex nature of the interaction potential, trajectories were followed for 0.65 ps for all surface coverages except for the fully covered surface. Trajectories at this surface coverage were integrated for a maximum time of 0.86 ps because in a few cases, hydrogen exchange resulting in chemisorption or desorption occurred, which took longer to study than the events for the other surface coverages. Energy was conserved to 0.005 eV. The time step used in the integration is given in Table III, Appendix.

H_2 on Si(111)

Model

The model used in this calculation consisted of 95 lattice atoms of which 25 are in the first layer and

35 are in each of the second and third layers. Only the first layers are permitted to move during trajectory integration and initial condition selection.

Initial Condition Selection

Initial conditions for the lattice atoms were selected by canonical Metropolis-Monte Carlo sampling (72) as described above. However, initially there will be no hydrogen atoms adsorbed on the Si(111) surface, and only the surface silicon atoms in the model will undergo the Monte Carlo sampling procedure. In this study, one Markov move is defined to be a step taken by each of four first-layer silicon atoms. Table III, Appendix gives the Metrepolis parameters used in this sampling procedure.

Initial conditions for the incoming H_2 molecule were selected as follows: The center-of-mass of the incoming H_2 molecule was placed 9 a.u. above the Si(111) surface. This distance was the minimum distance at which the potential between the lattice atoms and the hydrogen atoms was 0.01 eV or less. The orientation angles of the center-of-mass were selected as follows (See Fig. 15).

$$\Theta_{cm} = \text{Acos}\{1.0 + \zeta_6(\text{Cos } \theta_m - 1.0)\} \qquad (30)$$

$$\Phi_{cm} = 2\pi\zeta_7 \qquad (31)$$

where θ_m is described below. As in the H-Si(111) study, we ensured that the molecule would always start its trajectory from a position above the lattice surface.

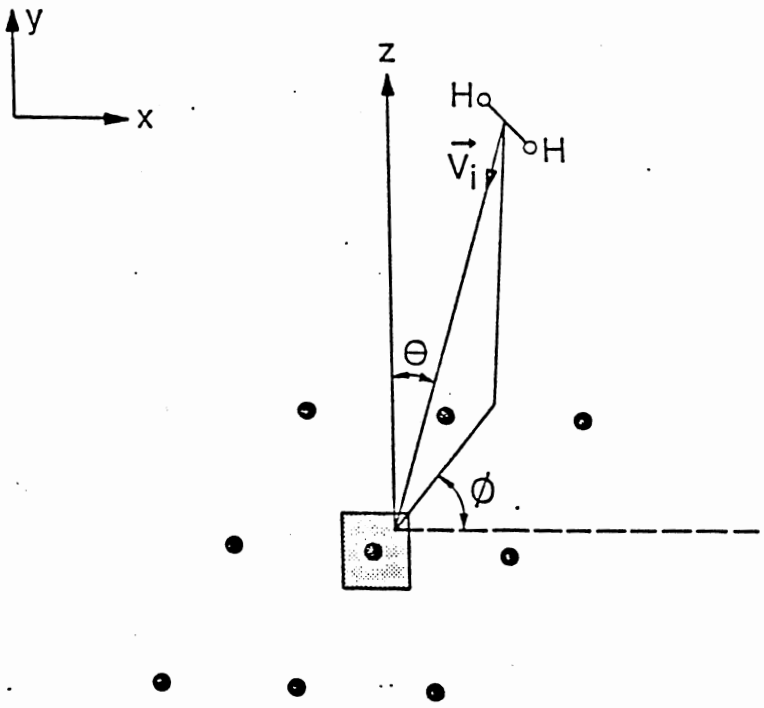

Figure 15. Schematic representation of the selection of initial conditions for H_2 scattering/dissociative chemisorption on Si(111) study. Same as Figure 14, except the shaded area is a rectangle with side length in x direction of 4.2 a.u. and side length in y direction of 7.82 a.u.

Therefore, a maximum limit θ_m was set on the initial azimuthal angle. The size of the model lattice, coupled with the requirement that the initial H_2 center-of-mass be located 9 a.u. above the surface plane, requires this limit to be 54.4°. Consequently, we were unable to study scattering/adsorption of molecules incident upon the Si(111) lattice at angles greater than θ_m.

The initial H_2 vibrational and rotational energies were either selected from a Boltzmann distribution at the same temperature as the lattice or they were state selected quasiclassically. The initial H_2 translational energy was either selected canonically at the lattice temperature or it was fixed at a value greater than the barrier height for H_2 adsorption on the Si(111) surface in order to increase the statistical accuracy of the chemisorption studies. The initial H_2 velocity vector is chosen so as to aim the H_2 center-of-mass at a rectangular area about the central lattice atom (see Fig. 15). The rectangular box had a side length in the x direction of 4.2 a.u. and a side length in the y direction of 7.82 a.u. Choosing the box in this manner ensures that all impact points within a unit cell will be sampled.

Trajectory Integration

Classical trajectories were integrated to give sticking probabilities and hydrogen-atom mobilities as

well as spatial and translational energy distributions for the scattered hydrogen molecules at each of three temperatures, 300, 1000 and 1500 K. The position and momenta of each moving particle as a function of time is determined by solving the 162 equations of motion. Energy was conserved to 0.01 eV and the time step for trajectory integration is given in Table III, Appendix. Trajectories were integrated until the maximum trajectory time was exceeded, or until the center-of-mass of a scattered H_2 molecule had reached 9 a.u. above the surface after impact, or, in the case of dissociative chemisorption, the adsorbed atoms remained on the surface for an integration period of 0.6 ps measured from the second-inner turning point of a lattice-adatom vibration in the surface normal direction. The maximum allowed integration time is 0.86 ps.

The instantaneous hydrogen atom mobility on the Si(111) surface at $t=t_0$ was calculated as a function of residence time on the surface for surface temperatures of 300, 1000, and 1500 K using the velocity autocorrelation function

$$\mu(t_o) = 0.5 \int_{t_o}^{\infty} \langle v(t_o) \cdot v(t) \rangle dt \qquad (32)$$

The velocity autocorrelation functions were obtained from the results of extended classical trajectories. During these trajectories, the hydrogen atoms were constrained to move on the surface within the area designated by the dashed lines in Fig. 16. When a hydrogen atom crossed

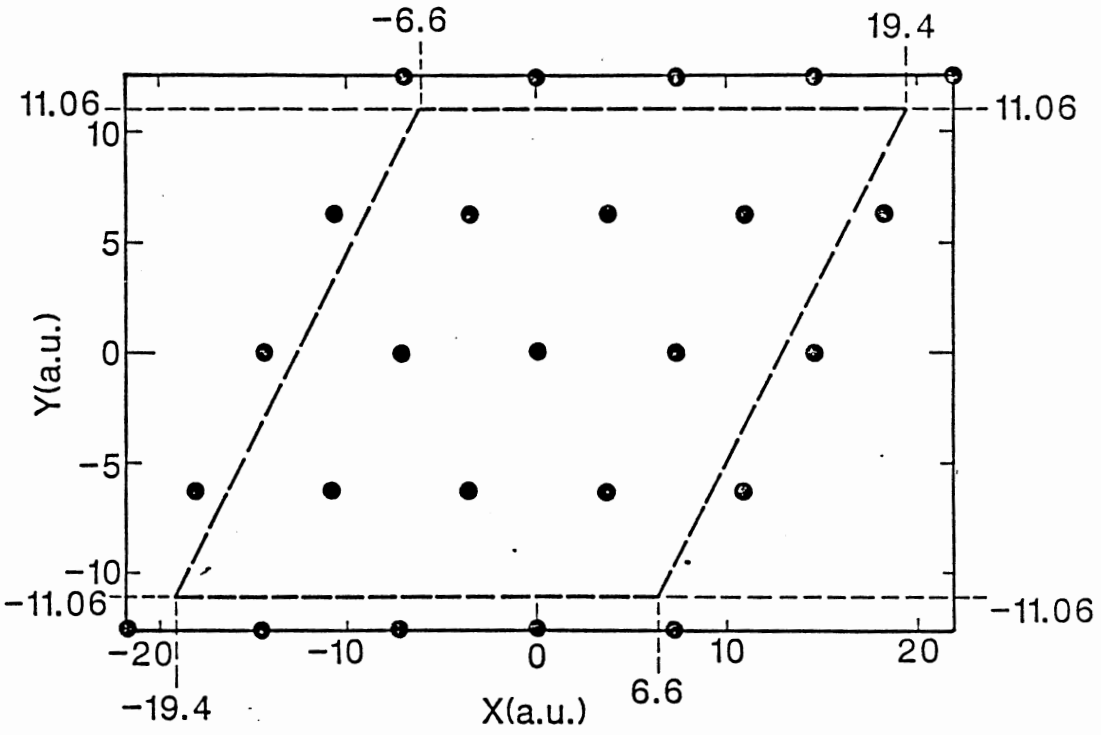

Figure 16. Relative equilibrium positions of the first-layer silicon atoms in the Si(111) lattice used in the study of scattering/dissociative chemisorption of H_2 on Si(111). See text for explanation of dashed line.

this line, the direction of the velocity components in the surface plane were changed to keep the atom within the surface area. Small energy discontinuities caused by this reversal are insignificant.

Hydrogen Atom Diffusion on Si(111)

In many chemical reactions on surfaces, the rate determining step for reaction is surface diffusion of reacting species. Often, the rate of migration of reacting species on the surface is rapid and the activation energy for surface diffusion is on the order of kT (2(a)). A system with these conditions would be amenable to classical trajectory study, and the diffusion coefficient could be obtained by calculating the velocity autocorrelation function of the adsorbate, from the Green-Kubo relation (73):

$$D = 0.5 \int_{t_o}^{\infty} \langle v(t_o) \cdot v(t) \rangle dt \qquad (33)$$

Doll and Voter (74) have reviewed several direct molecular dynamics studies of surface diffusion employing this approach. However, there are systems in which the time between adsorbate hops is very large. In such cases, the duration of the trajectories required to calculate the diffusion coefficient makes this approach computationally impractical. This is the case for hydrogen diffusion on Si(111), where the thermal rate is very small because of high energy barriers. We attempted to calculate the thermal diffusion coefficient for a

hydrogen atom on Si(111) from the velocity autocorrelation function using the Raff *et al.* (48) potential. The autocorrelation functions were obtained from trajectories integrated for periods of 2.7 ps. A typical result is shown in Fig. 17. This type of autocorrelation is typical of a system undergoing purely periodic motion. The integral in Eq. (33) is small and nonconvergent. Examination of the motion of the hydrogen atom giving rise to this autocorrelation fucntion shows that it does not diffuse at all but remains bound to the initial Si(111) binding site. Thermal hydrogen atom diffusion on Si(111) is a high-energy process whose rate is very small. Calculation of the thermal diffusion coefficient must be done by using techniques which simulate rare event processes, for example, transition-state theory (TST). We report here a variational transition-state theory calculation employing Metropolis Monte Carlo methods to evaluate the TST averages to study the diffusion of hydrogen on Si(111).

Doll (75) first suggested Monte Carlo sampling methods to calculate TST rate coefficients for unimolecular reactions. Viswanathan *et al.* (76) applied Monte Carlo Variational Phase-Space Theory (MCVPST) to unimolecular decomposition of CH_4 and obtained good agreement with trajectory calculations. Adams and Doll (77) have computed MCTST rate coefficients for desorption of Ar and Xe from solid Xe(111). Additionally, Voter and

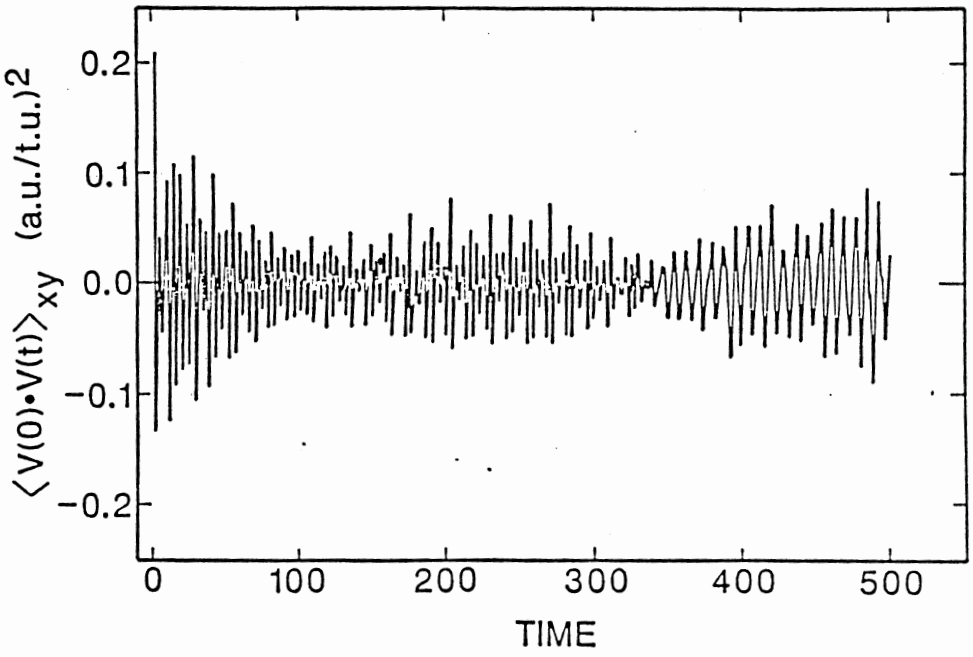

Figure 17. Velocity autocorrelation function for the thermal motion in the X-Y plane of a hydrogen atom on Si(111) at 300 K. Time is given in units of 0.00539 ps.

Doll have calculated self-diffusion constants for atoms on metal surfaces using MCVTST methods (78) and a Monte Carlo TST method with dynamical corrections (79).

Diffusion of hydrogen on Si(111) might involve appreciable quantum mechanical effects, such as tunneling, due to the small mass. We have thus far incorporated WKB tunneling corrections (80) into the Monte Carlo procedure to obtain an estimate of the tunneling for three-dimensional motion.

There have been a few approaches to quantum mechanical diffusion on surfaces. Freed (81) proposed a quantum mechanical model to explain the exponential increase with isotopic mass of the preexponential factor for the thermally activated diffusion rate for atomic hydrogen and its isotopes on the W(110) surface as observed in experiments by Wang and Gomer (82). They did not, however, perform numerical calculations for the model. Whaley, Nitzan, and Gerber (83) developed a model of hydrogen diffusion on metal surfaces based on band theory in a study of coverage dependence of diffusion.

Valone, Voter and Doll (84) studied quantum mechanical contributions to diffusion of H, D and T on Cu(100). They performed a MCTST calculation on a temperature dependent effective potential, that is, a potential with significant quantum mechanical corrections built in. This method avoids explicit calculation of the tunneling correction. The study shows mass and

temperature dependent decreases in the effective activation energy for H, D and T diffusion on Cu(100).

Lauderdale and Truhlar performed two variational transition-state theory (VTST) calculations (85,86) based on a reaction path formalism for hydrogen on Cu(100). Both studies used semiclassical methods for calculating multidimensional tunneling probabilities as well as other quantum effects. The first study was done on a rigid surface at equilibrium, and showed that tunneling increases the surface diffusion coefficients of H, D and T by factors of 3.0, 1.6 and 1.3, respectively at 100 K. (85) The second calculation allowed for motion of six of the surface atoms. (86) This calculation showed that diffusion is dominated by tunneling at low temperatures and that by allowing motion of the surface atoms, phonons and effects of surface relaxation were introduced into the reaction coordinate, giving an increase in diffusion rate compared to that of the rigid surface. They chose a tunneling path located on the concave side of the minimum energy path because it is shorter, rather than restricting the tunneling path to the minimum energy path. They concluded that restricting the tunneling path to the minimum energy path lowers the diffusion coefficient and that tunneling actually occurs with the Cu atoms near the vibrational turning points in the direction that shortens the tunneling path.

Jacquet and Miller (87), using Monte Carlo path integral methods, calculated the quantum mechanical diffusion rate of hydrogen on W(100). Their results show that surface atom motion increases the rate of H-atom tunneling from one site to another. They explain this in terms of the extreme limit of large surface amplitude motion. In a distorted surface-atom geometry, the surface atoms are close together and the tunneling probability so much larger that essentially tunneling occurs only for this configuration. This calculation included only one phonon.

Model

The model used in this calculation is the same used in the H-atom scattering/chemisorption study on a Si(111) with different degrees of hydrogen coverage, described above.

Initial Condition Selection

Initially, all of the lattice atoms and adsorbed hydrogen atoms are placed in their equilibrium positions, with all adsorbed hydrogen atoms occupying top binding sites on the surface. In this configuration the potential energy of the lattice and adsorbed atoms is zero. The total energy of each atom is taken to be 3kT where k is the Boltzmann constant and T is the desired surface temperature for the ensemble. The energy is

equipartitioned into the X, Y and Z momentum components of each atom. The signs of the individual momentum components are assigned randomly.

Monte Carlo Variational Phase-Space Theory (MCVPST)

The classical PST rate constant for migration from binding site A to binding site B may be expressed as the flux F across a dividing surface $\tilde{S}$ between the two binding sites,

$$F = \int dP \int dR\ \delta(\tilde{S}) |v_p| \exp(-\beta H) / \int dP \int dR\ \exp(-\beta H) \qquad (34)$$

where v_p is the velocity normal to the dividing surface $\tilde{S}$, $\beta = 1/kT$, $\delta(\tilde{S})$ is the Dirac delta function, and H is the system Hamiltonian. In the Monte Carlo application of Eq. (34), we write

$$F = \lim_{N\to\infty} [1/N \sum \delta_i(\tilde{S}) |v_p|_i] \qquad (35)$$

The summation is evaluated by Metropolis sampling methods which employ a canonical Markov walk through the 84-dimensional reactant phase space of the system. The summation in Eq. (35) runs over the N configurations generated in the walk.

However, there is a large barrier between the two binding sites on the Si(111) surface. Therefore, convergence of the Monte Carlo sum is very slow. To circumvent this problem, we introduced an importance sampling procedure which transforms Eq. (34) to the form

$$F = \int dG \delta(\tilde{S}) |v_p| P_0^{-1} / \int dG\ P_0^{-1} \qquad (36)$$

where

$$G(P,R) = \int dP \int dR \exp(-\beta H)\ P_0 \tag{37}$$

with the distribution function P_0

$$P_0 = \exp(\beta V_{dg}) \tag{38}$$

where V_{dg} is the adatom-lattice atom interaction potential for the diffusing hydrogen atom. Equation (36) is now evaluated using a Monte Carlo procedure based on a Markov walk in reactant phase space that is governed by the distribution function dG. This yields

$$F = N^{-1}\sum_i^{N_\delta} {}_i(\hat{S})\,|v_p|_i\,(P_0^{-1})_i / N^{-1}\sum_i^{N}(P_0^{-1})_i \tag{39}$$

This procedure allows the diffusing adatom to move in a potential-free phase space. Under such conditions, the phase-space points corresponding to the barrier to diffusion, which are rarely accessible with unbiased sampling, become freely accessible. The execution of the canonical Markov walk for evaluating the integrals has been described above. In this study, one Markov move is a step taken by a first-layer silicon atom and one adsorbed hydrogen atom in the reaction zone other than the diffusing hydrogen, with the choice of the lattice atom and adatom to be moved being cycled systematically among the 7 movable lattice atoms and the 6 adatoms other than the diffusing particle. A random step of the diffusing particle is attempted for every cycle. The parameters used for the walk are given in Table III, Appendix. After a Markov step has been chosen, if the diffusing particle has crossed the dividing surface, the

velocity of it perpendicular to the surface is calculated and added into the Monte Carlo sum. The reflecting surfaces are identical to the dividing surfaces, and the flux in only one direction is calculated.

The flux given in Eq. (39) is an upper limit to the true classical rate of crossing the dividing surface. There are recrossings of the dividing surface. A much closer upper bound can be obtained by using Eq. (39) in a variational calculation of the rate. In principle, to obtain the minimum flux, the dividing surface must be expressed as a general function of the 84 coordinates and momenta that define the phase space of the model system and the flux minimized with respect to this function. Since the problem must be solved numerically, the computational requirements of such a procedure are too large. Consequently, a more approximate minimization is employed.

We constructed a set of dividing surfaces that span the important regions of the phase space of the system. Figure 18 shows the central top site, and the three surrounding open sites. This is the region we focus on in this study. Due to the symmetry of the system, we have restricted the hydrogen to walk only within the area within Region I labeled on this plot. Additionally, the diffusing hydrogen atom was not allowed to penetrate the surface and was not allowed to walk farther than 5.0 a.u. above the surface. These

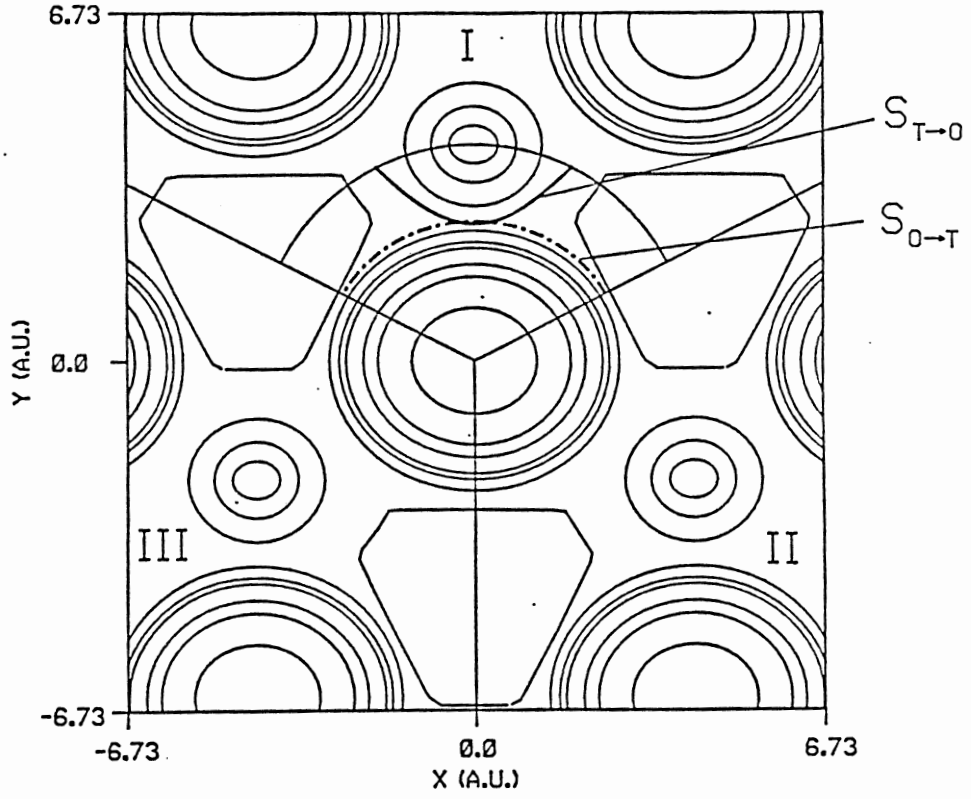

Figure 18. Same as Figure 11, except this contour plot shows the central portion of the model. Region I designates area in which diffusing atom was restricted to move (see text). S_{T-O} denotes dividing surface which gives minimum flux for top-to-open site jumps; S_{O-T} denotes dividing surface which gives minimum flux for open-to-top site jumps.

restrictions allowed faster convergence of the rates while averaging over the relevant region of the phase space of the system.

Three different dividing surfaces $\tilde{S}$ were used relative to the top site, located directly in the center of Fig. 18:

Circular cylinder $\tilde{S} = x^2 + y^2 - a^2 = 0$ (40)

Elliptical cylinder $\tilde{S} = b^2x^2 + a^2y^2 - a^2b^2 = 0$ (41)

Hyperbolic cylinder $\tilde{S} = a^2y^2 - b^2x^2 - a^2b^2 = 0$ (42)

In this calculation, x and y are the coordinates in the surface plane, and z is the coordinate in the surface normal direction. Our calculations show that the minimum flux calculated using circular cylinders are approximately 50% larger than those for elliptical and hyperbolic cylinders. There is no difference in the minimum flux when elliptical or hyperbolic cylinders are used.

With $\tilde{S}$ defined, we can calculate the component of velocity normal to $\tilde{S}$. The component of velocity normal to $\tilde{S}$ is:

$$v = v \cdot N_{\tilde{S}} \tag{43}$$

where $N_{\tilde{S}}$ is the unit normal of $\tilde{S}$ where

$$N_{\tilde{S}} = \nabla\tilde{S} / |\nabla\tilde{S}| \tag{44}$$

The parameters a and b in Eqs. (40)-(42) are variational parameters used to minimize the flux. Convergence of the values of the jump frequencies for diffusion from top to

open site and open to top site is obtained with 10^6 attempted steps.

Thermal Diffusion Coefficient

Direct calculation of the diffusion coefficient from the jump frequencies for the case of two types of binding sites is more complicated than for surfaces with a single type of binding site. NoorBatcha, Raff and Thompson, (64) in a study of silicon diffusion on Si(111), developed a general method to calculate a lower bound and an estimated upper bound for the surface diffusion coefficient using jump frequencies for different types of binding sites. The method involves solving a set of coupled first-order differential equations which describe the phenomenological process illustrated in Fig. 19, where top and open adsorption sites are numbered, for convenience. The equations are:

$$\dot{C}_1(t) = -3k'_1C_1(t) + k'_2[C_2(t)+C_3(t)+C_4(t)]$$

$$\dot{C}_2(t) = -3k'_2C_2(t) + k'_1[C_1(t)+C_6(t)+C_5(t)], \text{ etc.} \quad (45)$$

where $C_i(t)$ is the number of atoms present at adsorption site i and $k'_j = k_j/3$ (j=Top, Open). Equation (45) is expressed in terms of the k'_j rather than the jump frequencies k_j since the calculation of k_j counts jumps in all three equivalent directions. Integration of these equations gives $C_i(t)$ at any time t. The mean-square displacement is:

$$\langle r^2(t)\rangle = 1/C_T \sum_i C_i(t)r_i^2 \quad (46)$$

where r_i is the equilibrium distance of site i from site one and C_T is the total number of adatoms present at all sites. The diffusion coefficient can be obtained from the Einstein relation:

$$\langle r^2(t) \rangle = 2\alpha Dt \tag{47}$$

The model used in solving Eq. (45) treats 64 adsorption sites, 37 of which are top sites and the remainder are open sites. The initial concentrations at the adsorption sites are as follow: $C_T = 73000$, $C_1(t=0) = 10000$ and $C_i(t=0) = 1000$ for $i > 1$. The equations were sufficiently stiff to warrant use of a Gear integrator (88). If smaller initial values were chosen for the $C_i(t)$, underflow errors accumulated during the integration due to the small value of the jump frequencies. Edge effects were negligible except during the last stages of the calculation, as discussed by NoorBatcha *et al.* (64) We also calculated an estimate of the upper bound for D by modifying Eq. (45) such that all motions leading toward the initial adsorption site is excluded. The equations are

$$\begin{aligned} \dot{C}_1(t) &= -3k_1' C_1(t) \\ \dot{C}_2(t) &= -2k_2' C_2(t) + k_1' C_1(t), \text{ etc.} \end{aligned} \tag{48}$$

The approximate upper bound was obtained by solving Eq. (48) and using Eqs. (46) and (47).

Tunneling

We attempted to determine the importance of tunneling in hydrogen atom diffusion on Si(111) using the WKB semiclassical approximation (80). We assumed that the tunneling rate could be approximated as follows:

$$k(T)= \int dP \int dR\ \nu(E)\ T_p(E)\ \exp(-\beta H) / \int dP \int dR\ \exp(-\beta H) \quad (49)$$

where $\nu(E)$ is the frequency of hydrogen atom motion in the surface plane at a specific energy, and $T_p(E)$ is the tunneling probability which gives the largest value among tunneling probabilities calculated from nine different paths. The WKB approximation (88) of $T_p(E)$ has the form

$$T_p(E) = \exp(-2/\hbar \int [2m_H(V-E)]^{1/2} d\tau) \quad (50)$$

where

$$m_H = 1.00797 \text{ a.m.u.} \quad (51)$$

and m_H is the mass of the hydrogen atom. We solved this equation using the Monte Carlo procedure with biased Markov walk described in Eq. (39). Equation (49) transforms to

$$k(T)= [N^{-1} \sum \nu(E)_i T_p(E)_i (P_0^{-1})_i] / [N^{-1} \sum (P_0^{-1})_i] \quad (52)$$

The calculation proceeded as follows: A biased Markov walk as described above for the classical MCVPST calculation of hydrogen-atom diffusion was used to average over the reactant phase space. The diffusing hydrogen was initially placed in its equilibrium position in the central top site. It was restricted to walk within the confines of the top site phase space; i.e., it could not walk past the dividing surface which gave the minimum

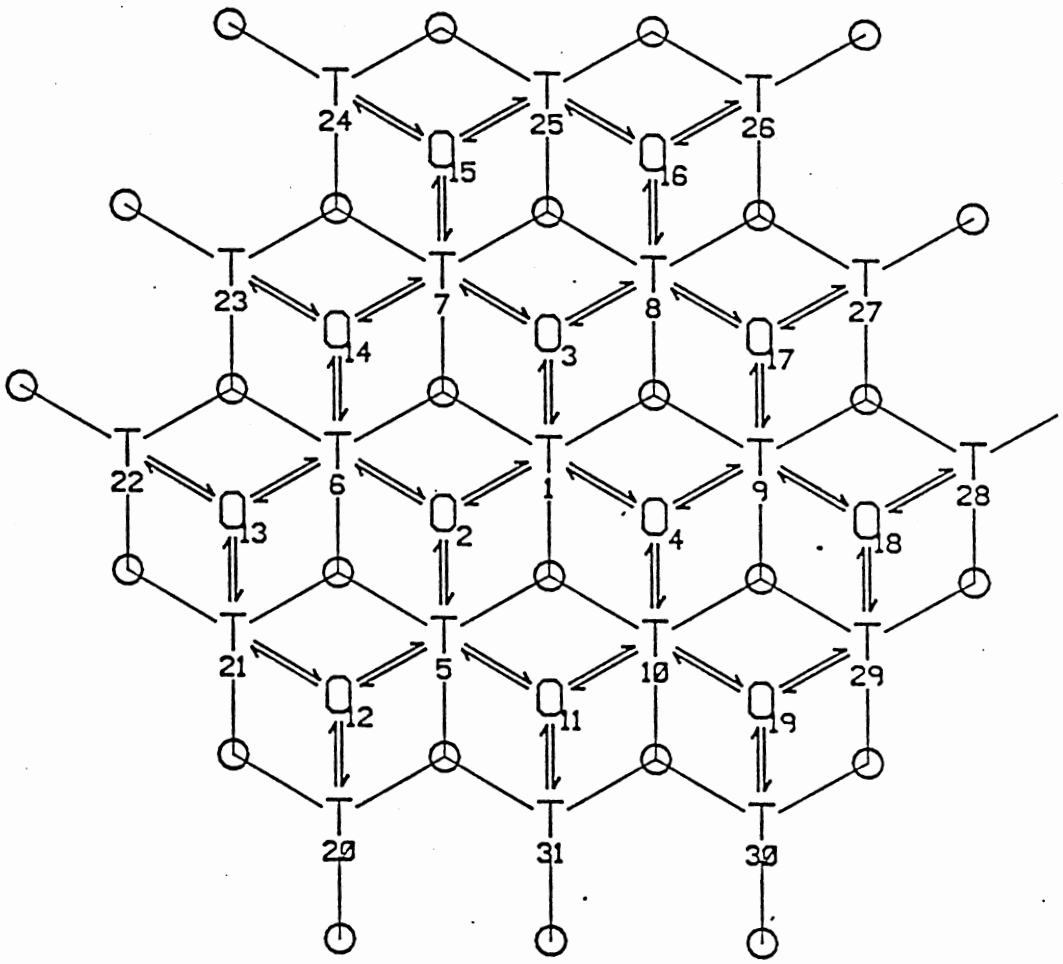

Figure 19. Phenomenological model used to describe the single jump, uncorrelated diffusion of hydrogen atoms on Si(111). T denotes a top binding site and O represents an open binding site. T also represents a first-layer Si atom and the small circles denote second-layer Si atoms.

flux in the calculation of the classical jump frequency of hydrogen from top site to open site. The energy of the diffusing hydrogen atom was calculated after each Markov step. If the energy was less than the classical barrier to diffusion and if the energy was greater than or equal to the minimum potential energy in the adjacent open site, nine tunneling paths were calculated. The tunneling paths are illustrated in Fig. 20. The nine paths were along lines parallel to the surface plane (the distance above the surface determined by the Markov walk selection of the z coordinate of the diffusing particle) connecting the diffusing particle with one of nine evenly-spaced points spanning the diameter of the open site well. The particle was moved by small increments along each path and the potential energy experienced by the hydrogen was calculated at each step. The particle was moved along a specific path until it reached an equal energy in the open site, at which time the one-dimensional WKB tunneling probability was calculated using the potential energy curve calculated along the path. If the particle never reached an equal energy in the open site for one of the nine paths, that tunneling path was discarded. The maximum tunneling probability of all the accepted paths was chosen, and multiplied by the frequency of hydrogen atom motion in the surface plane direction at that particular energy in the top site well and at that particular surface atom

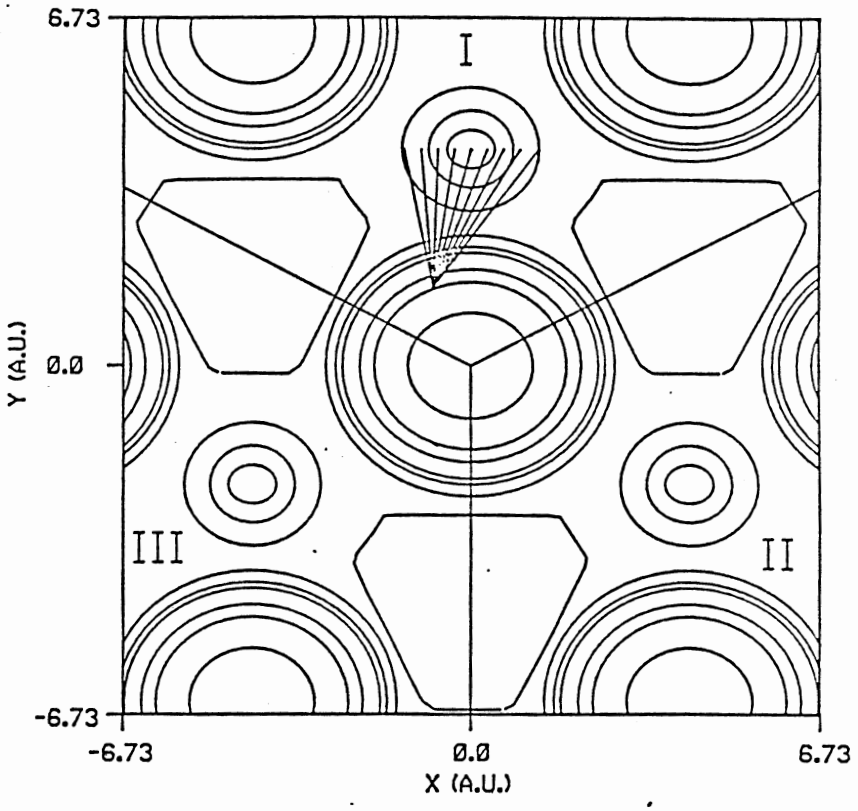

Figure 20. Same as Figure 18, except this plot shows the tunneling paths of a hydrogen atom in the central top binding site through the migration barrier between the top and open binding sites. (See text)

geometry. This product was added in to the Monte Carlo sum in Eq. (52). This procedure was repeated until the results converged. The frequency was calculated by integrating Hamilton's equations of motion for the diffusing particle for one vibration in the surface plane direction. All surface atoms and adsorbed atoms in the system were held fixed during trajectory integration.

CHAPTER IV

RESULTS

Hydrogen Atom Scattering/Chemisorption on Partially/Fully Covered Si(111)

Scattering and Adsorption Mechanisms

Each individual trajectory in this calculation was examined in detail in order to better understand the mechanism of scattering or chemisorption and to determine the effect of the heterogeneity of the binding sites on these processes.

The major processes observed are direct scattering, exchange scattering, direct chemisorption, and chemisorption with exchange;

$$H(g) + (* \text{ or } \#) \longrightarrow (* \text{ or } \#) + H(g) \qquad (R1)$$

$$_aH(g) + *\text{--}_bH \longrightarrow *\text{--}_aH + {}_bH(g) \qquad (R2)$$

$$H(g) + * \longrightarrow *\text{--}H \qquad (R3)$$

$$H(g) + \# \longrightarrow \#\text{--}H \qquad (R4)$$

$$_aH(g) + *\text{--}_bH + \# \longrightarrow *\text{--}_aH + \#\text{--}_bH \qquad (R5)$$

* = top site # = open site

These processes are represented by reactions (R1), (R2), (R3) and (R4), and (R5), respectively. In some cases, we observe indirect scattering via an adsorbed state,

$$H(g) + * \longrightarrow [*\text{--}H] \longrightarrow * + H(g) \qquad \text{(R6a)}$$

$$H(g) + \# \longrightarrow [\#\text{--}H] \longrightarrow \# + H(g) \qquad \text{(R6b)}$$

Subsequent to chemisorption, we also observe hydrogen-atom migration,

$$*\text{--}H + \# \longrightarrow * + \#\text{--}H \qquad \text{(R7)}$$

$$\#\text{--}H + \# \longrightarrow \# + \#\text{--}H \qquad \text{(R8)}$$

$$\#\text{--}H + * \longrightarrow \# + *\text{--}H \qquad \text{(R9)}$$

We find that the probability of each of these reactions is dependent upon the incidence angle and the degree of hydrogen-atom coverage present. Table IV, Appendix summarizes our observations of hydrogen atom behavior as it interacts with a Si(111) surface with different degrees of hydrogen coverage. The results include percentages of trajectories which migrate on the surface after adsorbing in an available binding site. In this study, migration of a hydrogen atom is defined to be diffusion by the incident hydrogen atom to at least one new binding site. For initial azimuthal angles of 0° and 15°, the statistical error is large because there are very few chemisorbing trajectories. Nevertheless, for the 0° series, there appears to be an increase in migrating trajectories with decreasing surface coverage (excluding the fully covered surface). In the case of the fully covered surface, half of the chemisorbing trajectories are a result of hydrogen exchange reaction (R5), which is not seen in any other coverage in this series. The only other case involving chemisorption via

hydrogen exchange occurs in the set of trajectories involving a fully covered surface and initial incidence angle of 15°. In this case, 5% (2 of 37 chemisorbing trajectories) are a result of hydrogen exchange. Therefore, the 0° case on the fully covered surface could be considered a special case. For the 15° series, there is an increase from fully covered surface to the partially covered surface with 1 available top site. The percentage of migrating trajectories for coverages with 1, 3 and 5 available top sites is approximately the same, and increases significantly with the surface which has all top sites available in the reaction zone. There seems to be an increase in the number of migrating trajectories with decreasing surface coverage in both the 0° and 15 series; however, this is not definitive due to the large statistical error. For the 30° series, the statistics are significantly better, due to the larger chemisorption probability. We see that the surfaces which are fully covered or have only one available top site have the same percentage of migrating trajectories. Decreasing the surface coverage to 3 and 5 available sites increases the percentage of migrating trajectories and they share the same percentages. There is, as in the other series, a significant increase in the number of migrating trajectories for the surface with all top sites available.

Table IV, Appendix also shows the percentage of all trajectories which are deflected by an open site (or an unoccupied outer top site) before reaching the initial aiming point. For all surface coverages, there is an increase in deflected trajectories with increasing initial azimuthal angle. A trajectory starting with a larger initial azimuthal angle will pass over more binding sites as it approaches its initial aiming point. For example, the hydrogen atoms with an initial 15° angle start 13 a.u. above the surface approximately over the center of the open site. The hydrogen atoms with 30° initial angle start 13 a.u. above the surface approximately over an outer top site. Therefore, the 30° trajectories can immediately be affected by the long-range nature of the available outer top sites, or by an open site as they approach the surface. A trajectory with a 30° initial azimuthal angle will be closer to the surface plane as it passes over an open site and subsequently feels a stronger attraction to that site than a trajectory whose initial angle is 15°. The 15° trajectories can be affected somewhat by the open site, but as they approach the surface they have moved past the largest attractive region of the open site.

Obviously, no trajectory aimed at the central occupied or unoccupied binding site at 0° is deflected by any other binding site before reaching its initial aiming point. For trajectories with an initial 15° angle, the

percentage deflected by the open site appears to be nearly independent of surface coverage if we exclude the fully covered surface. This result is due to the influence of the deep attractive well of the central top site which is available at these coverages. For the fully covered surface, this attraction does not exist; the open sites are the only attractions the hydrogen feels. Consequently, it is easily deflected. The same trend with regard to the open site is exhibited at 30° incidence as the 15° case. Except for the fully covered surface, the number of trajectories deflected by the open site is approximately the same. However, the increase in total deflected trajectories with decreasing surface coverage (except for the fully covered surface) is due to the deflection by the increasing number of available outer top sites.

All partially covered surfaces exhibited chemisorption or scattering only. The fully covered surface exhibited hydrogen exchange reactions resulting in scattering or chemisorption in adjacent open sites for trajectories with 0° or 15° initial azimuthal angles in addition to direct chemisorption and scattering. For the 0° case, 13% of the trajectories resulted in hydrogen exchange and subsequent desorption or adsorption in an adjacent open site. For the 15° case, 7% of the trajectories involved hydrogen exchange. For both 0° and 15° cases, approximately 80% of the exchange reactions

resulted in desorption of the exchanged hydrogen atom. However, the statistical error is large due to the small number of trajectories resulting in hydrogen exchange (23 and 13 trajectories for the 0° and 15° cases, respectively). In both of these cases, the incoming hydrogen atom directly strikes the hydrogen atom adsorbed on the central silicon atom. In most cases, exchange leading to desorption or adsorption in adjacent sites was not immediate. The two hydrogen atoms are observed to compete for the stable top site. After a relatively short time (less than 0.1 ps), one hydrogen atom is pushed into an adjacent open site, where it either adsorbs or desorbs. Additionally, in both the 0° and 15° cases, approximately 7% of the scattering trajectories did not directly scatter, but would compete with the previously adsorbed hydrogen for the top adsorption site before it subsequently scattered. At 0° and 15° incidence, most of the scattering trajectories are direct; they strike the surface and immediately desorb. Figure 21 shows the projection of a trajectory into the surface plane which results in hydrogen exchange ending in chemisorption in an adjacent site. The initial azimuthal angle is 15° . The incoming hydrogen hits the top site and displaces the previously adsorbed hydrogen into the adjacent open site. At 30° incidence, no hydrogen exchange on the fully covered surface was observed. As the incoming hydrogen atom approaches its

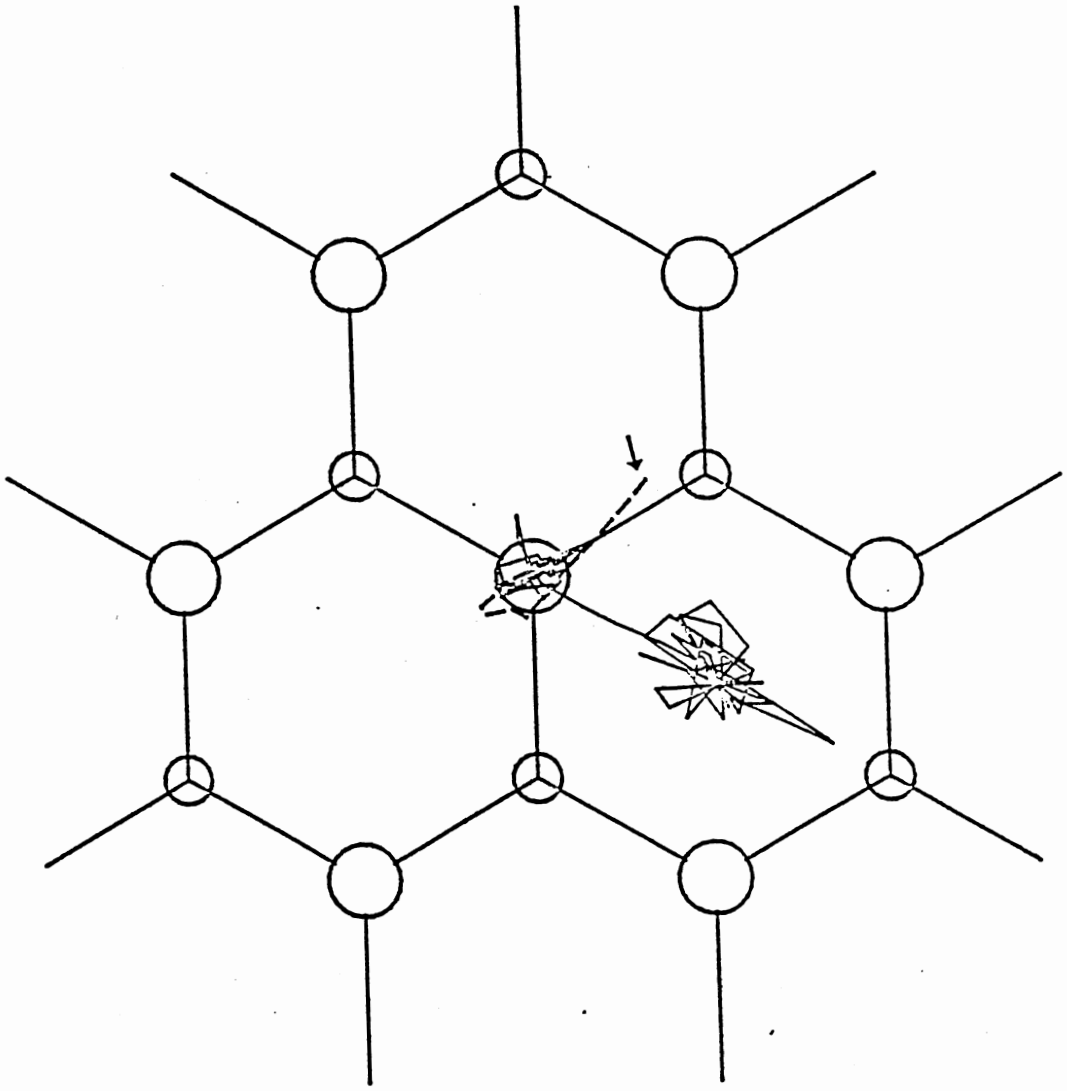

Figure 21. Projection of a trajectory onto the Si(111) surface plane which results in hydrogen exchange and subsequent adsorption in an adjacent open site. Initial incidence angle is 15°. All top binding sites on the surface are occupied. Arrow denotes beginning of trajectory. Dashed line denotes motion of incident hydrogen; solid line denotes motion of displaced hydrogen.

aiming point at a 30° angle on the fully covered surface, it passes over an open site. When this occurs, the hydrogen atom is slowed and drawn in toward the open site. This slowing of the motion and deflection of the trajectory, coupled with the strong repulsion the incoming hydrogen feels when it comes near to the adsorbed hydrogen in the top site, causes the incoming hydrogen to be deflected into the open site, where it subsequently adsorbs or scatters. Because the incoming hydrogen is slowed down, it does not have enough energy to displace the hydrogen atom already adsorbed in the top site.

For all other surface coverages, trajectories with normal incidence which resulted in scattering were relatively uninteresting. Scattering was predominantly direct, reaction (R1); a few cases (less than 5%) involved either bouncing out of the available top site into an open site and vibrating, or vibrating a few times in the available top site, before scattering.

Similarly, trajectories with 15° incidence angle undergoing reaction (R1) generally scattered directly from the top site, except for the fully-covered surface. However, as can be seen in Table IV, Appendix, there is a small percentage of trajectories which are deflected by the open site, but scattering from these sites is also mainly direct. The hydrogen does not stay in the sites and vibrate for a significant time.

Trajectories with a 30° incidence angle generally scatter indirectly via reaction (R6) at all surface coverages. The incident hydrogen atom interacts for a short time (less than five vibrations in the surface normal direction) with the surface before desorbing. The mechanism of scattering in this case can be explained in terms of energy rechannelling. For scattering trajectories with an initial angle of 0° , initially there is no energy in the components parallel to the surface plane, and apparently energy is not totally rechanneled into those components. A significant portion remains in the dissociative mode (component normal to surface plane), resulting in direct scattering. When a hydrogen atom approaches the surface at a 30° angle, there is some energy in the hydrogen atom's momentum components parallel to the surface plane. As discussed below, energy transfer in this system is not completely efficient; therefore, upon impact, energy remains in these parallel components. In some cases, energy is gained by the hydrogen. Although after impact with the surface, the hydrogen atom has enough energy to leave the surface, the energy must be directed to a dissociative mode before desorption can occur. That is, the energy must be rechanneled from momentum components parallel to the surface plane to the component normal to the surface plane. Figure 22 illustrates this type of trajectory.

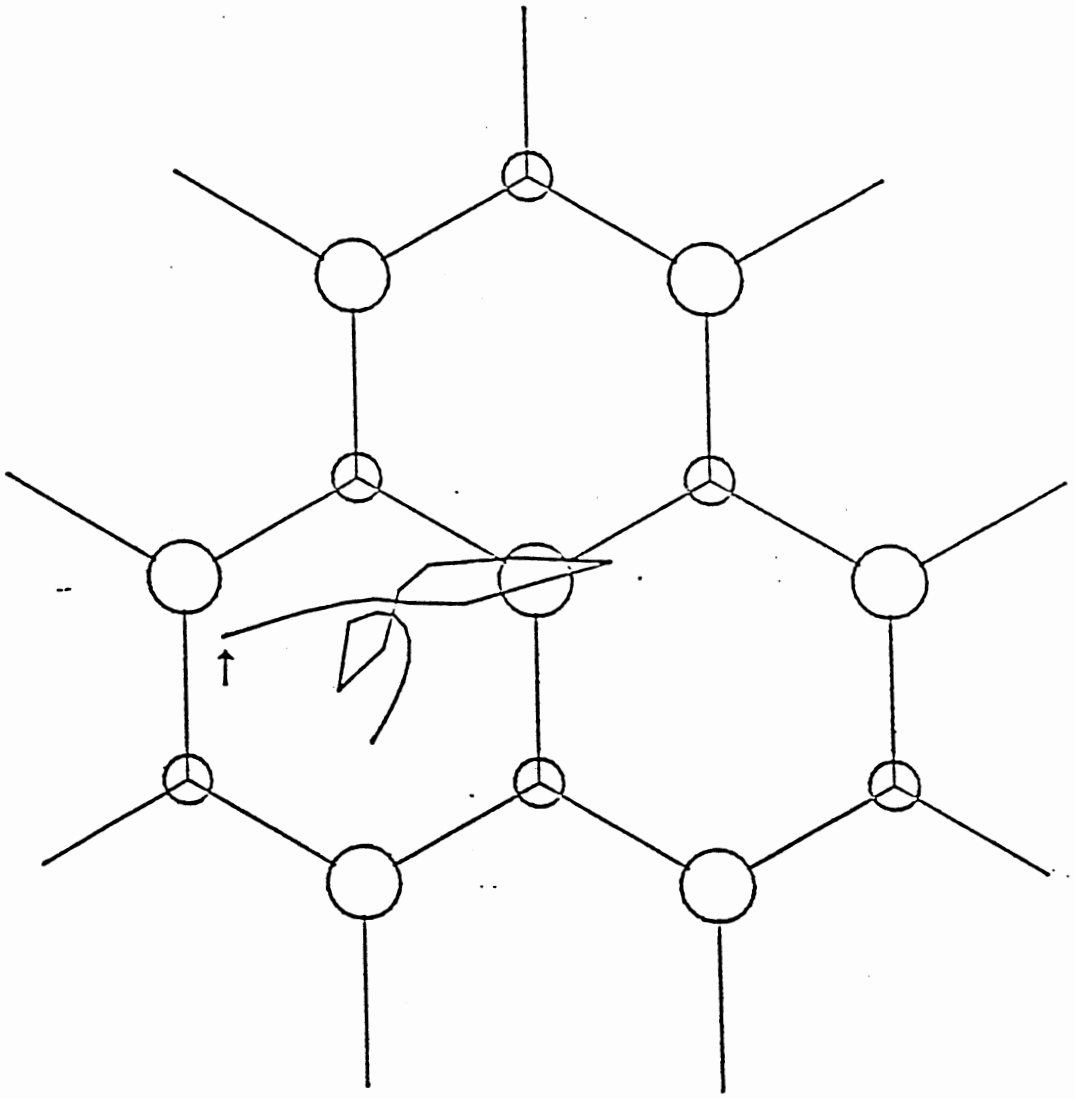

Figure 22. Projection of hydrogen atom trajectory onto the Si(111) surface plane which results in scattering after the hydrogen atom has adsorbed in the central top binding site and migrated to an adjacent open site. Initial angle is 30° and the surface has one available top binding site.

The hydrogen atom hits the available top site, migrates to an adjacent open site, undergoes a few vibrations, and then scatters from the surface. Chemisorbed trajectories also show this effect. The majority of trajectories incident at 30° which chemisorb for surface coverages with 3, 5 or 7 available top sites migrate, indicating that a good deal of energy is in parallel momentum components. Figure 23 shows a trajectory with initial angle of 15° which results in chemisorption, reaction (R3), and subsequently migrates from the central top site to the open site, reaction (R7), to an outer top site, reaction (R8). Figure 24 shows another 30° trajectory resulting in chemisorption which is deflected from its initial aiming point, adsorbed into the outer top site from which it migrates to an open site. Figure 25 shows a similar trajectory, which was deflected by the outer top site and which adsorbed in a non-migrating trajectory.

Energy Transfer and Scattering Distributions

Spatial and translational energy distributions of hydrogen atoms scattered from the Si(111) surface have been computed under various conditions. For distributions with initial azimuthal angles of 0°, 15°, and 30° results were obtained with approximately 185, 160, and 100 trajectories, respectively.

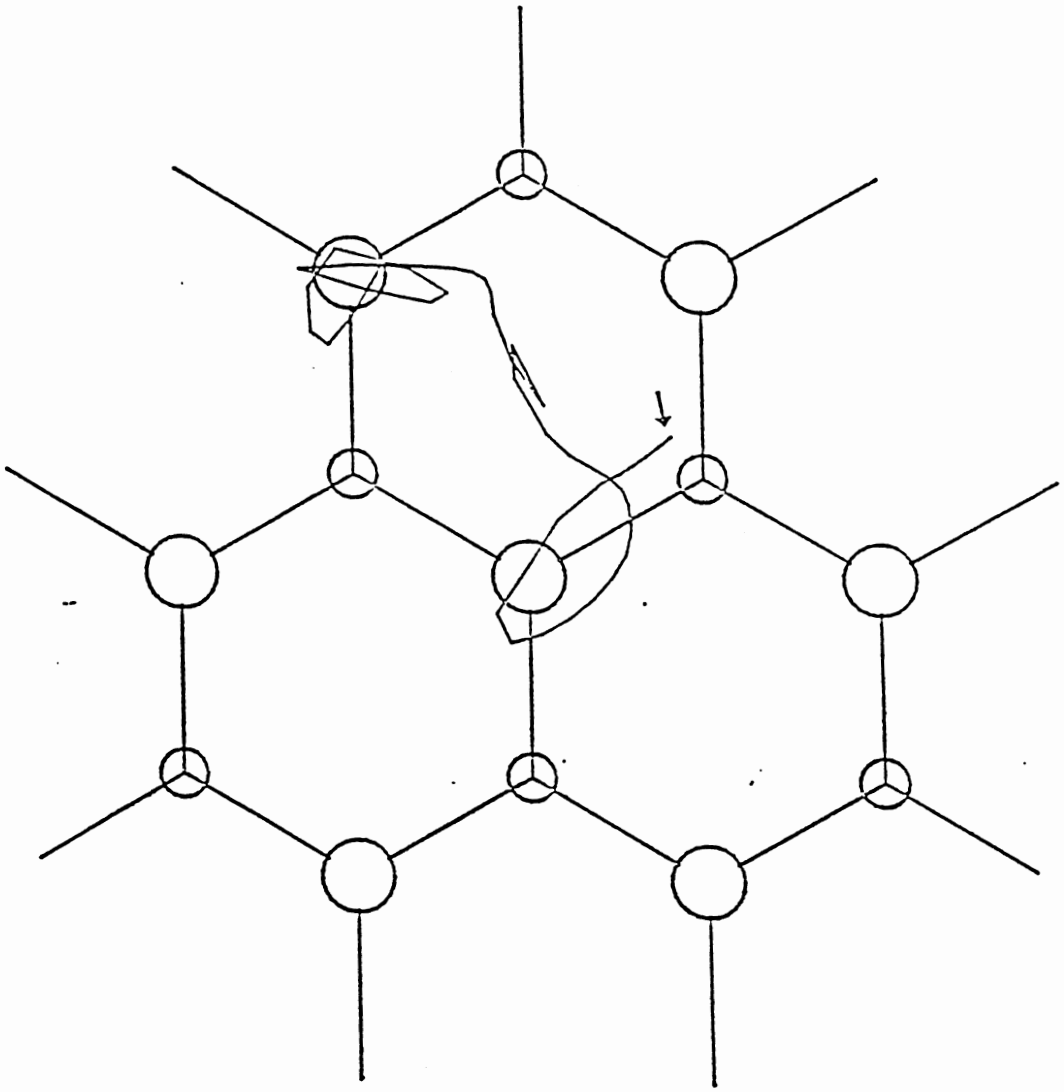

Figure 23. Projection of hydrogen atom trajectory onto the Si(111) surface plane which results in chemisorption at the central top site, migration to an adjacent open site and then to an available outer top site. Initial angle is 15° and the surface has five available top sites.

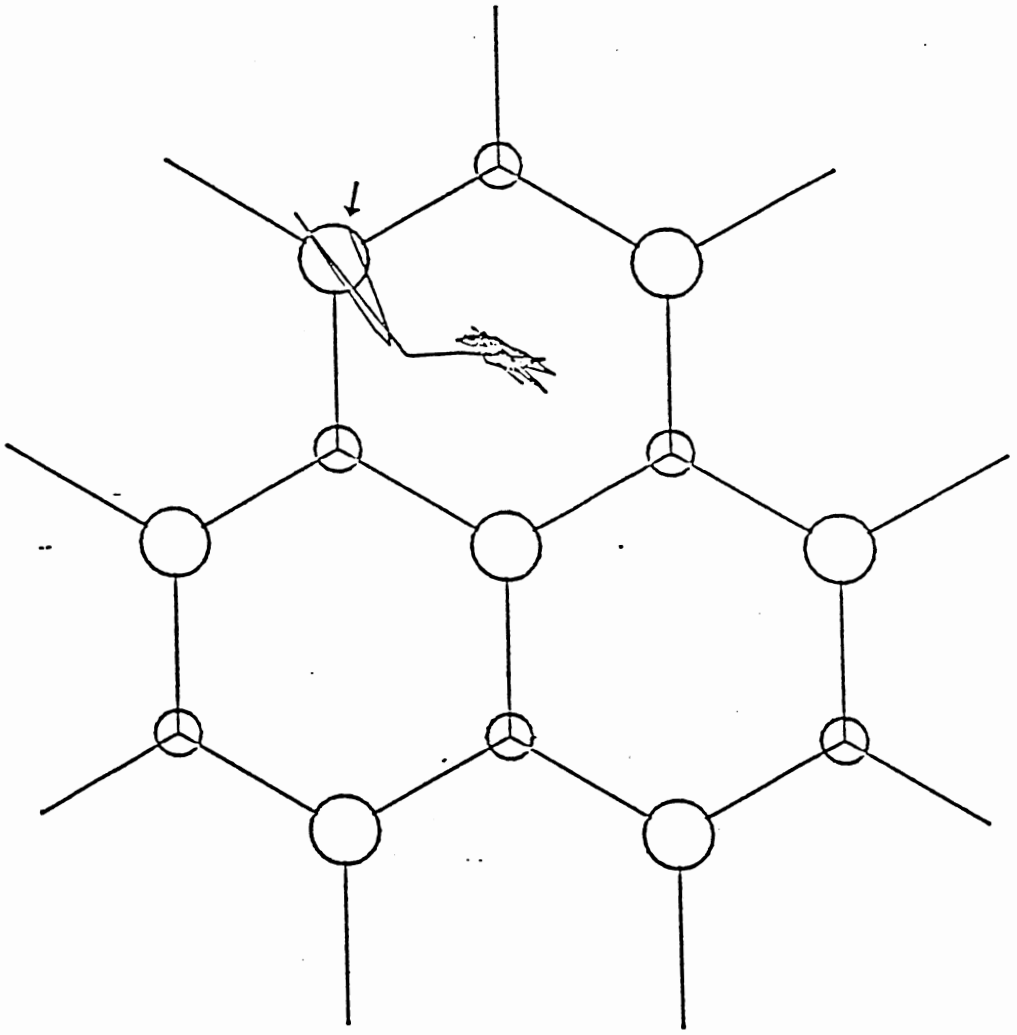

Figure 24. Projection of hydrogen atom trajectory onto the Si(111) surface plane showing deflection of the trajectory from its initial aiming point by an available outer top site. The atom adsorbed in outer top site and migrated to an open site. Initial angle is 15° and the surface has five available top sites.

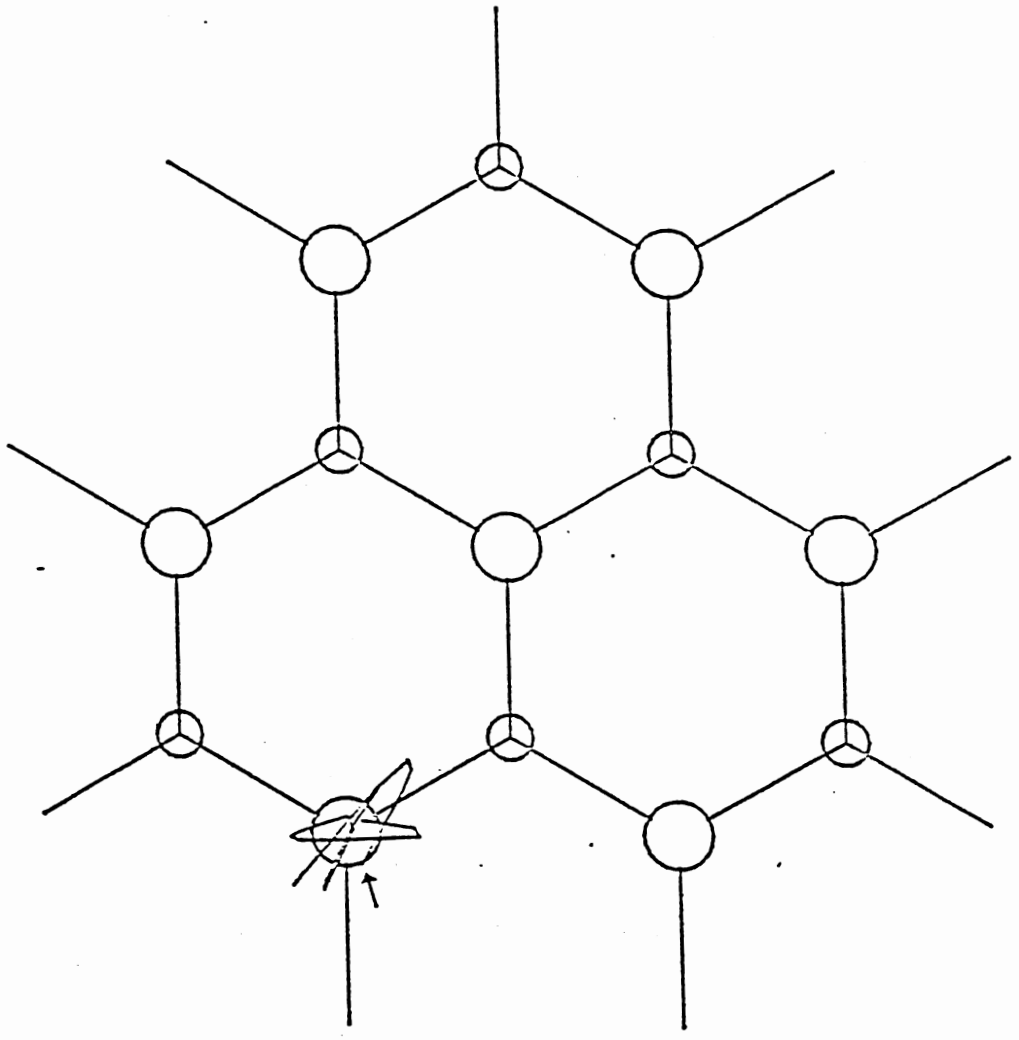

Figure 25. Projection of a hydrogen atom trajectory onto the Si(111) surface plane. The trajectory is deflected from its initial aiming point by an available outer top site. No migration occurs upon chemisorption in the outer top site. Initial incidence angle is 30° and the surface has five available top sites.

Figure 26 shows a series of translational energy distributions for various coverages of hydrogen on the Si(111) surface and three different initial azimuthal angles. In all cases, the initial hydrogen-atom relative translational energy is 0.126 eV. Figure 27 shows a similar series of scattering angle distributions for different coverages and different initial angles. Each row in the series shows the product translational energy or scattering angle distributions at a specific surface coverage of hydrogen. The rows are set up as follows:

Row 1: Each top site on the surface is covered with a hydrogen atom.

Row 2: Each top site on the surface, except for top site 1, is covered with a hydrogen atom.

Row 3: Each top site on the surface, except for top sites 1, 2, and 3, is covered with a hydrogen atom.

Row 4: Each top site on the surface, except for top sites 3 and 7, is unoccupied.

Row 5: Each top site on the surface is unoccupied.

Each column in the series shows the product translational energy or scattering angle distribution for the different coverages at a specific initial azimuthal angle. The columns have initial azimuthal angles as follow:

Column 1: 0°.

Column 2: 15°.

Column 3: 30°.

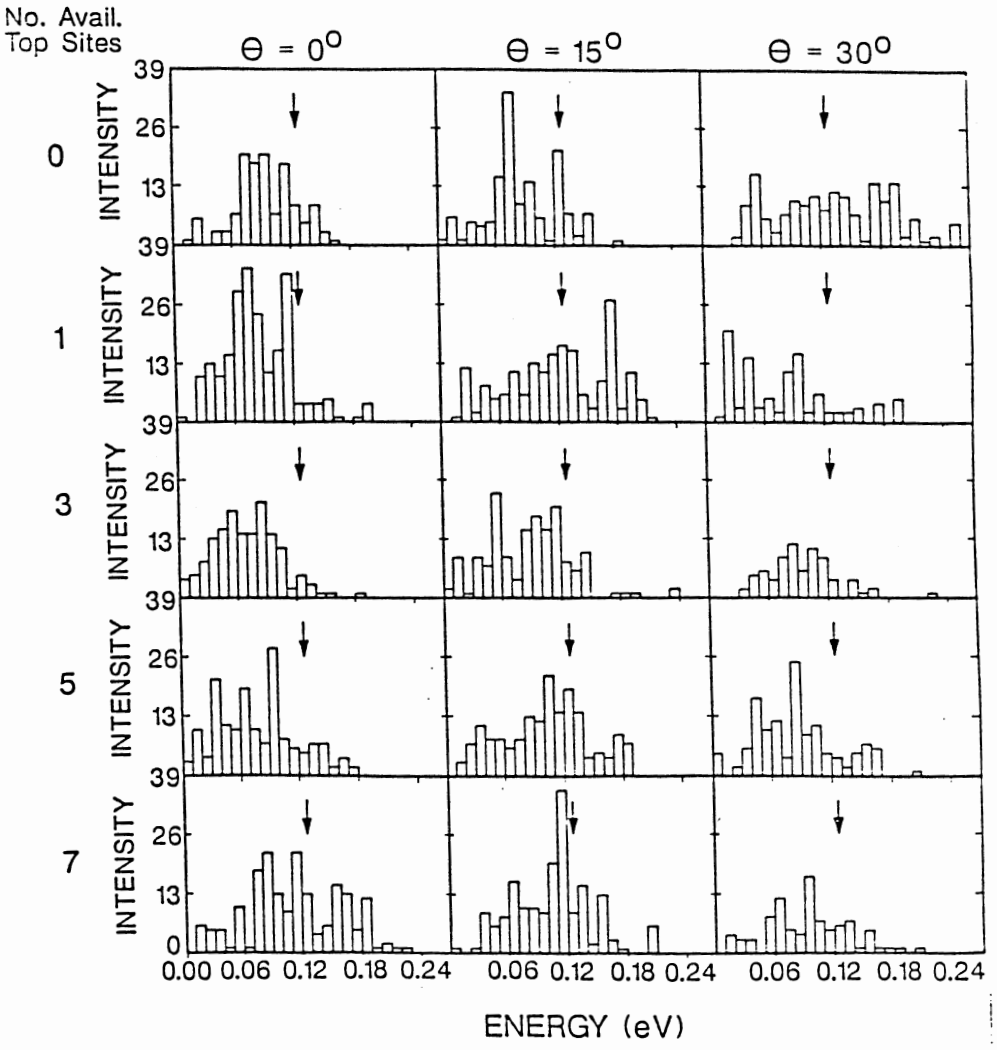

Figure 26. Product translational energy distributions for scattered hydrogen atoms. Each row specifies a surface coverage and each column specifies an initial incidence angle.
Row 1: Fully covered surface
Row 2: One available top site
Row 3: Three available top sites
Row 4: Five available top sites
Row 5: Seven available top sites
Column 1: Initial angle is 0°
Column 2: Initial angle is 15°
Column 3: Initial angle is 30°
Arrows designate initial translational energy.

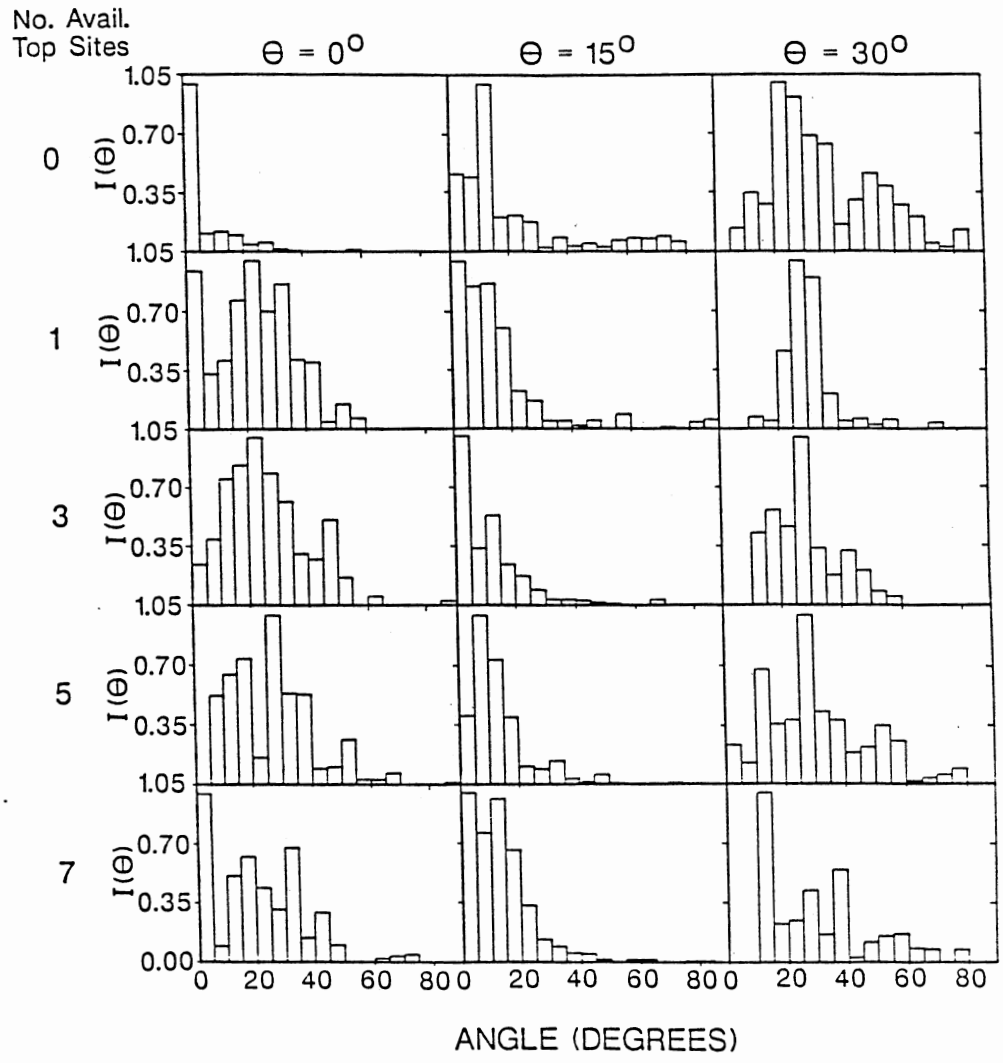

Figure 27. Scattering angle distributions for scattered hydrogen atoms. Ordering is the same as in Figure 26.

From these plots, direct comparison can be made of the scattering distributions as functions of surface coverage and initial azimuthal angle.

Product Translational Energies as a Function of Initial Angle. For the fully covered Si(111) surface, the distribution broadens as the initial azimuthal angle increases. For this surface coverage, the incoming hydrogen is aimed directly at a surface silicon atom which has a hydrogen occupying its top binding site. The distributions indicate that energy transfer is quite efficient when the hydrogen strikes the Si-H bond in a sideways manner. Energy transfer at 30° is efficient for both loss of energy and gain of energy by the incoming hydrogen atom, although energy transfer to the latter clearly predominates.

For all other coverages, the incoming hydrogen is directly aimed at a silicon atom with an unoccupied top site. There does not appear to be a trend among these series, other than showing that energy transfer occurs for all surface coverages and all initial angles and in all cases, energy transfer to the lattice predominates. Table V, Appendix gives the average product translational energies for each set of scattered trajectories.

Product Translational Energies as a Function of Surface Coverage. For an initial azimuthal angle of 0°, except for the surface in which all top sites in the

reaction zone are unoccupied, the amount of energy lost to the surface by the incoming hydrogen upon impact increases with decreasing surface coverage. The distributions broaden and flatten out with decreasing surface coverage. The "clean" surface is the most efficient in this series with regard to energy transfer from the lattice to the incident hydrogen atom.

For the 15° distributions, no trend is readily apparent among the different surface coverages. The most broad and flattest distribution is for scattered hydrogen atoms from a surface with one available top site.

For the series of distributions with an initial angle of 30°, the fully hydrogen-covered Si(111) surface is the most efficient for energy transfer to and from the surface. The rest of this series does not appear to have any remarkable features.

Scattering Angles as a Function of Initial Azimuthal Angle. For full surface coverage, the scattering distributions broaden with increasing initial azimuthal angle. The distribution at an initial angle of 30° is bimodal, with one peak at 20-25° and the other peak at 50-55° indicating classical rainbow scattering (2a,89). This effect is enhanced at the larger initial angle of 30° because as the incoming atom approaches the surface, it must travel over an open site and its course is diverted somewhat (See Table IV, Appendix; 98% of the

trajectories are deflected upon approach to initial impact point). Additionally, the surface atoms are moving. As a result, a partial averaging over impact points is achieved which produces rainbow scattering (2a,89). Coverages with 1, 3 and 5 available top sites do not exhibit rainbow scattering. This is due to the fact that these coverages do not have the translational symmetry required for rainbow scattering (2a,89). Although the "clean" surface (7 available top sites) has translational symmetry and a majority of the trajectories are deflected upon approach to initial impact point (see Table IV, Appendix), suggesting that there is at least partial averaging over impact points, statistics are not good enough to determine if the scattering distribution at 30° is showing a rainbow effect.

In most cases, specular scattering is observed. There are, however, some notable exceptions, especially at a 0° incidence angle.

Scattering Angles as a Function of Surface Coverage. For scattering trajectories with initial angle of 0°, the scattering angle distributions show the same general features for all surface coverages (with the exception of the fully covered surface). The large peak at 0° scattering angle could be a result of poor statistics. Generally, the scattering is non-specular with the peak occurring between 20-30°.

Distributions for atoms incident at 15° show the same structure with decreasing surface coverage; however, the distributions broaden with increasing coverage.

With the exception of the fully covered surface, scattering distributions for trajectories with initial angle of 30° broaden significantly with decreasing surface coverage. While this could be an artifact of the limited number of trajectories used in the distribution, it appears that specular scattering occurs at the surface with one available top site, and approaches a cosine-like distribution with decreasing surface coverage.

Sticking Probabilities as a Function of Angle.

Figures 28(a), (b), (c), (d), and (e) show sticking probabilities as a function of angle for the five different surface coverages. Figures 28(b), (c), (d), and (e) show similar behavior, with an increase in sticking probability with increasing angle. These correspond to partial coverages of surfaces. Figure 28(a) corresponds to the fully covered surface, where the incoming hydrogen atom is aimed directly at a silicon atom whose top site is occupied by another hydrogen. The remarkable difference in the behavior of the sticking probability for this surface is at 30°. In all other cases, the sticking probability is approximately 0.5. In this case, the sticking probability is approximately 0.12. This effect can be correlated with the scattering

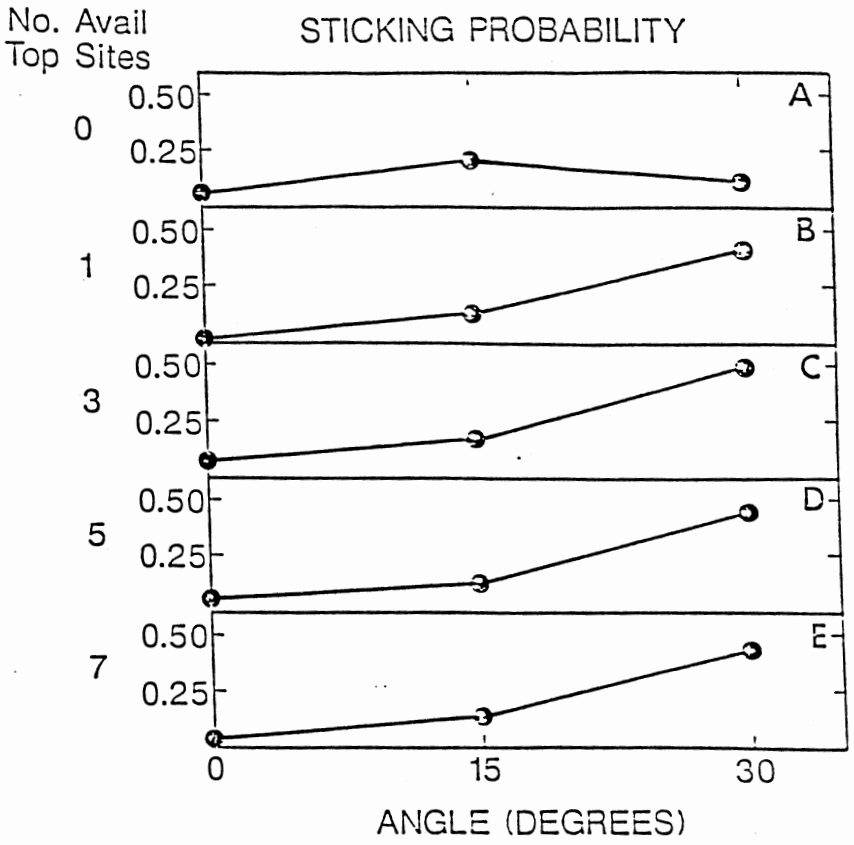

Figure 28. Sticking probabilities as a function of initial angle for five different surface coverages.
A. Fully covered surface
B. One available top site
C. Three available top sites
D. Five available top sites
E. Seven available top sites

results for this surface coverage shown in Figure 26. The translational energy distributions of the scattered atoms from a fully covered surface with initial angle of 30° shows energy transfer from the surface (or adsorbed hydrogen atom) to the incoming hydrogen atom to be quite efficient, with approximately half of the scattered hydrogen atoms gaining energy, rather than losing energy. To stick to the surface, either energy must be lost from the adsorbed hydrogen to the surface, or energy must be directed to a non-dissociative mode. Energy gain by an incoming hydrogen atom would decrease the likelihood of sticking in either case.

Sticking Probability as a Function of Surface Coverage. Figure 29 shows sticking probabilities as a function of available top sites in the reaction zone. For all coverages (with the exception of the fully covered surface at 30°, the sticking probabilities are constant as a function of available top sites.

There appears to be no difference in the number of chemisorbing trajectories with respect to surface coverage; however, as Table IV, Appendix shows, there is a difference in the number of migrating trajectories. In our investigation of energy transfer discussed below, we have concluded that although a migrating atom may lose some energy necessary to continue motion across the surface when it comes into contact with another adsorbed hydrogen, the main effect of hydrogen coverage on the

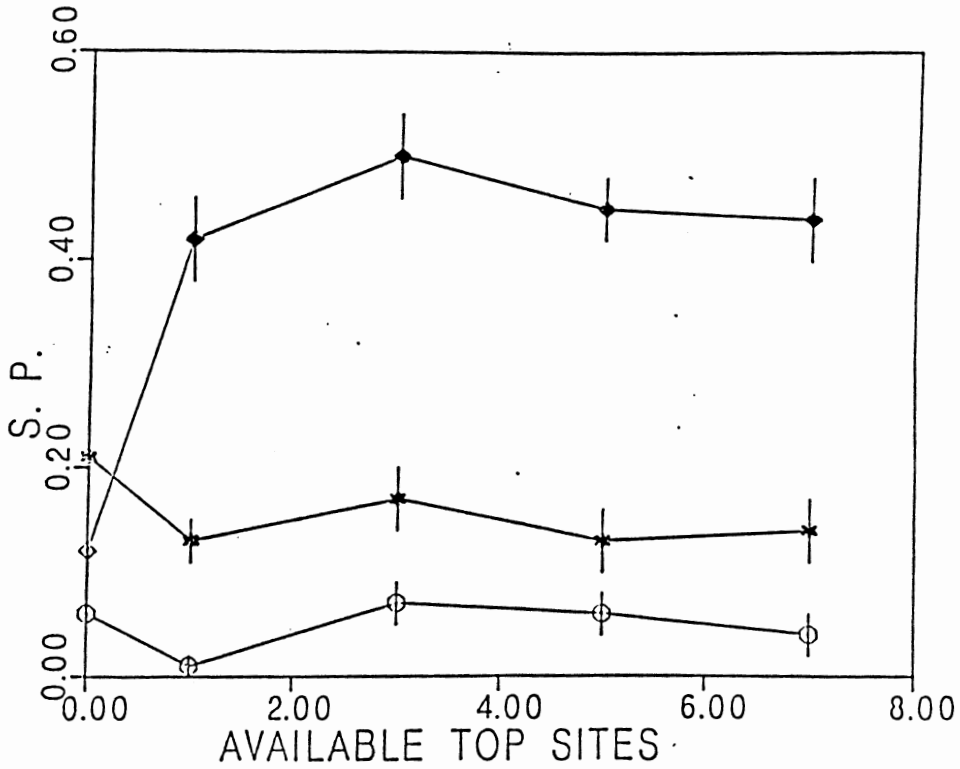

Figure 29. Sticking probabilities as a function of available top binding sites. Curve with points denoted by circles has 0° incidence. Curve with points denoted by stars has 15° incidence. Curve with points denoted by diamonds has 30° incidence.

surface with regard to migration is to block adsorption sites and hinder motion on the surface.

Energy Transfer Mechanisms. Examination of the trajectories and the scattering distributions shows that the main energy transfer mechanism is from the impacting hydrogen atom to the surface, unless the hydrogen atom hits an Si-H bond at an angle. Figure 30 shows the change in energy experienced by an impacting hydrogen atom and the Si(111) lattice during a typical chemisorptive trajectory. The plot shows a direct correlation of energy lost from the impacting hydrogen to the lattice. We investigated the possibility that energy would transfer through interaction with an adsorbed hydrogen. Figure 31 shows the changes in energy experienced by the adsorbing hydrogen, the Si(111) surface, and an adsorbed hydrogen atom on the surface. Note that at approximately 0.11 ps, the impacting hydrogen atom hits the surface hydrogen atom, and approximately 0.2 eV is transferred from the impacting hydrogen atom to the surface hydrogen atom. Approximately 0.1 eV is immediately regained by the impacting hydrogen. The remaining 0.1 eV retained by the surface hydrogen gradually flows into the surface.

To gain more understanding of the mechanism of energy transfer to the lattice, we carried out a series of calculations in which we monitored the energy in a hydrogen atom adsorbed in a top site on a Si(111)

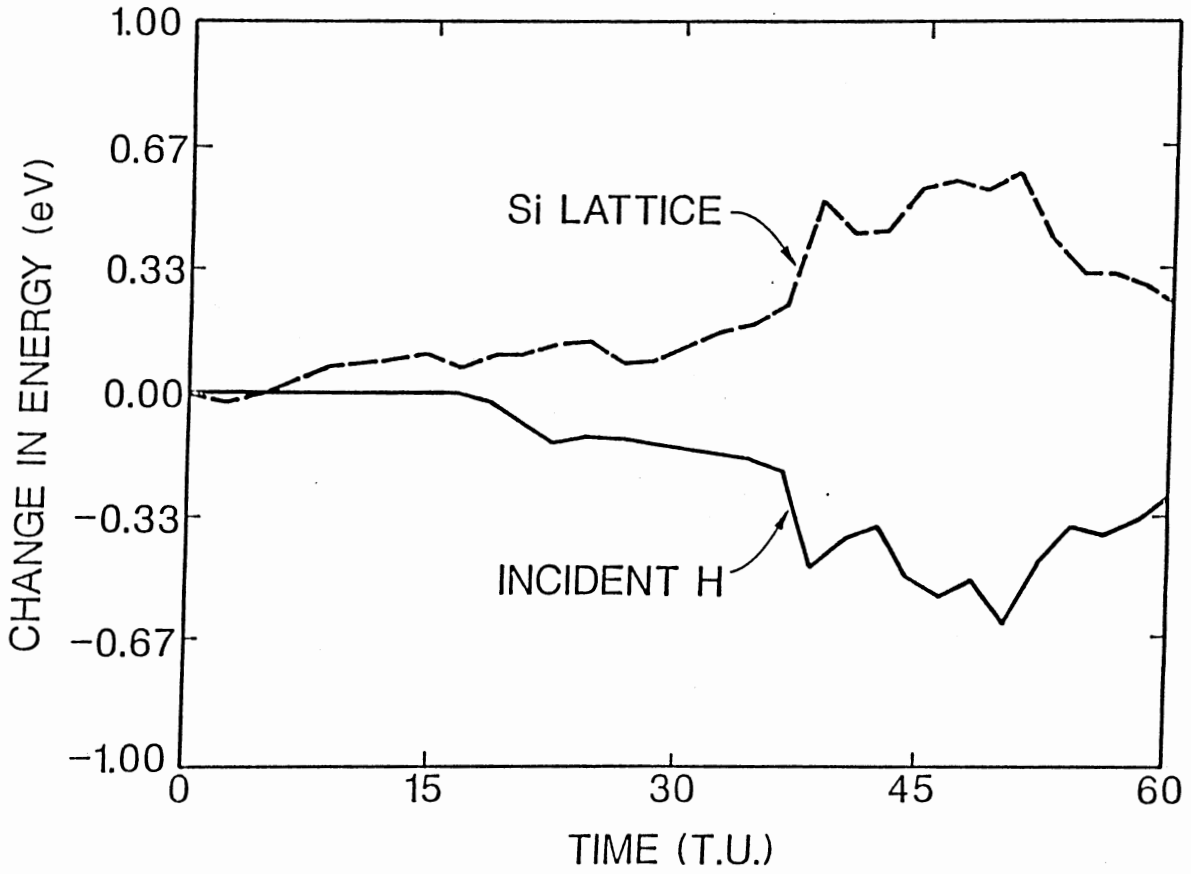

Figure 30. Change in energy of incident hydrogen atom (solid line) and the Si(111) lattice (dashed line) in a typical trajectory which results in chemisorption. Time is given in units of 0.00539 ps.

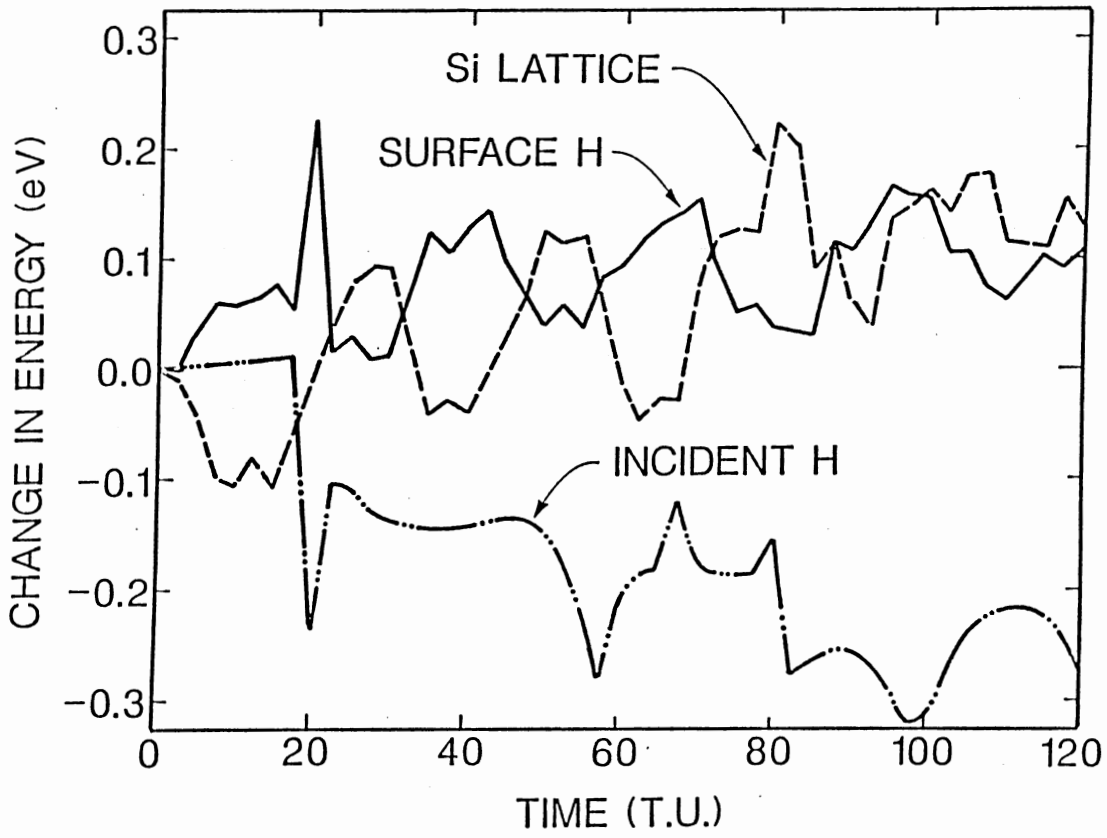

Figure 31. Change in energy of incident hydrogen atom (dot-dashed line), the Si(111) lattice (dashed line) and a surface hydrogen atom (solid line) in a trajectory which results in chemisorption. Time is given in units of 0.00539 ps.

surface. The first calculation involved putting one quantum of energy into the symmetric stretch of the Si-H bond, and zero point energy into the bend. The trajectory was monitored for 0.5 ps and energy did not flow from this bond. The next calculation involved exciting the stretch in a 2:1 resonance with the bending frequency, and following the trajectory for 0.5 ps. Again, energy did not leave the bond. We then put 2.75 eV into the symmetric stretch with thermal energy in the bending mode, and followed the trajectory for 1.0 ps. Energy did not flow out of the bond. A similar calculation with 2.75 eV equipartitioned into the X, Y and Z momentum components of the hydrogen atom showed the same result. Because we see energy transfer from scattered hydrogen atoms and from those trajectories resulting in chemisorption, it is clear that the mechanism of energy transfer is not from the symmetric stretch to the bending modes.

The next series of trajectories involved simulating the situation that corresponds to the instant of hydrogen-atom chemisorption. At the point of chemisorption, the hydrogen atoms are in a highly excited vibrational state. To accomplish this simulation, for each trajectory of an ensemble of 42 trajectories, the surface was allowed to undergo a long series of Markov steps to reach a non-equilibrium configuration. The surface temperature was 300 K. The hydrogen atom was

initially in a high vibrational state, selected as follows: The hydrogen atom was placed a distance of z' a.u. above the surface, where 2.6 a.u. $\leq$ z' $\leq$ 3.1 a.u. The orientation of the hydrogen atom with respect to the top binding site was selected in a random fashion, as follows: The initial azimuthal angle of the hydrogen atom was selected from a sine distribution between 0° and 30°. The polar angle was selected in the same manner as described in Eq. (29). The potential-energy experienced by the hydrogen atom in this orientation on the surface was calculated, and the kinetic energy of the hydrogen atom was randomly selected from the following range of energies:

$$|\text{P.E.}| - 0.2 \text{ eV} \leq \text{K.E.} \leq |\text{P.E.}| \qquad (53)$$

With this energy, the initial hydrogen velocity vector was assigned according to the selected orientation angles, so as to aim the hydrogen at a square area about the central lattice atom with a side length of 0.1 a.u. Limiting the initial conditions in this manner ensured a highly excited vibrational state. We followed an ensemble of 42 trajectories for 3.8×10^{-13} s and calculated the total energy of each hydrogen atom through its trajectory. Figure 32 shows the average energy of the ensemble of trajectories as a function of time. On the average, 0.2 eV of energy is lost to the surface within 0.05 ps. Therefore, the mechanism of energy transfer from the hydrogen atom to the lattice appears to

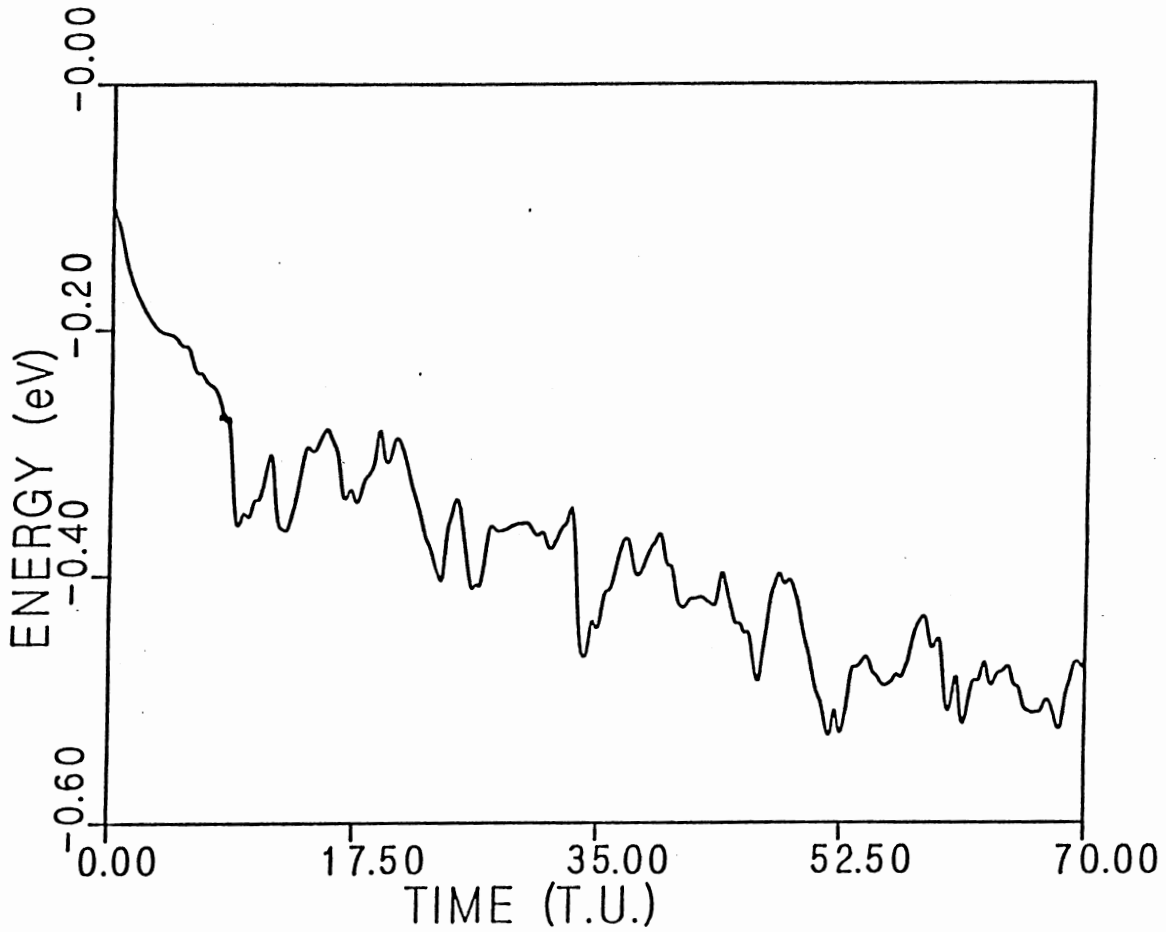

Figure 32. Average energy of initially excited hydrogen atom bound in top binding site. Surface temperature is 300 K. Time is given in units of 0.00539 ps.

involve asymmetric Si-H motion. Because our model allows motion only in the first layer silicon atoms, energy cannot transfer through the surface stretching modes; it can only transfer through the second-nearest neighbor bending terms. Asymmetric Si-H motion would cause excitation of surface bending phonon modes. This result is consistent with our observed chemisorption results as a function of angle. Chemisorption increases with increasing angle (except for the fully covered surface, discussed above). Trajectories striking the surface at a larger angle have a greater likelihood of exciting the surface bending modes and causing significant energy transfer leading to chemisorption. Trajectories striking the surface at a small angle excite the surface symmetric stretching mode, which, in our model, is inefficient in promoting energy transfer and therefore leads to little sticking.

In the study of dissociative chemisorption of H_2 on Si(111), we measured the rate of energy transfer from a highly excited chemisorbed hydrogen atom to the surface. Additionally, Agrawal *et al.* studied effect of lattice model on energy transfer in this system. (71) The studies showed energy transfer to be a first-order process with rate coefficients on the order of 10^{12} s^{-1} (discussed below). The rates are much larger than those found for thermal systems with one Si-H vibrational quantum of excess energy (90). The study on dissociative

chemisorption of H_2 on Si(111) showed no significant difference in the rate of energy transfer with different surface temperatures. The Agrawal *et al.* study (71) investigated the sensitivity of the energy transfer to surface relaxation, the number of lattice atoms explicitly included in the system Hamiltonian, and the functional form of the potential-energy surface of the lattice. We found that the rate of energy transfer is not sensitive to any of these factors. We calculated the rate of energy transfer for the ensemble of 42 trajectories. A decay plot of the results is shown in Fig. 33. The energy transfer is found to be a first-order decay process, with a rate coefficient of 1.74×10^{12} s^{-1}. The results from the dissociative chemisorption study gave similar results (see below).

Although the functional forms of the gas-surface interaction potentials used in the current calculation and previous calculations (48,49,71) were different, we obtained the same rate coefficient for energy transfer in both systems. Comparison of the two gas-surface interaction potentials is given in Figure 34. The figure shows potential energy curves for an Si-H bond used in the dissociative chemisorption of H_2 on Si(111) study, developed by Raff *et al.* (48,49) and in the H-atom scattering/chemisorption calculation. In Figure 34, the direction of the bond is 30° from the normal to the plane. The curves have significant differences. They

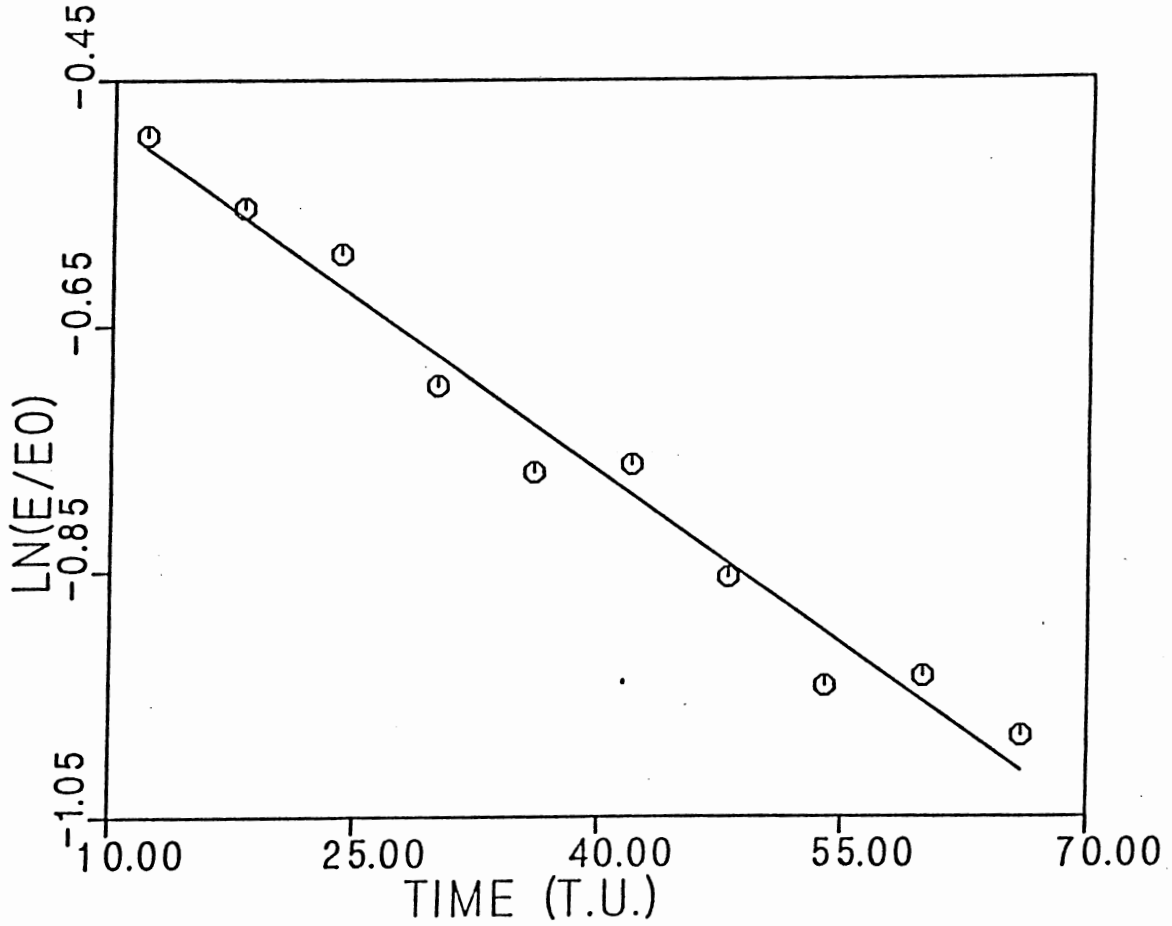

Figure 33. First-order decay plot of energy transfer from Si-H bond to Si(111) lattice. Time is given in units of 0.00539 ps.

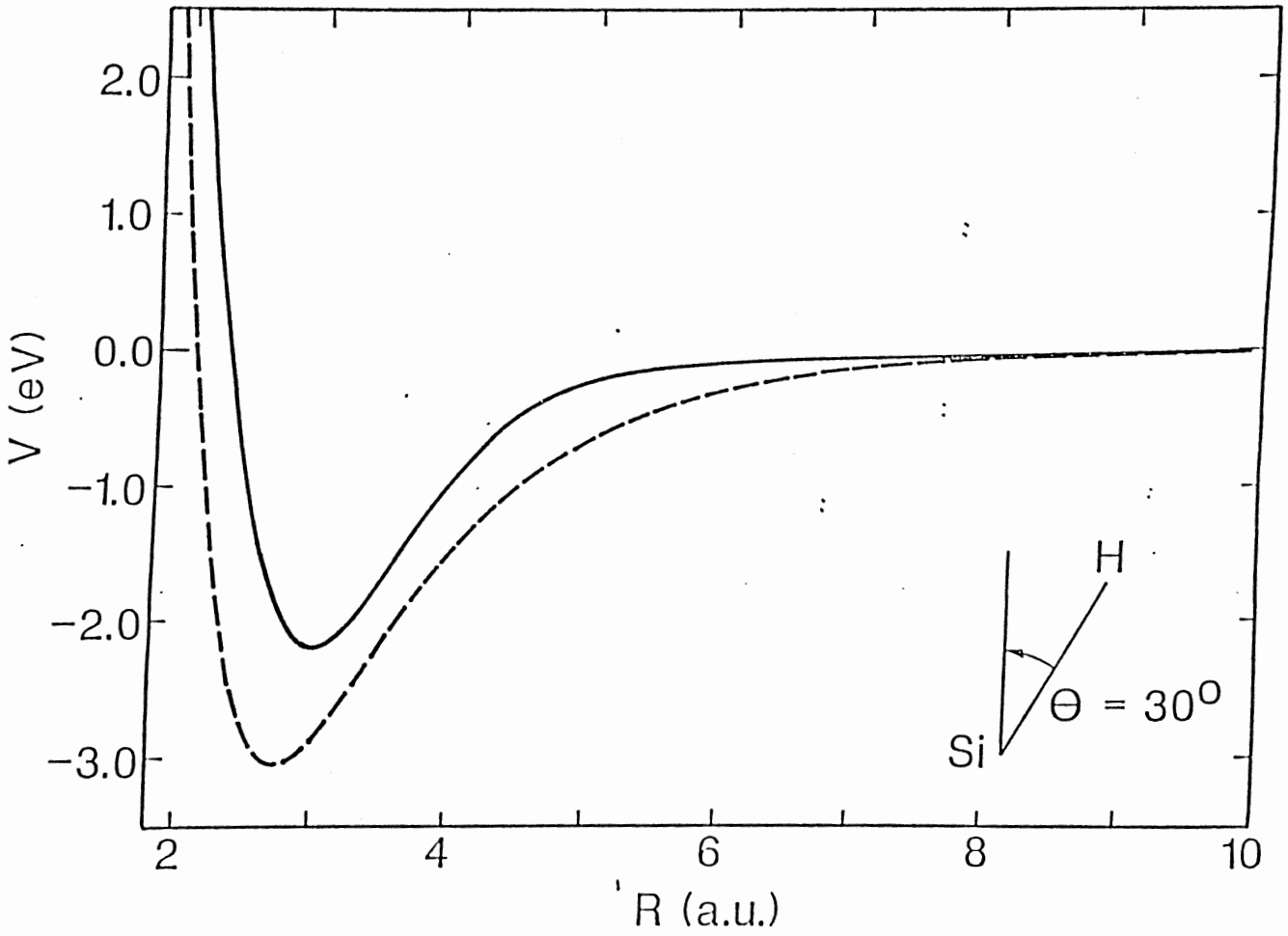

Figure 34. Si-H stretching potential for hydrogen in top site. Direction of bond is 30° normal to surface plane.

differ in well depth by 1 eV and the equilibrium positions differ by 0.2 a.u. The energy transfer is dependent upon ability to excite the surface bending phonon modes and is essentially unaffected by the variation of the gas-surface interaction potential. Both curves in Figure 34 show that upon chemisorption at this angle, enormous amounts of energy are released to surface, sufficient to excite the surface bending phonon modes although the fine detail of the curves are significantly different. To further substantiate this conclusion, Agrawal (91) calculated a 50% increase in rate of energy transfer upon reducing the bending force constant of the Keating potential to 80% of its original value. Thus, energy transfer in this sytem is not dependent on the fine detail of the gas-surface interaction potential, but rather the capacity to excite the surface bending phonon modes. The fine detail of the gas-surface interaction potential affects sticking probabilities (71), scattering distributions, and behavior of adsorbed and scattered atoms. Additionally, there are only 7 moving lattice atoms in this study; there were 25 moving lattice atoms in the previous study. This indicates that the energy transfer rate is not dependent on model size. Similar results were obtained in previous studies (71).

Dissociative Chemisorption/Scattering of H_2 on Si(111)

The spatial and translational and internal energy distributions of H_2 molecules scattered from the Si(111) surface have been computed under various conditions. Each distribution curve was obtained from the results of approximately 200 scattered trajectories.

In general, H_2 scattering from Si(111) tends to be specular and elastic. Figures 35(a) and 35(b) show the incident and scattered distributions, respectively, of H_2 azimuthal angles at 1500 K. The distributions truncate at 54° for reasons discussed in Chapter III. A point-by-point comparison of the two distributions shows them to be nearly identical, which is the expected result for predominately specular scattering.

Figures 36 and 37 give the final translational energy distributions for scattering of a beam of H_2 molecules with an initial translational energy of 0.50 eV from a Si(111) surface at 300 and 1500 K, respectively. Although there is some broadening of the distributions which increases with increasing surface temperature, the scattering is predominately inelastic, particularly at lower surface temperatures. The net energy transfer is near zero as shown by the first moments of the distributions given in Table VI, Appendix.

Figures 38 and 39 show the resulting distributions of H_2 vibrational energy for surface

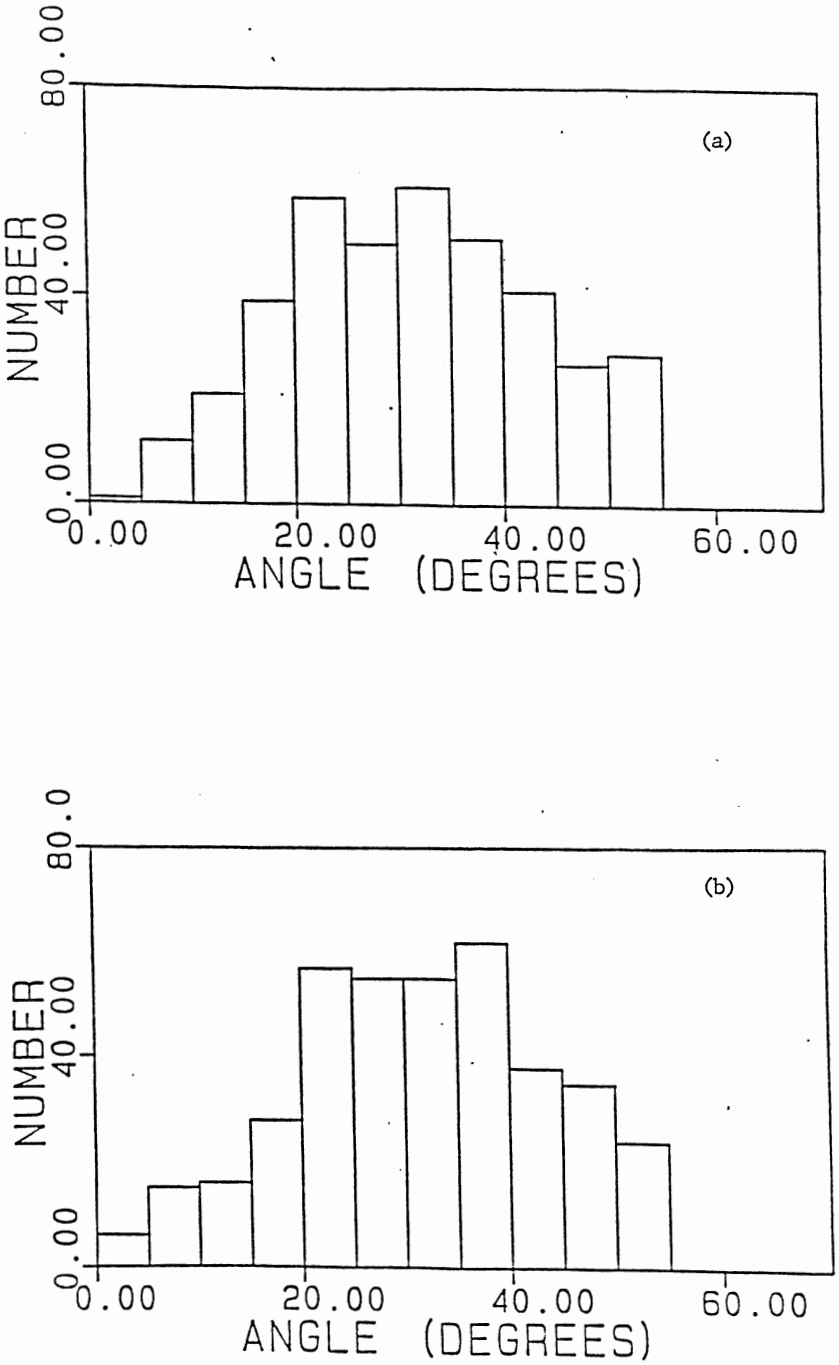

Figure 35. Distributions of (a) incidence angles and (b) scattering angles of H_2 molecules at T = 1500 K.

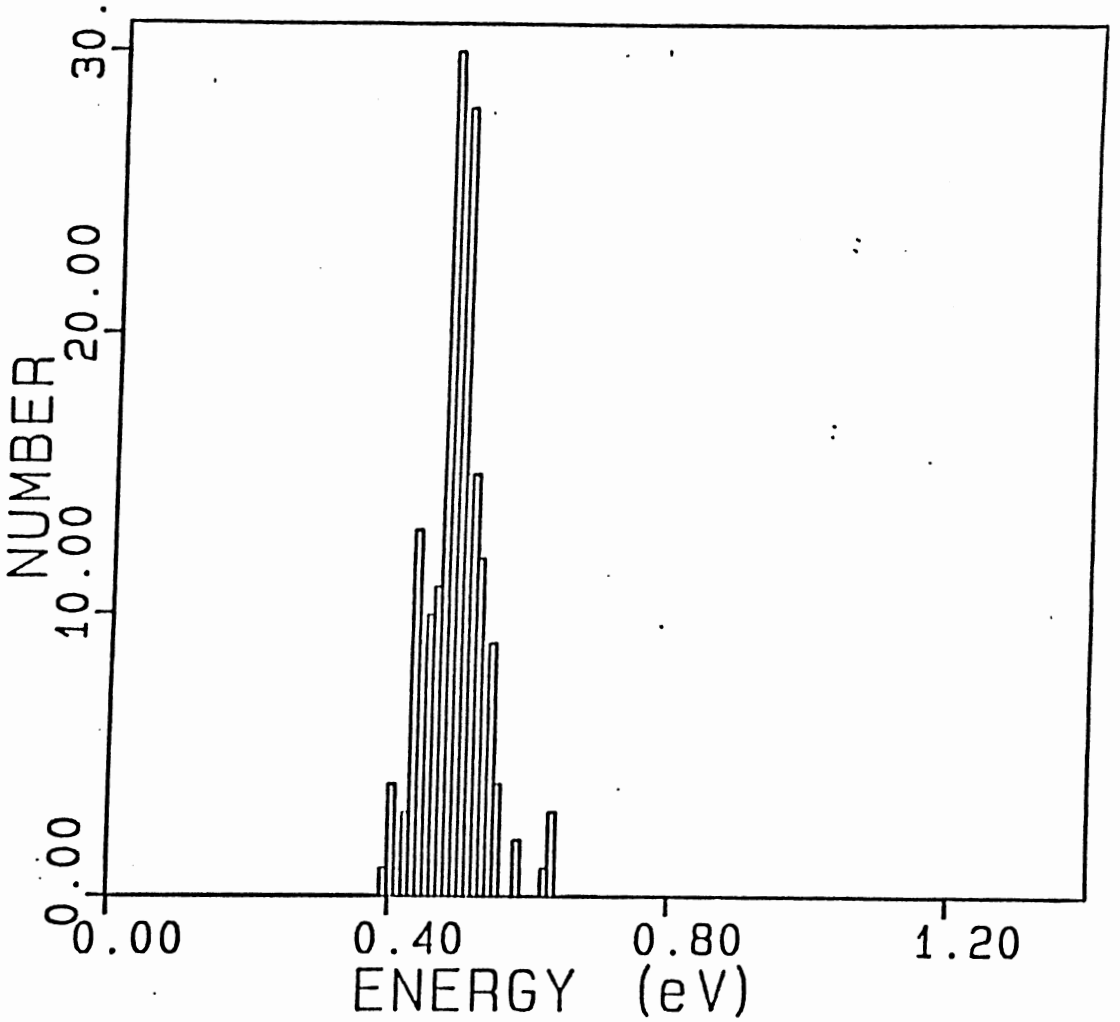

Figure 36. Product translational energy distribution of scattered H_2. $\langle E \rangle_i$ = 0.5 eV, T = 300 K.

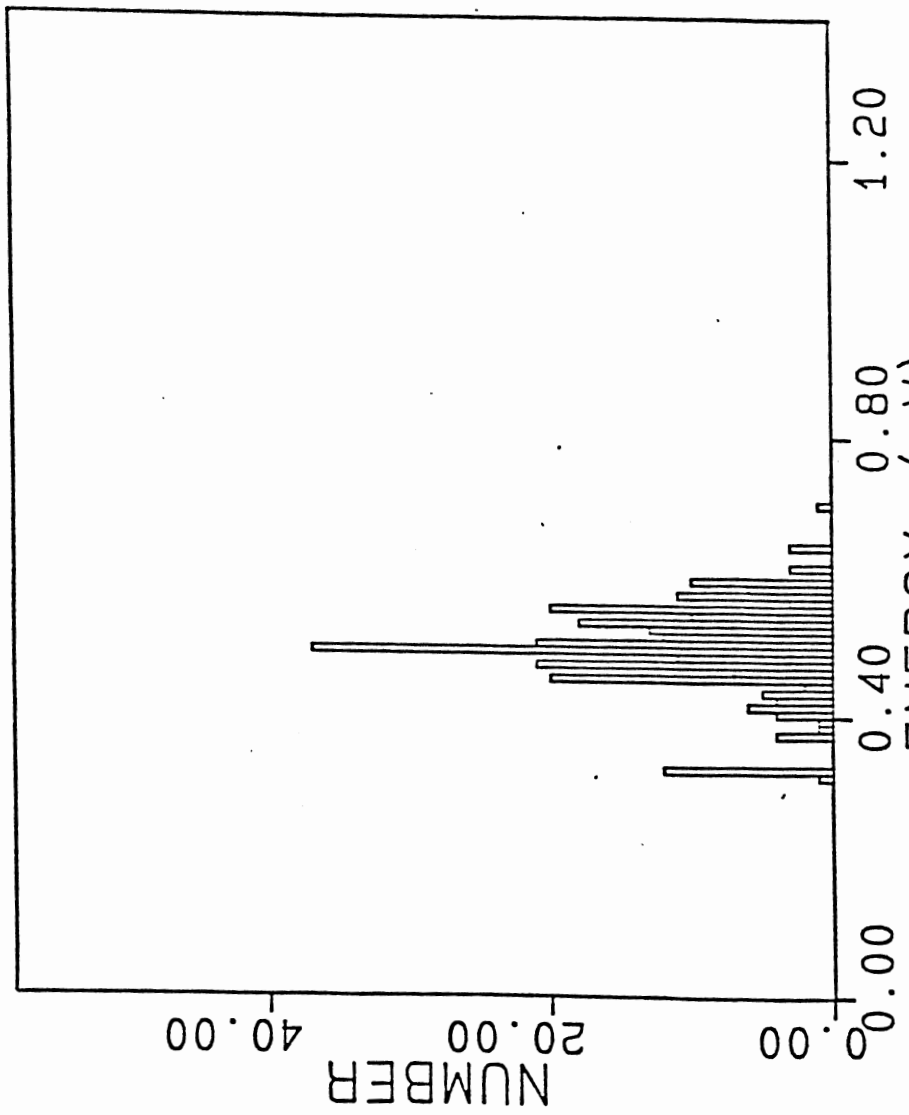

Figure 37. Same as Figure 36, except T = 1500 K.

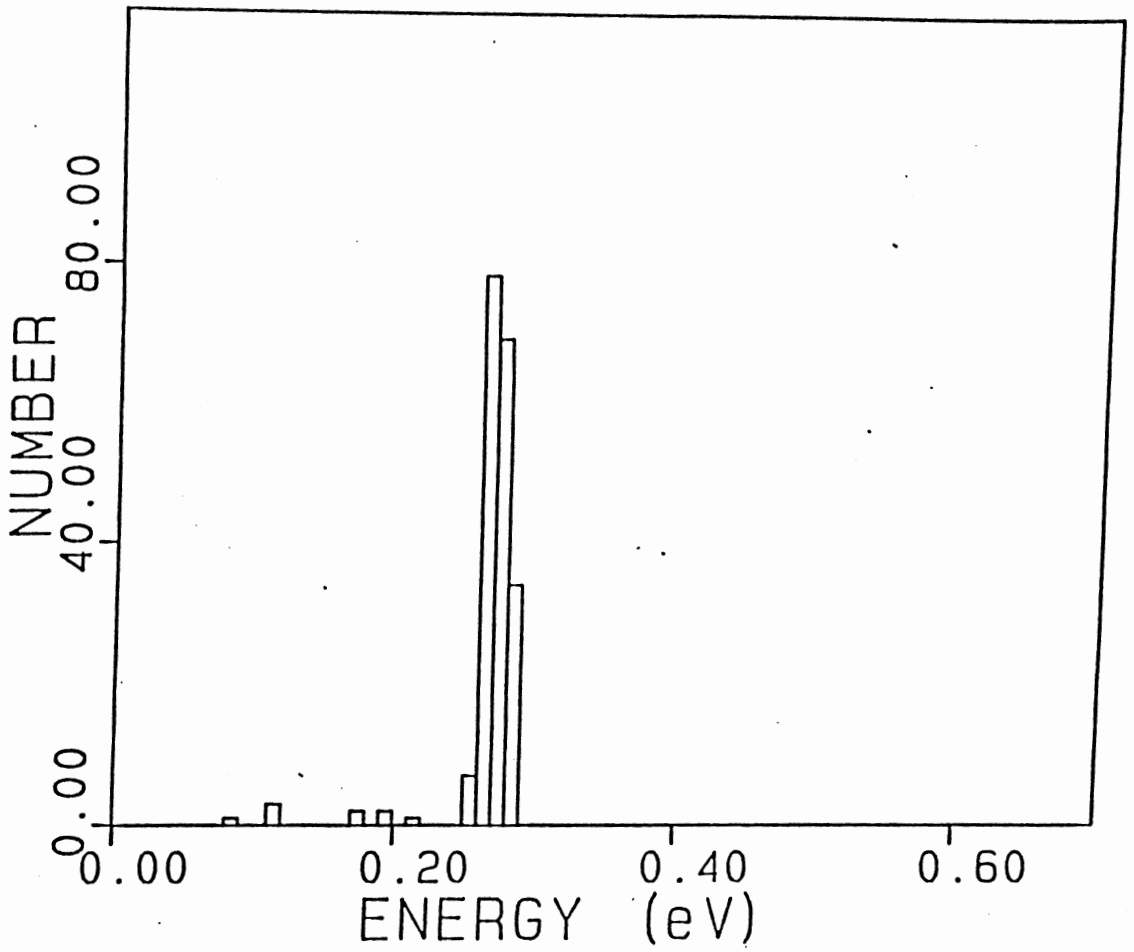

Figure 38. Product vibrational energy distributions of scattered H_2 molecules. $\langle E(vib)\rangle_i$ = 0.2729 eV, T = 300 K.

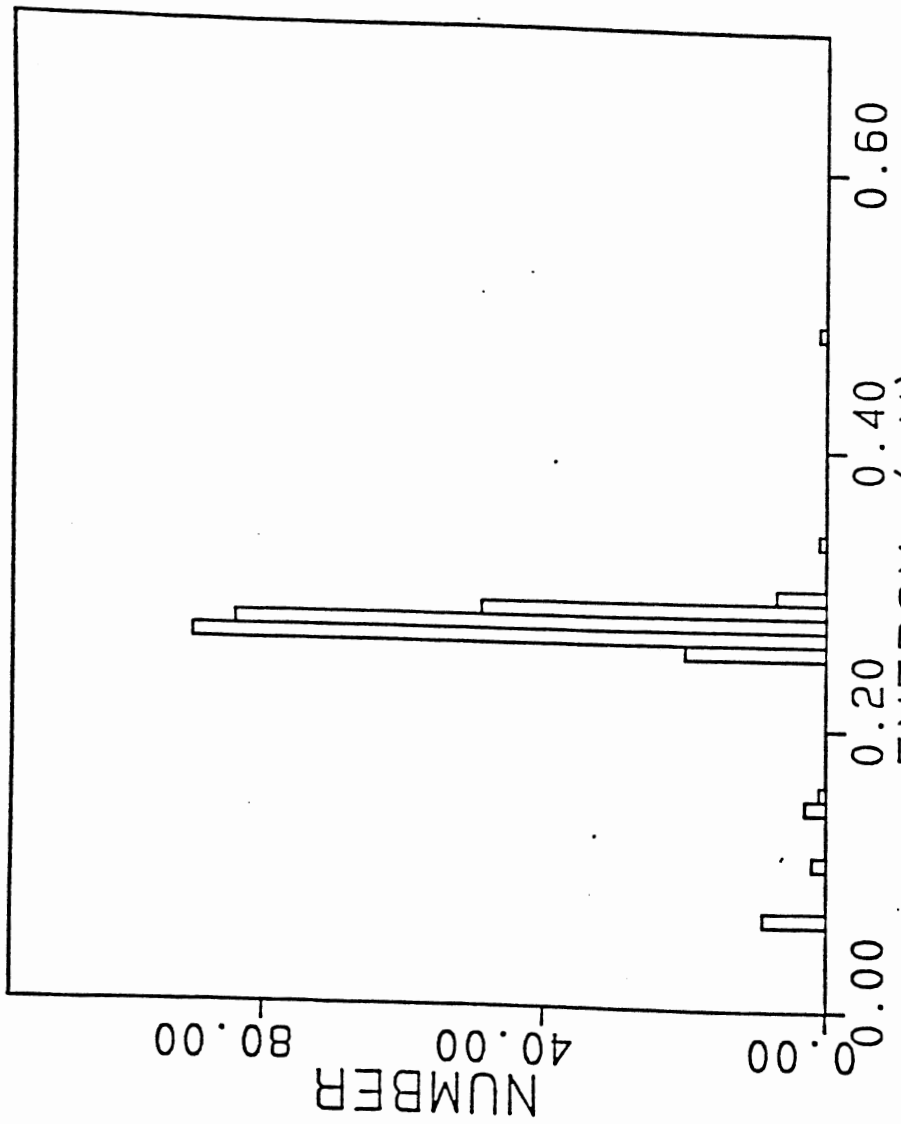

Figure 39. Same as Figure 38, except T = 1500 K.

temperatures of 300 and 1500 K, respectively. In each case, the initial H_2 energy corresponds to zero-point vibrational energy and 0.5 eV in translation. Since the calculations are classical, some broadening of the vibrational distributions is obtained upon scattering. However, there are no root trajectories corresponding to the transfer of a single vibrational quantum for T=300 K and only a few at T=1500 K. There is consequently little vibrational energy transfer in the scattering process. This is reflected in the nearly unchanged first moments given in Table VI, Appendix.

Figures 40 and 41 give the H_2 rotational distributions for surface temperatures of 300 and 1500 K, respectively. In each case, the initial H_2 rotational energy corresponds to J = 1 (0.0151 eV) with an H_2 translational energy of 0.50 eV and zero-point energy in the H_2 vibrational mode. As can be seen,, there is very little rotational energy transfer. At T = 300 K, there are only a few root trajectories corresponding to the J=1-->J=2 transitions. At 1500 K, the probability of energy transfer increases, but it is still relatively small. The first moments of the distributions are given in Table VI, Appendix.

Lower limits for sticking probabilities of dissociated H_2 molecules were calculated from the results of 200 trajectories at each of three temperatures, 300, 1000, and 1500 K. Because there exists a 0.18 eV barrier

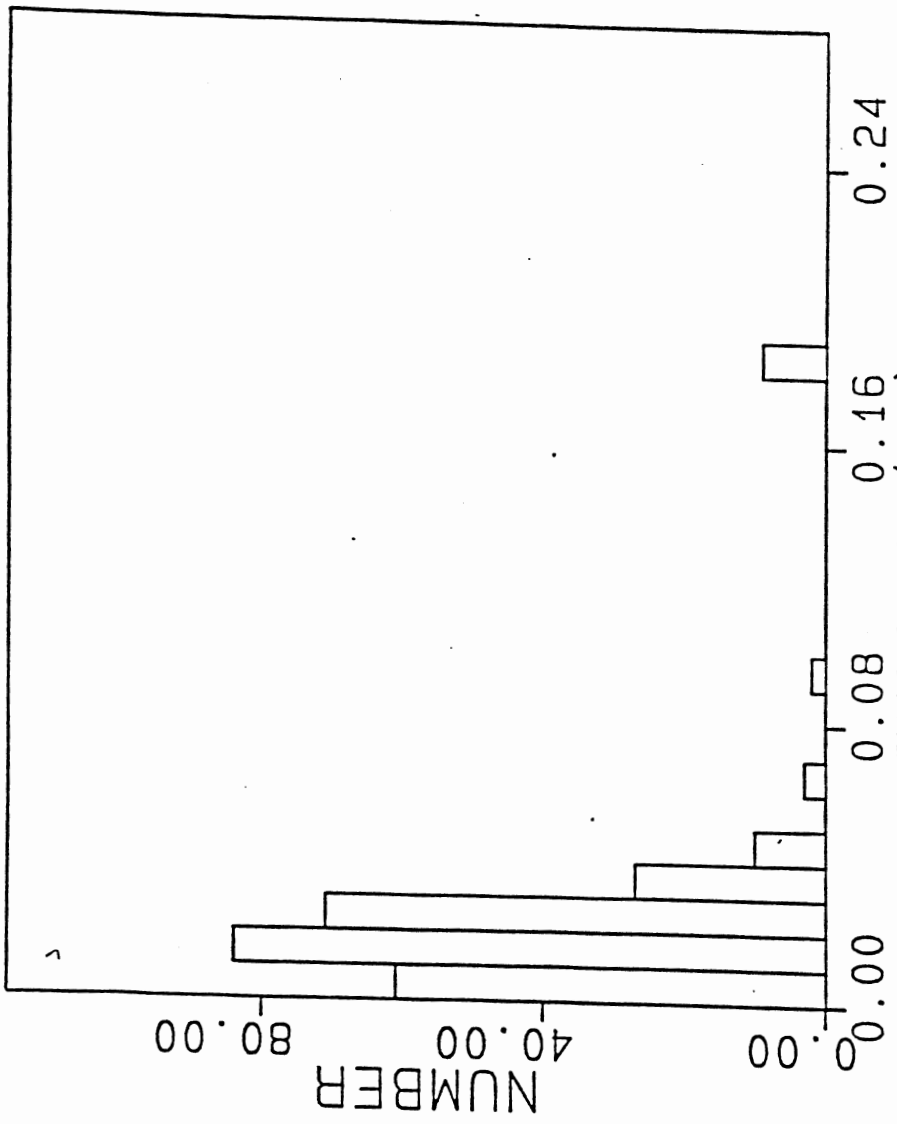

Figure 41. Same as Figure 40, except T = 1500 K.

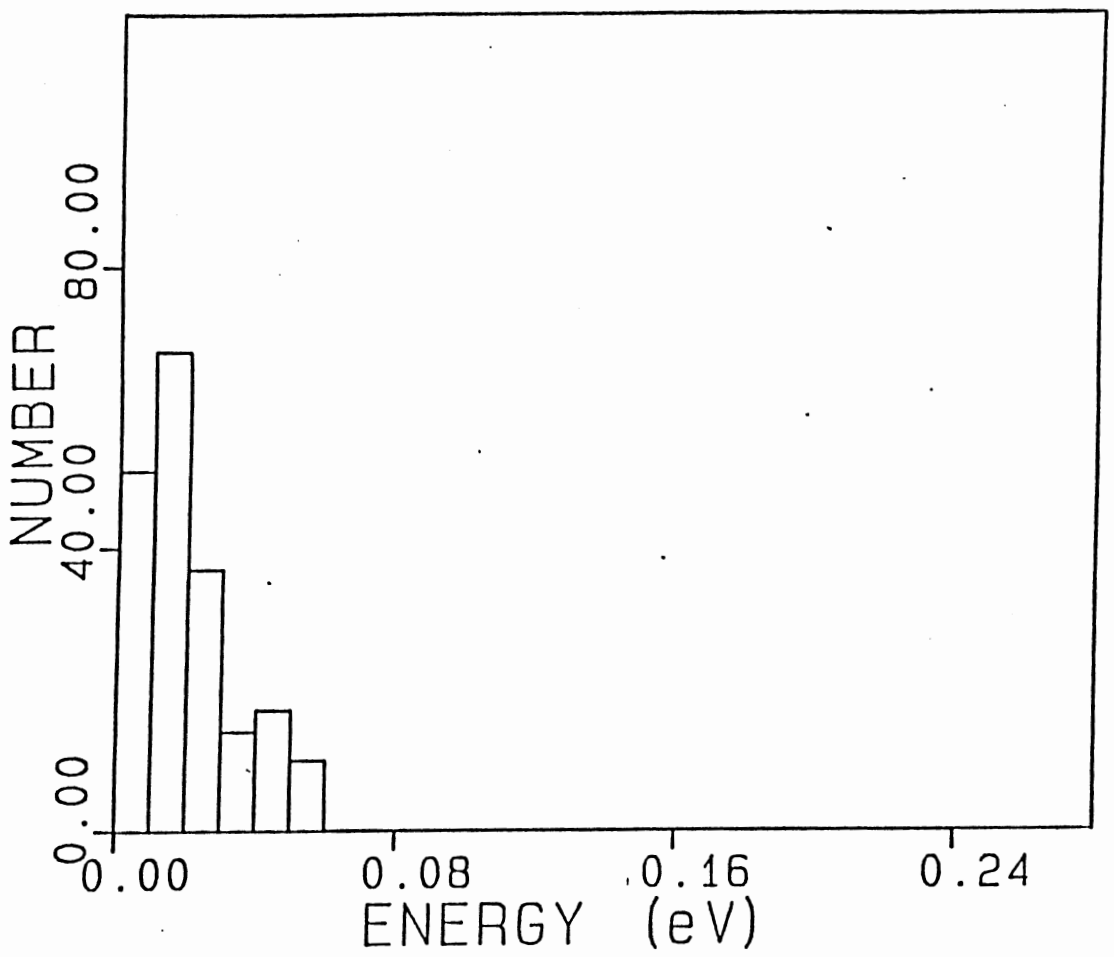

Figure 40. Product rotational energy distributions for scattered H_2 molecules. $\langle E(rot) \rangle_i$ = 0.0151 eV, T = 300 K.

to dissociative chemisorption, molecules with incident kinetic energy in the normal momentum component less than this barrier have a high probability of scattering from the surface. Because integration of trajectories in this system is very expensive in terms of computer time, we have assumed that trajectories with incident kinetic energy in the normal momentum component less than this barrier will uniformly result in scattering from the surface and have omitted their integration. Since some of these trajectories will actually result in sticking and subsequent dissociative chemisorption, our calculated sticking probabilities represent lower limits to the true values. At 300 K, the calculated sticking probability is too small to compute without a much larger statistical sample. At 1000 and 1500 K, we obtain lower limits of 0.00461 and 0.0327, respectively. Orientation of the incoming H_2 molecule with respect to the surface is an important factor in sticking on our potential-energy surface. The molecules approaching with the H-H bond parallel to the Si(111) surface plane have a much higher sticking coefficient than those which approach with a perpendicular orientation. Similar results have previously been otained for dissociative chemisorption on metallic surfaces. (92)

All of the H_2 molecules dissociate upon adsorption. In every case, both hydrogen atoms were chemisorbed. Adsorption of molecular hydrogen was not

observed, in agreement with experimental studies (7,20). Figures 42 and 43 show a typical trajectory which results in dissociative chemisorption for both hydrogen atoms. Figure 42 shows the H-H separation as a function of time during the trajectory. The two atoms first move far apart on the surface and then once again approach to within 6-8 a.u. as the highly mobile atoms move about on the surface. Figure 43 shows the distance between the two hydrogen atoms and the Si(111) surfce plane. Clearly both atoms are chemisorbed. The figure also illustrates that their binding sites are located near the open site in the surface plane as expected. This is shown by the fact that the vibrational motion oscillates about the surface plane [R(Si-H) = 0] rather than above the plane as would be the case if the on-top site were involved.

Upon dissociative chemisorption, between 2.5-4.3 eV is released. This energy is primarily deposited into the vibrational motion of the hydrogen atoms relative to the Si(111) surface. The large vibrational amplitudes seen in Fig. 43 illustrate this point. Although this excess energy is rapidly dissipated among the phonon modes of the lattice, the hydrogen atoms are initially very mobile on the surface as shown by Fig. 42. Using Eq. 32, we computed the hydrogen atom mobility on the surface at 300, 1000, and 1500 K. The results are shown in Fig. 44. Initially, the mobility is very large, as expected. It is also somewhat independent of surface

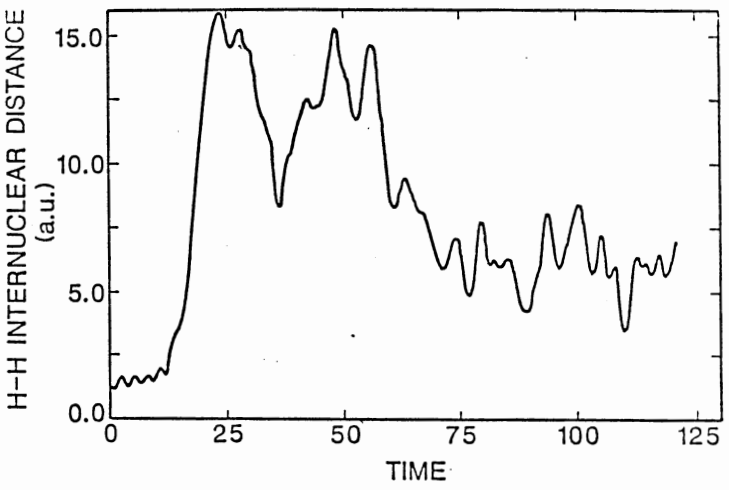

Figure 42. H-H internuclear distance as a function of time for typical trajectory resulting in dissociative chemisorption. Time is given in units of 0.00539 ps.

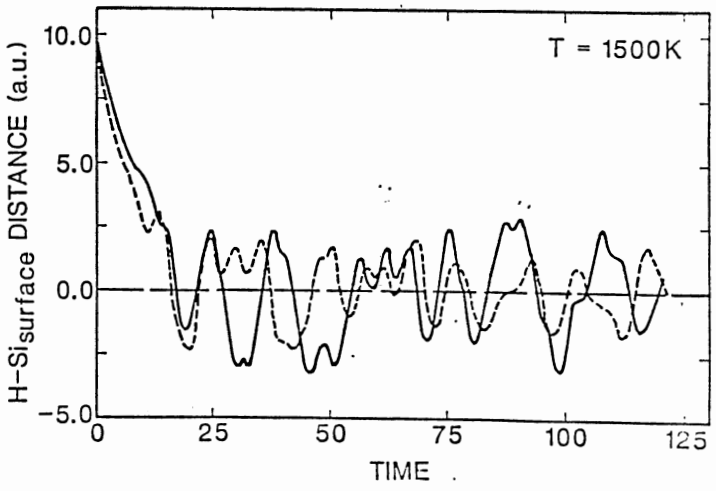

Figure 43. Same as Figure 42, except for Si-H internuclear distance.

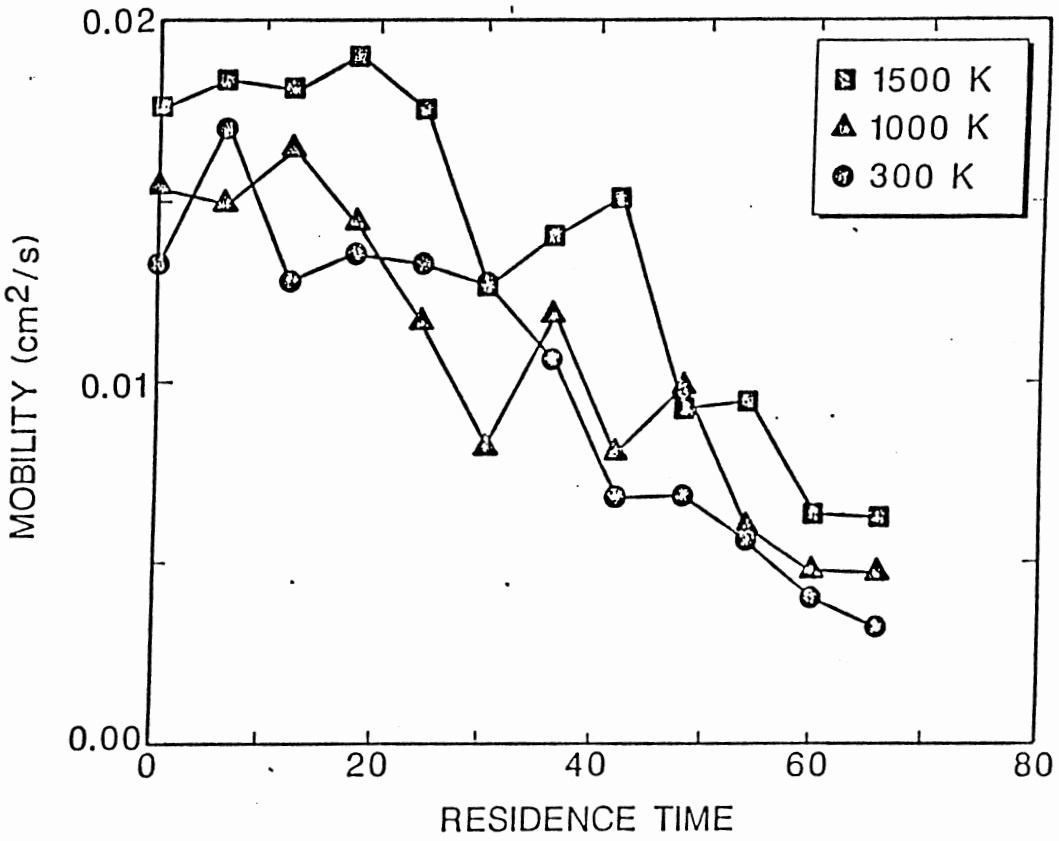

Figure 44. Instantaneous hydrogen atom mobilities computed from Eq. 32 as a function of residence time on Si(111) surface at 300, 1000, and 1500 K. Time given in units of 0.00539 ps.

temperature in that the mobilities are sometimes found to be inverted. This is due to the fact that the surface energy is a relatively minor perturbation when the hydrogen atom surface energy is 2.5 eV or more. As the residence time on the surface increases, the system moves toward thermal equilibrium and the mobilities are seen to decrease and approach the thermal diffusion coefficient with the values increasing in order of increasing temperature.

The initial hydrogen atom energy is large and is rapidly dissipated to the phonon modes of the lattice. We have computed the rate for this dissipation as a function of surface temperature. The average kinetic energy of the hydrogen atoms was computed over two Si-H vibrational periods and this quantity plotted as a function of time. The result is an exponential decay. Figs. 45 and 46 show first-order decay plots for the results at 300 and 1000 K, respectively. Clearly, the energy transfer is well described by a first-order rate law. The corresponding rate coefficients are 1.79×10^{12} and 1.03×10^{12} s^{-1}, respectively.

Hydrogen Atom Diffusion on Si(111)

Classical Results

We have calculated jump frequencies, activation energies, and pre-exponential factors for H-atom diffusion from a top to an open binding site and from an

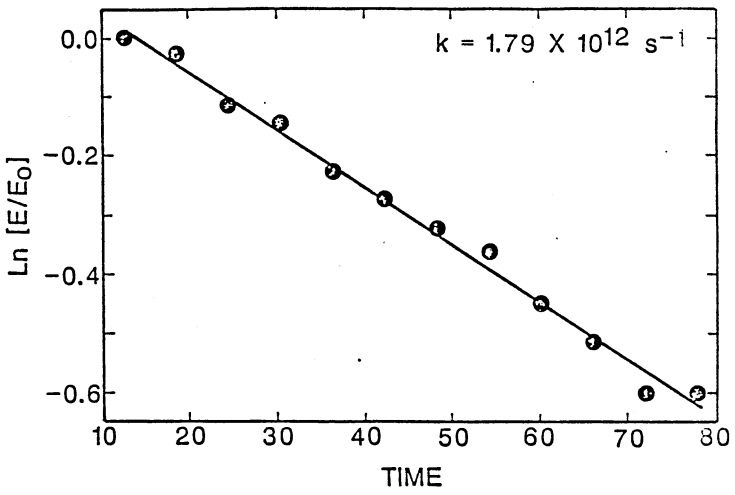

Figure 45. First-order decay plot of energy transfer from Si-H bond to Si(111) lattice. T = 300 K. Time is given in units of 0.00539 ps.

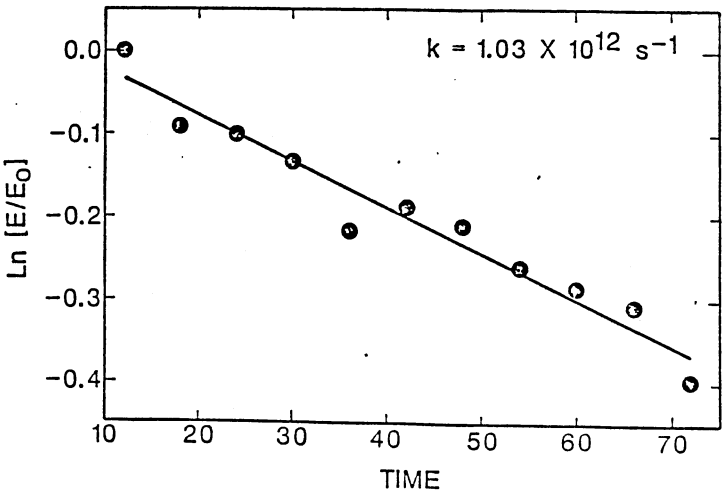

Figure 46. Same as Figure 45, except T = 1500 K.

open to a top binding site on a partially covered Si(111) surface by using Monte Carlo variational phase-space theory with a biased Markov walk containing 10^6 attempted moves. The computations were performed at 300, 600, 900 and 1200 K. The shape of the dividing surfaces and corresponding variational parameters which gave the minimum flux are given in Table VII, Appendix.

The calculated classical rate coefficients for diffusion from the top to the open site and from the open to the top site are given in Tables VIII and IX, Appendix. The rate coefficients for top to open site diffusion range from 1.5×10^{-33} s^{-1} at 300 K to 34 s^{-1} at 1200 K. This strong temperature dependence is expected for a process with such a large barrier (2.79 eV on the rigid equilibrium surface). These classical rates suggest, as we will see below, that tunneling from top to open sites is very important for this process. The classical rate coefficients for open to top site diffusion are significantly larger, ranging from 7.1×10^2 s^{-1} at 300 K to 3.1×10^{10} s^{-1} at 1200 K. Even at 1200 K, the rate of diffusion from top to open site is considerably smaller than the rate of diffusion from open to top site at room temperature. Activation energies and frequency factors were calculated from the Arrhenius plots shown in Figs. 47 and 48, which are for the classical jump frequencies for top-to-open site jumps and open-to-top site jumps, respectively. The activation

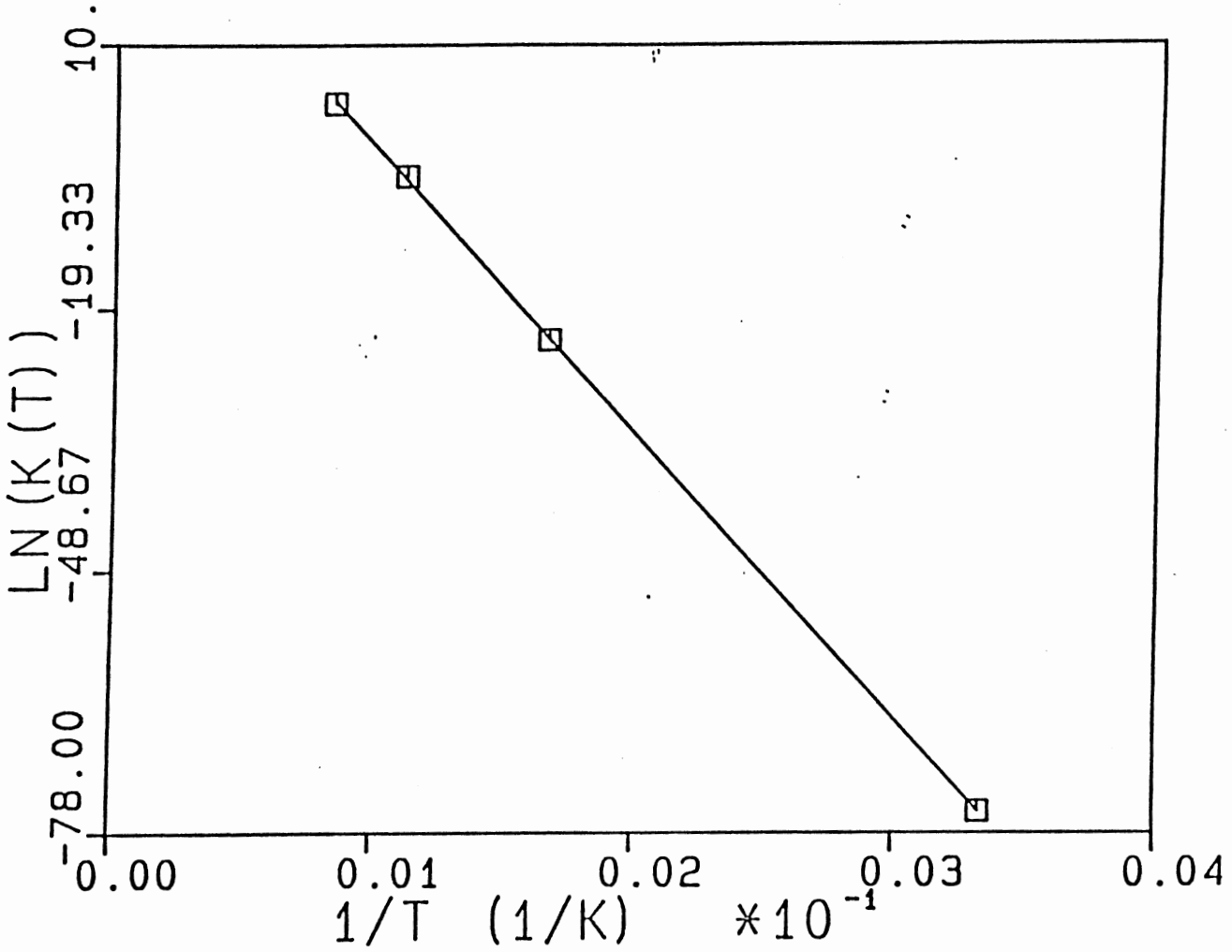

Figure 47. Arrhenius plot of jump frequencies for top-to-open site jumps.

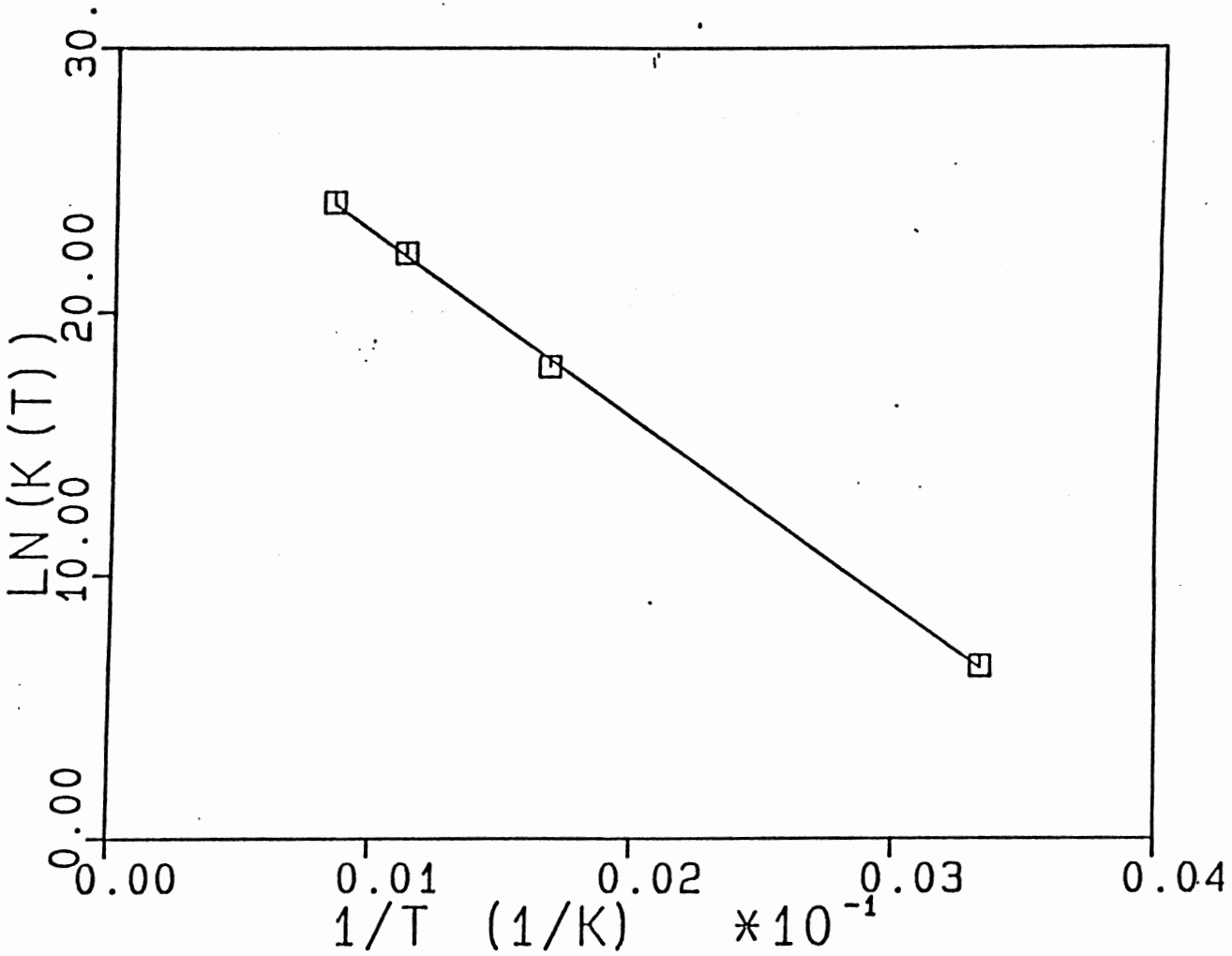

Figure 48. Arrhenius plot of jump frequencies for open-to-top site jumps.

energies for top to open site jumps is 2.74 eV and the activation energy for open to top site jumps is 0.61 eV. The pre-exponential factor for top to open site jumps is 1.4×10^{13} s^{-1} and the pre-exponential factor for open to top site jumps is 1.0×10^{13} s^{-1}.

A lower bound for the diffusion coefficient of hydrogen on Si(111) was obtained by solution of Eq. (45) at each of the temperatures for which the classical jump frequencies were calculated. An Arrhenius plot of the lower bound for the diffusion coefficient gives an activation energy of 2.77 eV and a pre-exponential factor of 0.008 cm^2/s. An Arrhenius plot of the estimated upper bound for diffusion gives an activation energy of 2.74 eV and a pre-exponential factor of 0.022 cm^2/s. Note that the activation energy calculated from the jump frequencies for top-to-open site migration is equal to activation energy calculated from the estimated upper bound of the diffusion coefficient and is very close to the lower-bound value. This indicates that the diffusion of hydrogen on Si(111) is energetically controlled by jumps from top sites to open sites. The rate-limiting step in diffusion is top-to-open site jumps, and the rate of diffusion due to open to top site jumps is significantly faster, particularly at lower temperatures (at T = 300 K, the open-to-top site jump frequency is 34 orders of magnitude greater than the top-to-open site jump frequency).

Figure 49 shows the minimum-energy diffusion path between top site and open site. The solid line corresponds to the minimum-energy diffusion path for the system at equilibrium. The points correspond to the minimum-energy configuration at circular cylindrical dividing surfaces set up along the reaction path. The points were obtained by the method that Raff *et al.* (48) suggested for extracting the minimum-energy path from Monte Carlo variational phase-space theory calculations. The procedure consists of setting up an ensemble of dividing surfaces which span the important regions of phase space and as the Markov walk is executed the minimum-energy configuration for the crossing of each surface in the ensemble is stored and continuously updated. By allowing the system to walk sufficiently long to adequately cover the entire phase space of the system, the energy values and configurations thus obtained will be the minimum energy pathway for the process. The distance at which the points in Fig. 49 are plotted correspond to the radii of the circular cylinders used in the series of dividing surfaces. This plot, and the calculated activation energies, show that dynamical effects (surface motion) lower the barrier relative to the equilibrium value. In the equilibrium system, the barrier to diffusion is 2.79 eV and 0.65 eV for diffusion from top to open site and from open to top site, respectively. The "dynamical" barrier is 2.65 eV (see

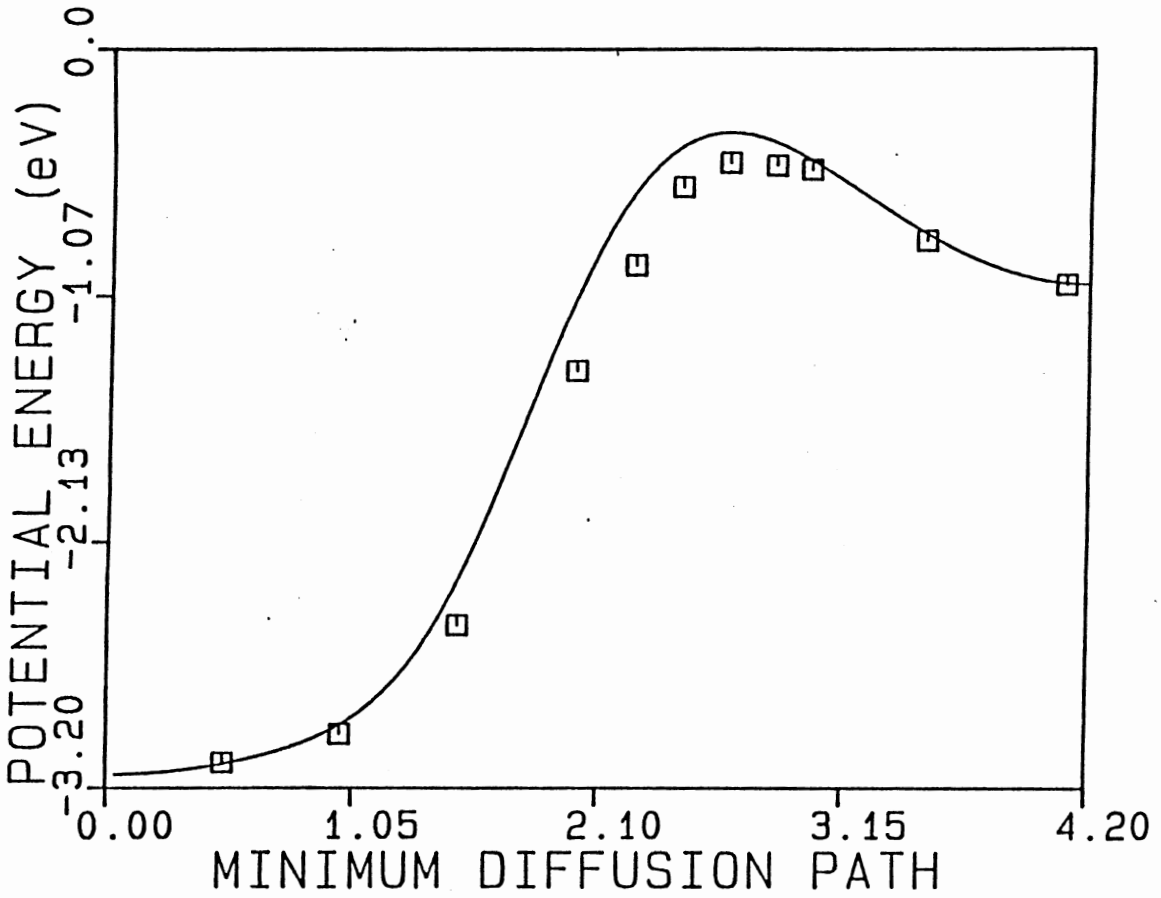

Figure 49. Minimum energy path of hydrogen diffusion from top to open binding sites. Solid line is equilibrium rigid surface minimum energy path; points correspond to minimum-energy configuration at dividing surfaces (see text). Distance given in units of a.u.

Fig. 49) and E_a=2.74 eV for the top-to-open site migration.

Tunneling Calculations

An approximate rate of tunneling through the barrier separating the top and open binding sites has been computed from the results of a biased Markov walk containing 85000 attempted moves. The calculation was performed at 300 K. Tunneling may contribute to jumps from the open to the top sites, however, we have not considered it in the present study. This step, open to top jumps, is not the rate limiting step and has little effect on surface diffusion. Thus, tunneling from open site to top site was not calculated.

Approximately 9000 sets of tunneling paths were calculated during the biased Markov walk and tunneling probabilities were calculated for each path in a set. Each set contained nine or less tunneling paths and the majority of sets had between three and six paths. The largest tunneling probability from the set was included in the Monte Carlo sum used to calculate the rate of tunneling.

The calculated frequencies of the diffusing particle which correspond to the sets of selected tunneling paths are plotted as a function of energy in Fig. 50. The frequencies range from 1.0×10^{13} s^{-1} and 3.2×10^{13} s^{-1}. The values plotted in Fig. 50 are for

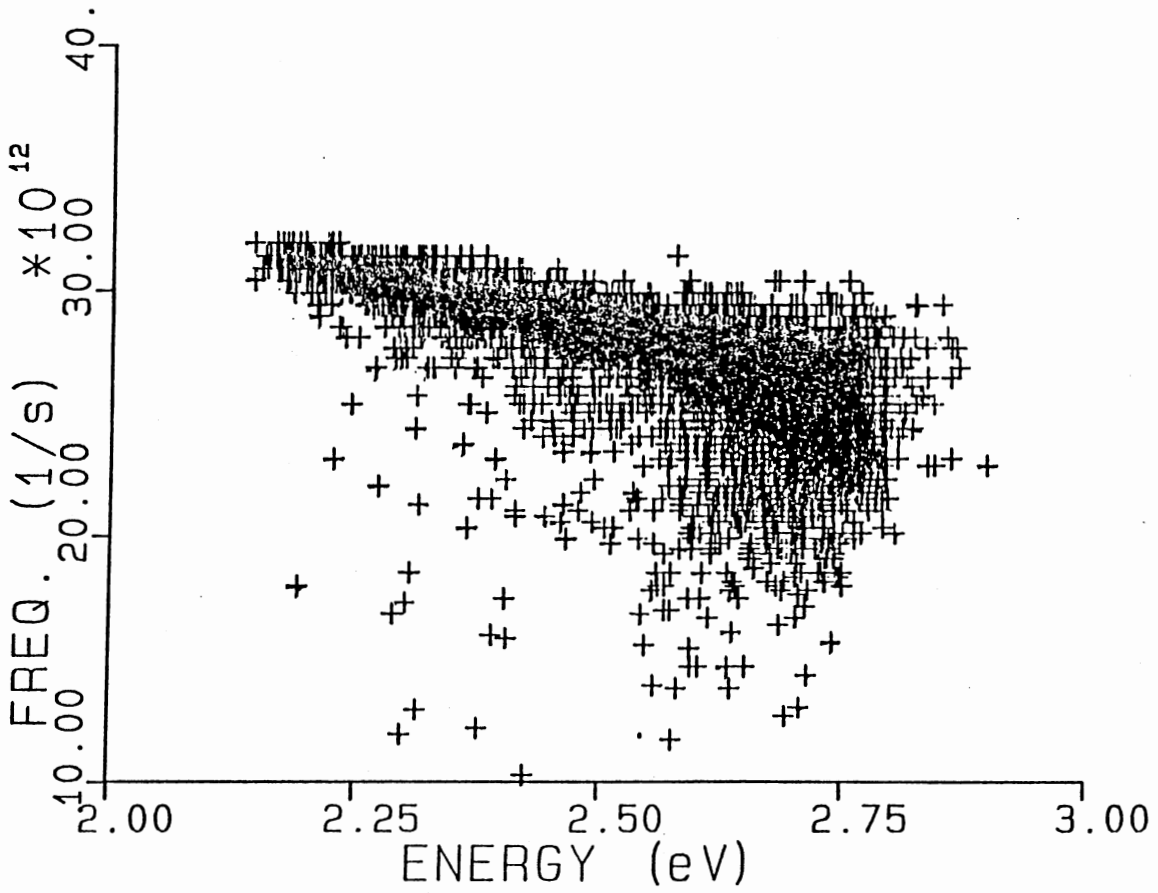

Figure 50. Frequency of surface-plane vibrations of H in top-site well as a function of energies ≥ threshold for tunneling.

energies greater than 2.1 eV, the threshold for tunneling from the top site to the open site, to the top of the well. The average frequency of vibration in the surface plane of the diffusing hydrogen, using the frequencies in Fig. 50, is 2.71×10^{13} s^{-1}. Figure 51 is a plot of average frequency of vibration in the surface plane as a function of energy above the threshold for tunneling. The frequencies of vibration vary very little over the range of energies for the tunneling calculations. This can be understood because of the shape of the top site potential (see Fig. 6); the shape of the top site potential is approximately parabolic.

Figure 52 shows the tunneling probabilities for the random walk as a function of energy. The solid line is the WKB approximation of tunneling through the minimum energy path on the equilibrium surface. The points are the probabilities calculated from the random paths selected in the Markov walk.

The rate of tunneling calculated at 300 K is 7.7×10^{-30} s^{-1}. This is 5133 times larger than the classical rate at 300 K. Because this was a very expensive calculation in terms of computer time (15 hours on an IBM 3081), we made the following approximations and calculated the tunneling of hydrogen from top to open site at 600, 900, and 1200 K. The approximations are that the frequencies and the tunneling probabilities do not change with temperature. Each phase space point of

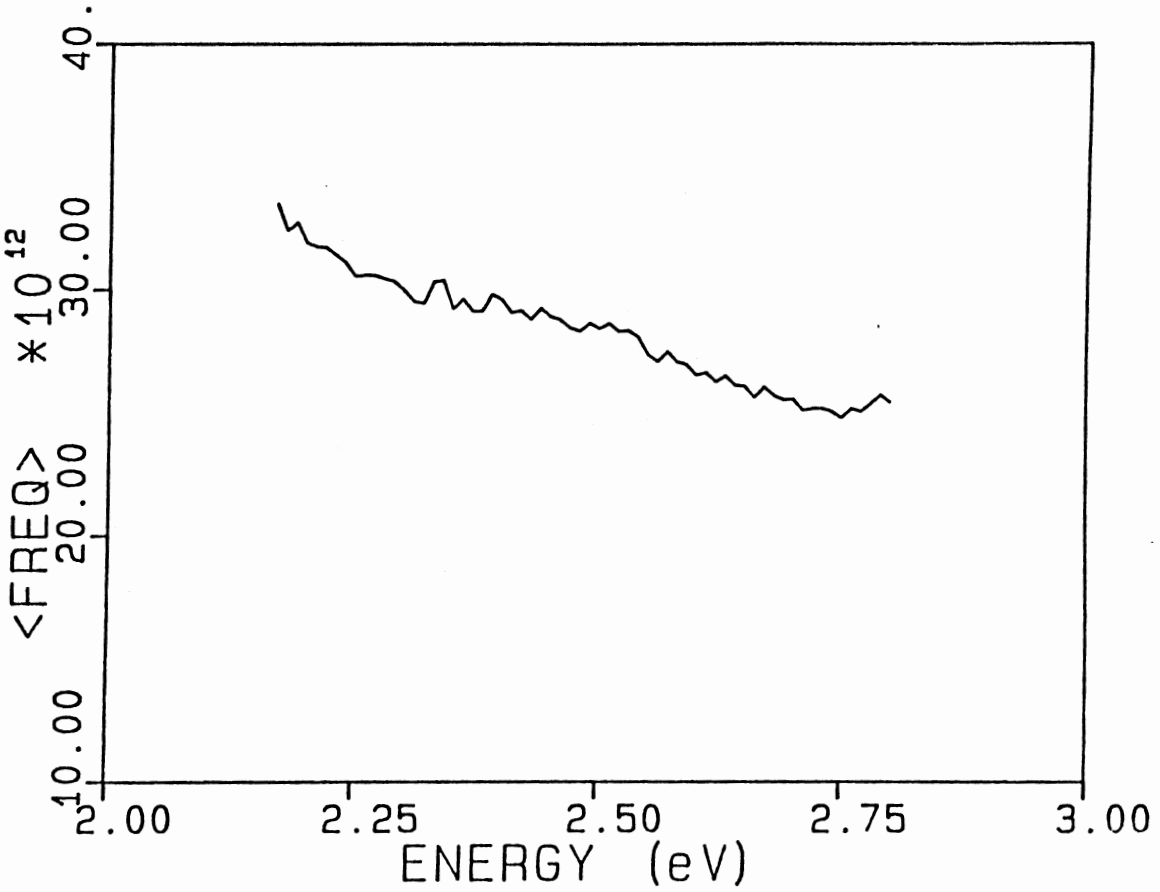

Figure 51. Average frequency of surface-plane vibration of H in top-site well as a function of energies $\geq$ threshold for tunneling.

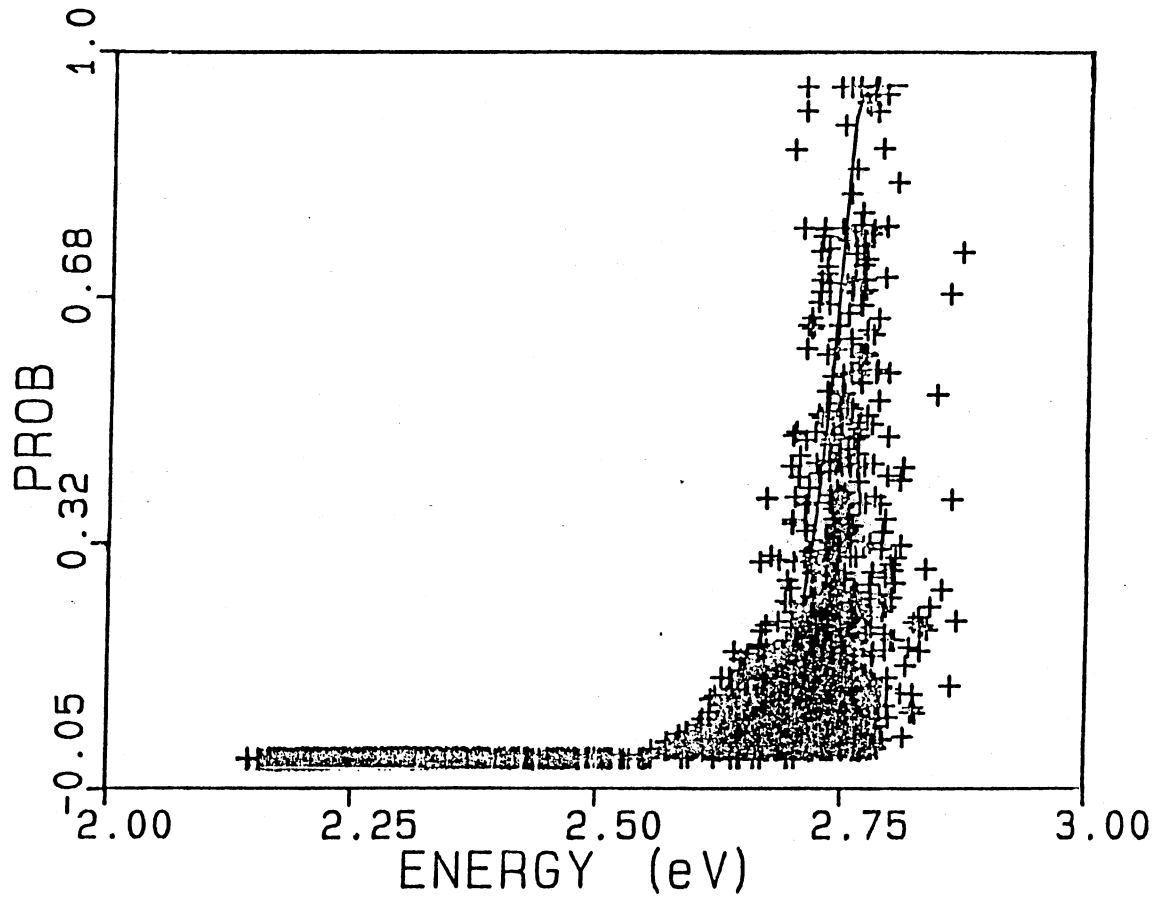

Figure 52. Tunneling probabilities as a function of energies $\geq$ threshold for tunneling. Points correspond to probabilities calculated in random walk; solid line is probability using minimum energy path of rigid surface.

the diffusing particle which was selected during the Markov walk was stored and used along with the frequencies and tunneling probabilities calculated in the Markov walk at 300 K in solving Eq. (52) at temperatures other than 300 K. Using these data and these approximations, we find that the rate of tunneling is larger than the classical rate at all temperatures studied in this calculation, with the ratio of tunneling rate to classical rate decreasing with increasing temperature. Table VIII, Appendix summarizes the results.

We used these tunneling rates for top-to-open site jumps in Eqs. (45) and (48) to calculate a lower bound and an estimated upper bound for diffusion described above. An Arrhenius plot of the lower bound for the diffusion coefficient gives an activation energy of 2.47 eV and a pre-exponential factor of 1.5×10^{-4} cm^2/s. A similar plot of the estimated upper bound for the diffusion coefficient yields an activation energy of 2.46 eV and a pre-exponential factor of 7.03×10^{-4} cm^2/s. The effective activation energy is approximately 0.3 eV less than the classical result.

Rate of tunneling on the equilibrium surface was calculated using Eq. (49), where (E) is the average frequency calculated in the Markov walk, and $T_p(E)$ is the tunneling probability calculated along the minimum energy path of the equilibrium surface. The assumptions

regarding temperature independence of frequencies and tunneling probabilities were made and the rates calculated in this manner are summarized in Table VIII, Appendix. Note that at 900 and 1200 K, the rate of tunneling calculated by using the equilibrium minimum energy path is the same as that calculated by using the Monte Carlo selected tunneling probabilities and frequencies. However, this is not true at lower temperatures. The rate of tunneling calculated from the Markov walk is 93 times larger than that calculated using the minimum energy path at 300 K. The fact that the tunneling probability calculated on the phase averaged surface is greater than that obtained using the equilibrium surface is is due to the difference in tunneling probabilities as a function of energy at the lower temperatures. This is illustrated in Fig. 52. At higher temperatures, the rates become comparable because the influence of the Boltzmann factor overrides the differences in the tunneling probabilities. Thus, the tunneling rate is significantly enhanced by surface motion.

It is interesting to compare the magnitudes of the rates of tunneling on the silicon surface to those computed by Lauderdale and Truhlar (85,86) on a Cu(100) surface. Tunneling is significantly more important in hydrogen atom diffusion on Si(111). Jumps from a top site to an open site on the Si(111) surface is a

physically different problem than that studied by Lauderdale and Truhlar (85,86), where tunneling occurs between interstitial sites on a Cu(100) surface. Tunneling between interstitial sites on the Cu(100) surface occurs through a barrier which is approximately 5.0 a.u. wide at the tunneling threshold, whereas tunneling in the hydrogen-Si(111) system occurs through a barrier which is approximately 2.0 a.u. wide at the tunneling threshold. Therefore, tunneling of hydrogen on Si(111) from top to open sites is through a much thinner barrier than that on a Cu(100) surface.

Our main interest in the present study was to present a new approach for treating tunneling through three-dimensional barriers to diffusion. The results of the calculations reported here provide at best only an estimate of the importance of tunneling of hydrogen on Si(111). They are based on a number of approximations.

Previous studies by others have illustrated with restricted treatments that tunneling is enhanced by phonon effects. Jacquet and Miller (87) found such an effect in a treatment in which they included one phonon. Lauderdale and Truhlar (86) also observed this effect in a variational transition-state theory treatment of surface diffusion of H on Cu(100) for a model which included 18 phonon modes. In the method presented here, the full effects of the phonon modes are explicitly included in a manner that is easy and straightforward to

apply. As discussed above, this study shows that surface motion significantly enhances the tunneling rate at temperatures of 600 K or less for this system.

We have made the approximation of continuum-to-continuum tunneling paths. While we have not carried out calculations to assess the importance of this assumption, it is supported by the results of Lauderdale and Truhlar (85) in a study of H, D and T diffusion on Cu(100). They found the effect of restricting tunneling to discrete energies as opposed to allowing continuum-to-continuum tunneling is small. For example, at 100 K, the difference in the two treatments is less than 20% and this difference decreased to 1% at 180 K. We did not consider other quantum effects, such as zero-point energy in this study.

The approach used to determine the tunneling paths is perhaps overly simplified. We simply selected nine possible paths connecting a particle in its random position in the top site to the nine points spanning the diameter of the open site well. We did not attempt to locate the maximum path for tunneling, but instead used the path with the largest tunneling probability from each set of nine.

In the specific application we have made here for H on Si(111), we have made some approximations to obtain temperature dependence over the range of 300 K to 1200 K from the calculations at 300 K. The main approximations

were that the frequencies of surface-plane vibration of hydrogen in the top site and the tunneling probabilities were temperature independent. This approximation that the frequencies are temperature independent is reasonable due to the nature of our potential-energy surface, wherein the top binding site well is approximately parabolic. Temperature dependent surface motion might render the approximation that the tunneling probabilities are independent of temperature invalid. We have assumed the dominant factor is the Boltzmann weighting.

CHAPTER V

CONCLUSIONS

Hydrogen Atom Scattering/Chemisorption On Partially/Fully Covered Si(111)

We have performed molecular dynamics calculations on hydrogen atom scattering and chemisorption on fully and partially covered Si(111) surfaces. Beam experiments were simulated for hydrogen atoms which had initial translational energy of 0.126 eV and three different angles incident on a Si(111) surface. The model used in the calculations involved 7 possible top sites and 3 available open sites in the reaction zone. Calculations were done on surfaces with 0, 1, 3, 5, and 7 available top sites in the reaction zone. All calculations were done with no hydrogen atoms initially in an open site.

The potential-energy surface employed in this study was assumed to be the sum of a lattice interaction potential, a repulsive adsorbate-adsorbate interaction potential, and an adsorbate-lattice interaction potential. The adsorbate-lattice interaction potential describes two types of binding states on the Si(111) surface with a migration barrier between them. This

surface was developed according to available experimental data and theoretical information about the well-defined on-top adsorption site (7-11,13,15,20-21,23-24,32), the interstitial or open site (7,35,39), and migration barrier (67-68). Fourier analysis of the motion of hydrogen atoms in the top and open sites on a fully covered surface gave frequencies in good agreement with experimental data and theoretical values (7-11,13,15,20-21,23-24,32,35,39).

The major processes observed are direct scattering, exchange scattering, direct chemisorption, and chemisorption with exchange;

$$H(g) + (* \text{ or } \#) \longrightarrow (* \text{ or } \#) + H(g) \qquad (R1)$$

$$_aH(g) + *\text{--}_bH \longrightarrow *\text{--}_aH + {}_bH(g) \qquad (R2)$$

$$H(g) + * \longrightarrow *\text{--}H \qquad (R3)$$

$$H(g) + \# \longrightarrow \#\text{--}H \qquad (R4)$$

$$_aH(g) + *\text{--}_bH + \# \longrightarrow *\text{--}_aH + \#\text{--}_bH \qquad (R5)$$

* = top site # = open site

These processes are represented by reactions (R1), (R2), (R3) and (R4), and (R5), respectively. In some cases, indirect scattering via an adsorbed state was observed,

$$H(g) + * \longrightarrow (*\text{--}H) \longrightarrow * + H(g) \qquad (R6a)$$

$$H(g) + \# \longrightarrow (\#\text{--}H) \longrightarrow \# + H(g) \qquad (R6b)$$

Subsequent to chemisorption, we also observe hydrogen-atom migration,

*--H + # ---> * + #--H (R7)

#--H + # ---> # + #--H (R8)

#--H + * ---> # + *--H (R9)

We find that the probability of each of these reactions is dependent upon the incidence angle and the degree of hydrogen-atom coverage present.

The results show that surface coverage does not have an effect on sticking probabilities, but affects the behavior of the highly excited adsorbed hydrogen atom on the surface. Energy transfer from the impinging hydrogen atom to a previously adsorbed hydrogen atom can be effected, but only if the impinging hydrogen atom collides with the adsorbed hydrogen as it undergoes migration. However, examination of trajectories indicates that the major effect of partial coverage of the surface is that the adsorbed partial/full monolayer coverage of hydrogen provides a cage effect on a chemisorbing hydrogen in that it blocks potential binding sites or hinders migration to another site.

For all surface coverages except the fully covered surface, the sticking probability is strongly dependent on angle, increasing with increasing angle. This indicates that hydrogen atoms impacting with the surface at a larger angle excite the surface bending modes, which are favorable for energy accomodation, and thereby produce a greater likelihood of sticking in our model, whereas hitting the surface at a smaller angle

excites the surface stretching modes, which, in our model, are inefficient with respect to energy transfer. For the fully covered surface, the sticking probabilities for the set of trajectories whose hydrogen atoms have initial azimuthal angles of 0° or 15° show the same behavior as the other surface coverages. However, the sticking probability decreases for 30° incidence. Product translational energy distributions show that at this surface coverage and initial angle, energy transfer to the impinging hydrogen atom is very efficient, and half of the trajectories impacting with this surface leave the surface with more than their initial energy. This gain of energy is not conducive to sticking.

Translational energy distributions were calculated from the results of scattering trajectories at different surface coverages and with different initial azimuthal angles. Energy transfer between the surface and the scattered hydrogen atoms is apparent in all distributions. For the fully covered surface, the energy distributions broaden and flatten with increasing angle. Energy transfer from the lattice to the impinging hydrogen predominates at this coverage at 30° incidence; all other coverages and all other angles exhibit the reverse situation. The other coverages do not show any remarkable trends with increasing azimuthal angle. Product energy distributions as a function of surface coverage also show no remarkable trends.

Spatial distributions were also calculated from the results of the scattering trajectories at different surface coverages and with different initial azimuthal angles. There are no striking features of the distributions with increasing initial angle, except for the fully covered surface. It exhibits an increase in rainbow scattering with increasing initial azimuthal angle. This is due to the translational symmetry of the system and to deflection of trajectories by the open site and repulsion of the hydrogen already adsorbed in the top site which result in a partial averaging over aiming points. Rainbow effects were not seen in the other distributions at the 30° angle as in the fully covered. surface. Except for the fully covered surface, the series of trajectories with initial angle of 30° show specular scattering with increasing development of a cosine distribution with decreasing surface coverage. The series of trajectories at 15° incidence show distributions similar to one another, with broadening of the distributions with increasing surface coverage. The series of trajectories at 0° incidence show non-specular scattering for all coverages (except for the fully covered surface).

Hydrogen exchange reactions resulting in chemisorption or desorption were observed for the fully covered surface when the initial azimuthal angle was 0° or 15°. Exchange reactions were not observed in the 30°

case because the incoming hydrogen was slowed as it passed over the open site and repelled by the hydrogen atom on the central top site. In the other two cases, the open site was not effective in slowing down the impacting hydrogen and subsequent exchange occurred.

At 30° incidence, a significant number of trajectories at each surface coverage were deflected by an open site or an available outer top site, with the total number of deflected trajectories increasing with increasing available outer top sites, except for the fully covered surface. At 15° incidence, a lesser, but constant percentage of trajectories was deflected with increasing surface coverage, except for the fully covered surface.

At 30° incidence, the percentage of trajectories which migrate (occupy more than one binding site on the surface during the time of the trajectory) increases with decreasing surface coverage. This trend is also exhibited at the smaller incidence angles, but the statistical error is large in these cases due to small number of chemisorbing trajectories.

Energy transfer mechanisms were examined, and we found that the major energy transfer pathway was from translational or asymmetric stretching motion of the adsorbate to the bending modes of the silicon surface. A rate of energy transfer was calculated for a surface at 300 K which is the same as that found in a previous study

using a different adsorbate-substrate interaction potential and a larger lattice model. Energy transfer does not appear to be sensitive to these factors.

Dissociative Chemisorption/Scattering of H_2 on Si(111)

We have investigated the dissociative chemisorption and scattering of H_2 on a Si(111) surface using classical trajectories. The potential-energy surface employed was developed by Raff *et al.* (48). The results shows that H_2 scattering from Si(111) is elastic and predominately specular. The H_2 translational energy distributions are broadened by the scattering process, but the first moments of the distributions are essentially unaltered. Based on the absence of root trajectories, there is essentially no energy transfer to or from the H_2 vibrational mode upon collision with the Si(111) surface. There is some inelasticity associated with rotational energy transfer, but it is small.

Lower limits to the sticking probabilities were computed as a function of surface temperature. Due to the presence of a barrier to H_2 adsorption, the sticking coefficients at 300 K are too small to compute with a statistical sample of a few hundred trajectories. At 1000 and 1500 K, sticking coefficients were found to be at least 0.0046 and 0.0327, respectively. On our potential-energy surface, adsorption of H_2 on Si(111) is always followed by dissociative chemisorption of both

hydrogen atoms. Adsorption of molecular hydrogen is not observed.

The reaction exothermicity for dissociative chemisorption is deposited primarily in Si-H vibrational motion. This leads to a very high initial hydrogen atom mobility of approximately 0.015 cm^2/s.

The mobility decreases rapidly with increasing residence time on the surface due to energy transfer to the phonon modes of the lattice, and approaches the thermal diffusion rate. The calculations indicate that the activation energy for thermal diffusion is large and the associated rate coefficient is very small.

Energy transfer to the phonon modes of the lattice is found to be a first-order process with rate coefficients on the order of 10^{12} s^{-1}. These rates are much larger than those found for thermal systems with one Si-H vibrational quantum of excess energy (90).

Hydrogen Atom Diffusion on Si(111)

The surface diffusion of hydrogen on a Si(111) surface with partial hydrogen coverage has been studied. The potential-energy surface of the system is the same one used in the study of hydrogen atom scattering and chemisorption on a Si(111) surface with full or partial hydrogen coverage. The diffusion coefficient of hydrogen on the surface was computed using phenomenological rate equations.

Monte Carlo variational phase-space theory rate calculations were carried out by defining dividing surfaces between the two binding sites on the surface and minimizing the calculated flux across the surface with respect to the parameters defining the dividing surfaces. Importance sampling was used in the Monte Carlo calculation due to the presence of large energy barriers to diffusion. Circular, elliptical, and hyperbolic cylinders relative to the top binding site on the surface were used in the MCVPST calculation. The circular cylindrical dividing surfaces gave a minimum flux three times larger than that given by elliptical or hyperbolic cylindrical surfaces for top to open site jumps. There was no difference in the minimum flux using elliptical or hyperbolic cylinders in the MCVPST calculation. Circular cylinders and elliptical cylinders were used to calculate the minimum flux for open-to-top site jumps; both types of surfaces gave the same result. Classical jump frequencies from the two different types of binding sites were computed at 300, 600, 900 and 1200 K. Arrhenius plots of the calculated jump frequencies yield activation energies of 2.74 and 0.61 eV for top-to-open site jumps and open-to-top site jumps, respectively. Corresponding frequency factors are 1.4×10^{13} s^{-1} and 1.0×10^{13} s^{-1} for top-to-open site jumps and open-to-top site jumps, respectively.

Lower bounds and estimated upper bounds for the classical diffusion coefficient at 300, 600, 900, and 1200 K were computed by integrating the phenomenological rate equations describing diffusion of hydrogen on this surface using the calculated classical jump frequencies. Arrhenius plots of these values give activation energies of 2.77 and 2.74 eV for lower and upper bounds, respectively. Corresponding pre-exponential factors are 0.008 and 0.022 cm^2/s for lower and upper bounds, respectively. These results indicate that diffusion is energetically controlled by jumps from top sites to open sites.

The minimum-energy path for hydrogen atom migration from a top to an open site is obtained by using a Monte Carlo random walk procedure with importance sampling. This calculation shows that the classical dynamical barrier to diffusion is 2.65 while the equilibrium barrier to diffusion is 2.79 eV.

The rate of tunneling of a hydrogen from the top site to the open site was calculated at 300 K using a Metropolis Monte Carlo sampling method and the WKB tunneling approximation. Random tunneling paths, corresponding tunneling probabilities, and frequencies of vibration of the diffusing particle in the surface plane were averaged in a random walk consisting of 85000 steps. We calculated a rate of tunneling of 7.7×10^{-30} s^{-1}, which is approximately 5000 times larger than the

classical jump frequency of top-to-open site jumps. By assuming that the frequencies of vibration and the tunneling probabilities are independent of surface temperature, we used the tunneling data calculated at 300 K to obtain tunneling rates at 600, 900, and 1200 K. We used these values in the phenomenological rate equations described above to get lower and upper bounds for diffusion due to tunneling of the hydrogen atom. Arrhenius plots of the calculated lower and upper bounds for diffusion due to tunneling yield activation energies of 2.47 and 2.46 eV for lower and upper bounds, respectively, and pre-exponential factors of 0.00015 and 0.00070 cm^2/s for lower and upper bounds, respectively. The rate of tunneling was also calculated using the minimum energy path on a rigid equilibrium surface. This gives equal results to the Monte Carlo random walk method at 900 and 1200 K, but gives much smaller rates at 300 and 600 K, indicating that surface motion plays a significant role in tunneling probabilities.

Suggestions for Future Work

One of the more interesting results in the gas-surface studies have been the energy transfer from nascent adsorbate-surface bonds to the bath modes of the lattice. In the study of hydrogen atom scattering/chemisorption on a Si(111) surface with full or partial coverage of hydrogen, we found that the Si-H

bonds on the surface did not provide additional bath modes into which energy could flow as compared with a clean Si(111) surface. The energy transfer from a nascent Si-H bond to the lattice in this study did not differ from that found in the study done on the dissociative chemisorption of H_2 on a clean ideal Si(111) surface. It is possible that our conclusions would be affected by inclusion of second- and third-layer Si atom motion. Agrawal *et al.* (71) found a decrease in the rate of energy transfer upon inclusion of second-layer motion. However, their results cannot predict what changes would take place upon inclusion of such motion in our system because they used a different lattice interaction potential (93), and the system did not include hydrogen coverage on the surface. It is possible that by allowing motion of second- and third-layer Si atoms in the lattice, an energy-transfer pathway from the nascent Si-H bond to the Si-H bonds on the surface might be opened.

Further studies need to be done on tunneling effects in the surface diffusion of hydrogen. The methods developed in the course of this thesis research will be useful in providing information on the importance of phonon coupling on rates of tunneling.

Corrosion of the Si(111) surface by hydrogen is an important phenomenon which needs to be investigated. Although there are a considerable number of studies done on the possible corrosion of the Si(111)

surface by hydrogen, detailed information about the interaction potential must be determined before a theoretical study can be carried out. Although information has been given about the binding sites on the Si(111) surface, in order to model corrosion properly, Si-Si bond weakening in the surface due to hydrogen must be determined and transition states for formation of multihydride species must be found. The hydrogen-Si(111) interaction potential developed in this thesis and the dynamical studies done using the potential have provided a foundation for a theoretical study on corrosive modification of a Si(111) surface once experimental data and theoretical information has been provided.

BIBLIOGRAPHY

1. (a) J. J. Lander and J. Morrison, J. Chem. Phys. 37, 729 (1962); J. E. Rowe and J. C. Phillips, Phys. Rev. Lett 32, 1315 (1974); (b) K. C. Pandey, T. Sakurai, and H. D. Hagstrum, Phys. Rev. Lett. 35, 1728 (1975).

2. (a) G. A. Somorjai, "Chemistry in Two Dimensions: Surfaces", (Cornell University Press, Ithaca, 1981) and references therein; (b) W. Monch, Surf. Sci 86, 672 (1979).

3. W. A. Harrison, Surf. Sci. 55, 1 (1976).

4. H. Ibach, and J. E. Rowe, Surf. Sci. 43, 481 (1974).

5. J. T. Law, J. Appl. Phys. 32, 600 (1961).

6. T. Sakurai and H. D. Hagstrum, Phys. Rev. B 12, 5349 (1975).

7. G. Schulze and M. Henzler, Surf. Sci. 124, 336 (1983).

8. H. Wagner, R. Butz, U. Backes, and D. Bruchmann, Solid State Comm. 38, 1155 (1981).

9. G. E. Becker and G. W. Gobeli, J. Chem. Phys. 38, 2942 (1963).

10. H. Froitzheim, H. Ibach, and S. Lehwald, Phys. Lett. 55A, 247 (1975).

11. K. D. Brzoska and Ch. Kleint, Thin Solid Films 34, 131 (1976).

12. J. E. Rowe, Surf. Sci. 53, 461 (1975).

13. H. Kobayashi, K. Edamoto, M. Onchi, and M. Nishijima, J. Chem. Phys. 78, 7429 (1983).

14. R. Butz, R. Memeo, and H. Wagner, Phys. Rev. B 25, 4327 (1982).

15. Y. J. Chabal, Phys. Rev. Lett. 50, 1850 (1983).

16. B. A. Joyce and J. H. Neave, Surf. Sci. 34, 401 (1973).

17. T. Sakurai, E. W. Muller, R. J. Culbertson, and A. J. Melmed, Phys. Rev. Lett. 39, 578 (1977).

18. K. Fujiwara, Phys. Rev. B 26, 2036 (1982).

19. P. Klimesch, G. Meyer, and M. Henzler, Surf. Sci. 137, 79 (1984).

20. H. Froitzheim, H. Lammering, and H. L. Gunter, Phys. Rev. B 27, 2278 (1983).

21. Y. J. Chabal, G. S. Higashi, and S. B. Christman, Phys. Rev. B 28, 4472 (1983).

22. S. Ciraci, R. Butz, E. M. Oellig and H. Wagner, Phys. Rev. B 30, 711 (1984).

23. M. Nishijima, K. Edamoto, Y. Kubota, H. Kobayashi, and M. Onchi, Surf. Sci. 158, 422 (1985).

24. H. Froitzheim, U. Kohler and H. Lammering, Surf. Sci. 149, 537 (1985).

25. Y. J. Chabal, J. Electron Spectrosc. Related Phenom. 29, 35 (1983).

26. A. P. Webb and S. Veprek, Chem. Phys. Lett. 62, 173 (1979).

27. A. Thanailakis, D. E. Ioannou, and C. M. Reed, Solid State Comm. 44, 669 (1982).

28. K. Fujiwara, Phys. Rev. B 24, 2240 (1981).

29. J. A. Appelbaum, H. D. Hagstrum, D. R. Hamann, and T. Sakurai, Surf. Sci. 58, 479 (1976).

30. K. C. Pandey, IBM J. Res. Develop. 22, 250 (1978).

31. K. C. Pandey, Phys. Rev. B 14, 1557 (1976).

32. J. A. Appelbaum, and D. R. Hamann, Phys. Rev. Lett. 34, 806 (1975).

33. K. Hermann and P. S. Bagus, Phys. Rev. B 20, 1603 (1979).

34. K. M. Ho, M. L. Cohen, and M. Schluter, Phys. Rev. B 15, 3888 (1977).

35. M. Seel and P. S. Bagus, Phys. Rev. B 23, 5464 (1981).

36. J. A. Appelbaum, D. R. Hamann, and K. H. Tasso, Phys. Rev. Lett. 39, 1487 (1977).

37. T. S. Shi, S. N. Sahu, and J. W. Corbett, Surf. Sci. 130, L289 (1983).

38. W. S. Verwoerd, Surf. Sci. 125, 575 (1983).

39. M. Seel and P. S. Bagus, Phys. Rev. B 29, 1070 (1984).

40. S. Ciraci, Solid State Comm. 49, 43 (1984).

41. T. Katterle and W. Lorenz, Phys. Stat. Sol. (b) 132, 225 (1985).

42. J. A. Appelbaum and D. R. Hamann, Phys. Rev. Lett. 31, 106 (1973).

43. E. G. McRae and C. W. Caldwell, Phys. Rev. Lett. 46, 1632 (1981).

44. M. Tsukada and T. Hoshino, Inter. J. of Quantum Chem.: Quantum Chem. Symp. 15, 445 (1981).

45. A. Selioni and C. M. Bertoni, Solid State Comm. 45, 475 (1983).

46. T. Hoshino and M. Tsukada, Surf. Sci. 115, 104 (1982).

47. G. V. Gadiyak, A. A. Karpushin, I. V. Korolenko, Yu. N. Morokov, I. Yu. Semenova, A. N. Sorokin, and M. Tomasek, Phys. Stat. Sol. (b) 137, 633 (1986).

48. L. M. Raff, I. NoorBatcha, and D. L. Thompson, J. Chem. Phys. 85, 3081 (1986).

49. B. M. Rice, I. NoorBatcha, L. M. Raff, and D. L. Thompson, J. Chem. Phys. 86, 1608 (1987).

50. T. S. Shi, S. N. Sahu, G. S. Oehrlein, A. Hiraki, and J. W. Corbett, Phys. Status Solidi (a) 74, 329 (1982).

51. S. N. Sahu, T. S. Shi, P. W. Ge, J. W. Corbett, A. Hiraki, T. Imura, M. Tashiro, and V. A. Singh, J. Chem. Phys. 77, 4330 (1982).

52. M. H. Brodsky, M. Cardona and J. J. Cuomo, Phys. Rev. B 16, 3556 (1977).

53. G. Lucovsky, R. J. Nemanich and J. C. Knights, Phys. Rev. B 19, 2064 (1979).

54. E. C. Freeman and W. Paul, Phys. Rev. B 18, 4288 (1978).

55. D. Haneman, Phys. Rev. 170, 705 (1968).

56. (a) E. G. McRae, Surf. Sci. 124, 106;
(b) M. Cardillo, Phys. Rev. B 23, 4279 (1981).

57. M. H. Brodsky, M. Cardona, and J. J. Cuomo, Phys. Rev. B 16, 3556 (1977).

58. G. Lucovsky, R. J. Nemanich, and J. C. Knights, Phys. Rev. B 19, 2064 (1979).

59. W. S. Verwoerd, Surf. Sci. 108, 153 (1981).

60. K. C. Pandey, Phys. Rev. Lett. 47, 1913 (1981); 49, 223 (1982).

61. D. L. Miller, H. Lutz, H. Wiesmann, E. Rock, A. K. Ghosh, S. Ramamoorthy and M. Strongin, J. Appl. Phys. 49, 6192 (1978).

62. D. J. Chadi, Phys. Rev. B 30, 4470 (1984).

63. W. A Harrison, Surf. Sci. 55, 1 (1976).

64. I. NoorBatcha, L. M. Raff, and D. L. Thompson, J. Chem. Phys. 82, 1543 (1985).

65. P. N. Keating, Phys. Rev. 145, 637 (1966).

66. W. Weber, Phys. Rev. B 15, 4789 (1977).

67. A. Van Wieringen and N. Warmoltz, Physica 22, 849 (1956).

68. T. Ichimiya and A. Furuichi, Internat. J. Appl. Radiat. Isot. 19, 573 (1968).

69. A. Ralston and P. Rabinowitch, "A First Course in Numerical Analysis", (McGraw-Hill, New York, 1978).

70. L. M. Raff and D. L. Thompson, in "Theory of Chemical Reaction Dynamics", edited by M. Baer (Chemical Rubber, Boca Raton, Florida, 1985), Vol III.

71. P. M. Agrawal, L. M. Raff, and D. L. Thompson. Surf. Sci., in press.

72. N. Metropolis, A. W. Rosenbluth, M. N. Rosenbluth, A. H. Teller, and E. Teller, J. Chem. Phys. 21, 1087 (1953); J. W. Brady, J. D. Doll, and D. L. Thompson, *ibid.* 74, 1026 (1981); J. D. Doll, *ibid.* 74, 1074 (1981).

73. R. Zwanzig, Annu. Rev. Phys. Chem. 16, 67 (1965).

74. J. D. Doll and A. F. Voter, Annu. Rev. Phys. Chem. 38, xxxx (1987).

75. J. D. Doll, J. Chem. Phys. 73, 2760 (1980); 74, 1074 (1981).

76. (a) R. Viswanathan, L. M. Raff, and D. L. Thompson, J. Chem. Phys. 81, 828 (1984), (b) 82, 3083 (1985).

77. (a) J. E. Adams and J. D. Doll, J. Chem. Phys. 74, 1467 (1981); (b) 74, 5332 (1981); (c) 77, 2964 (1982).

78. A. F. Voter and J. D. Doll, J. Chem. Phys. 80, 5832 (1984)

79. A. F. Voter and J. D. Doll, J. Chem. Phys. 82, 80 (1985).

80. See, for example, Donald Raff, "Quantum Mechanics", (Holt, Rinehart and Winston, Inc., Dallas, 1971).

81. K. F. Freed, J. Chem. Phys. 82, 5264 (1985)

82. S. C. Wang and R. Gomer, J. Chem. Phys. 83, 4193 (1985).

83. K. B. Whaley, A. Nitzan and R. B. Gerber, J. Chem. Phys. 84, 5181 (1986).

84. S. M. Valone, A. F. Voter and J. D. Doll, Surf. Sci. 155, 687 (1985).

85. J. G. Lauderdale and D. G. Truhlar, Surf. Sci. 164, 558 (1985).

86. J. G. Lauderdale and D. G. Truhlar, J. Chem. Phys. 84, 1843 (1986).

87. R. Jacquet and W. H. Miller, J. Phys. Chem. 89, 2139 (1985).

88. DGEAR, IMSL package.

89. J. D. McClure, J. Chem. Phys. 52, 2712 (1970).

90. J. C. Tully, Y. J. Chabal, K. Raghavachari, J. M. Bowman, and R. R. Lucchese, Phys. Rev. B 31, 1184 (1985).

91. P. M. Agrawal, private communication.

92. See, for example, (a) A. C. Diebold and G. Wolken, Surf. Sci. 82, 245 (1979); (b) A. Gelb and M. Cardillo, Surf. Sci. 59, 128 (1976); 64, 197 (1977); 75, 199 (1978); (c) G. F. Tantardini and M. Simonetta, Surf. Sci. 105, 517 (1981); (d) J. C. Polanyi and R. J. Wolf, J. Chem. Phys. 82, 1555 (1985); (e) R. J. Wolf and R. C. Davis, J. Phys. Chem. 89, 2757 (1985).

93. D. W. Brenner and B. J. Garrison, Phys. Rev. B 34, 1304 (1986).

APPENDIXES

TABLE I

EXPERIMENTAL DATA AND THEORETICAL INFORMATION
ON H-Si(111) INTERACTION POTENTIAL

Ref.	Si(111) surface	Method	Re (a.u.)	D (eV)	Force constant ($eV/a.u.^2$)	Frequency (1/cm) Stretch	Bend
Top Binding Site:							
9		IR				2062	
10		HREELS			4.300	2073	
11	thin film	TDS		3.19			
7	(2 x 1) (7 x 7)	TDS, LEED		3.5			
33	(7 x 7)	HF LCAO caln.	2.808	3.02	5.366	2274	
34		self-consist. pseudopoten.	2.93		6.803		
13	(7 x 7)	HREELS			4.245	2057	637
15	(7 x 7)	HRIRS				2073	

TABLE I (continued)

Ref.	Si(111) surface	Method	Re (a.u.)	D (eV)	Force constant ($eV/a.u.^2$)	Frequency (1/cm) Stretch	Bend
Top Binding Site (continued):							
8	(7 x 7)	HREELS				2100	630
20	(2 x 1)	ELS				2072	621
21	(7 x 7) (1 x 1)	HRIR				2073	
24	(7 x 7) (2 x 1)	HREELS, LEED				2089	637
23	(7 X 7)	EELS, LEED, AES				2057	637
32		Self-consist. pseudopoten.	2.73		4.762		
This caln.	Hydrogen covered		2.80	3.14	4.473	2115[a]	642[a]

TABLE I (continued)

Ref.	Si(111) surface	Method	Re (a.u.)	D (eV)	Force constant (eV/a.u.^{2})	Frequency (1/cm) Stretch	Bend
Open Binding Site:							
7		TDS, LEED		3.2[b]			
35, 39		HF LCAO (outer well)	2.646	1.0	0.696	823[c]	
35		HF LCAO (inner well)	2.268	.3	1.121	1044[c]	
This caln.	Hydrogen covered						
	Outer well		2.646	1.15	0.796	846[a,c]	
	Inner well		2.268	.3	1.121		

a. Resolution = 15.11 cm^{-1}
b. Calculated from desorption energy; see text.
c. Motion perpendicular to surface plane

TABLE II

POTENTIAL ENERGY PARAMETERS

Lattice Interaction	
f_a (eV/a.u.^{2})	0.84769
f_b (eV/a.u.^{2})	0.24120
Gas Interaction	
A_{H-H} (eV-a.u.^{9})	0.050
Gas-Lattice Interaction	
Top Site	
D (eV)	3.142861
α (a.u.$^{-1}$)	0.84359610
z_e (a.u.)	2.797228
A_{Top} (a.u.$^{-2}$)	0.34
k_θ (eV/rad^2)	2.0
θ_{eq} (rad)	1.91114
β (a.u.$^{-2}$)	0.2
ρ (a.u.$^{-2}$)	1.0
r_e (a.u.)	2.797228
Open Site	
k_{in} (eV/a.u.^{2})	1.12105
ze_{in} (a.u.)	-2.26772
D_{in} (eV)	0.3
E_{pb} (eV)	1.8
k'_{in} (eV/a.u.^{2})	1.12249594

TABLE II (continued)

Open Site (continued)	
k_{out} (eV/a.u.^{2})	0.83581061
D_0 (eV)	1.15
γ (a.u.$^{-1}$)	0.58850450
ze_0 (a.u.)	2.64567
A_{Open} (a.u.$^{-4}$)	0.0125
$r_{e_{xy}}$ (a.u.)	4.18766
Second-Layer Interaction	
B_{H-Si} (eV-a.u.^{9})	1.0
C (a.u.$^{-2}$)	0.10

TABLE III

VALUES OF PARAMETERS USED IN METROPOLIS SAMPLING AND TRAJECTORY CALCULATIONS

Atomic Hydrogen Scattering/Chemisorption on Si(111)

Metropolis sampling parameters

Surfaces with partial or full hydrogen coverage:

Δq (lattice) a.u.	0.070
Δp (lattice) m.u. (a)	0.070
Δq (hydrogen) a.u.	0.100
Δp (hydrogen) m.u. (a)	0.100

Surfaces with no hydrogen coverage:

Δq (lattice) a.u.	0.120
Δp (lattice) m.u. (a)	0.120

Trajectory integration parameters

Step Size	5.39×10^{-16} s

Molecular Hydrogen Dissociative Chemisorption/Scattering on Si(111)

Metropolis sampling parameters

Temperature	300 K	1000 K	1500 K
Δq (lattice) a.u.	0.075	0.15	0.20
Δp (lattice) m.u. (a)	0.075	0.15	0.20

Trajectory integration parameters

Step Size	5.39×10^{-16} s

TABLE III (continued)

Hydrogen Diffusion on Si(111)

Metropolis sampling parameters

	Temperature (K)			
	300	600	900	1200
Δq (lattice) a.u.	0.075	0.105	0.120	0.125
Δp (lattice) m.u.	0.075	0.105	0.120	0.125
Δq (adatom) a.u.	0.100	0.140	0.160	0.175
Δp (adatom) m.u.	0.100	0.140	0.160	0.175

(a) 1 m.u. = 1.63×10^{-18} g-cm/s

TABLE IV

FEATURES OF TRAJECTORIES

Percentage of migrating trajectories (a)

No. Avail. Top Sites	Angle (Deg) 0(b)	15(c)	30(d)
0	10	8	38
1	0	39	38
3	18	29	60
5	30	32	61
7	100	83	86

(a) includes only chemisorbed trajectories
(b) approximately 10 trajectories.
(c) approximately 35 trajectories
(d) approximately 100 trajectories, except for fully covered surface, which has 21 trajectories.

Percentage of trajectories (e) deflected by open (or outer top) site before reaching initial aiming point (f)

No. Avail. Top Sites	Angle (Degrees) 0 Open	0 Out. Top	0 Tot.	15 Open	15 Out. Top	15 Tot.	30 Open	30 Out. Top	30 Tot.
0	0	-	0	73	-	73	98	-	98
1	0	-	0	18	-	18	56	-	56
3	0	0	0	26	0	26	59	5	64
5	0	0	0	11	0	11	58	16	74
7	0	0	0	18	0	18	58	24	82

(e) includes all trajectories
(f) Surface coverages with 0 or 1 available top sites have no available outer top sites

TABLE V

FINAL AVERAGE ENERGIES FOR HYDROGEN SCATTERING

No. Avail. Top Sites	Initial Angle (Degrees) 0	15	30
0	0.095 (a)	0.872 (a)	0.132 (a)
1	0.084	0.120	0.081
3	0.070	0.087	0.094
5	0.077	0.101	0.085
7	0.112	0.103	0.093

(a) Values are in eV. Initial energy is 0.126 eV.

TABLE VI

INITIAL AND FINAL AVERAGE ENERGIES (a)
FOR H_2 SCATTERING

Energy (eV)	Temperature (K) 300 (b)	1500 (c)
$\langle Trans \rangle_i$	0.5000	0.5000
$\langle Trans \rangle_f$	0.4881	0.4990
$\langle Vib \rangle_i$	0.2729	0.2729
$\langle Vib \rangle_f$	0.2664	0.2628
$\langle Rot \rangle_i$	0.0151	0.0151
$\langle Rot \rangle_f$	0.0203	0.0259

(a) i and f denote initial and final, respectively.
(b) Averaged over 197 trajectories.
(c) Averaged over 267 trajectories.

TABLE VII

DIVIDING SURFACES AND VARIATIONAL PARAMETERS USED IN MCVPST CALCULATION OF MINIMUM FLUX

Dividing Surface	Variational Parameters (a) (a.u.)	Flux (1/s)
Dividing Surfaces for Top-To-Open Jumps: (b)		
$\tilde{S} = x^2+y^2-a^2=0$	a = 2.64766	2.8×10^{-33}
$\tilde{S} = b^2x^2+a^2y^2-a^2b^2=0$	a = 2.84766 b = 2.74766	1.1×10^{-33}
$\tilde{S} = a^2y^2-b^2x^2-a^2b^2=0$	a = 1.9 b = 2.65	1.5×10^{-33}
Dividing Surfaces for Open-to-Top Jumps:[c]		
$\tilde{S} = x^2+y^2-a^2=0$	a = 2.9	$4.7 \times 10^{+09}$
$\tilde{S} = b^2x^2+a^2y^2-a^2b^2=0$	a = 2.9 b = 2.7	$4.6 \times 10^{+09}$

(a) Values of the parameters which gave the minimum flux

(b) Flux at 300 K.

(c) Flux at 600 K.

TABLE VIII

TOP SITE TO OPEN SITE JUMP FREQUENCIES

T(K)	Classical Rate (a) (1/s)	Tunneling Rates (1/s) Equil. surface (b)	Markov Walk
300	1.5×10^{-33} (5133)	8.3×10^{-32} (93)	7.7×10^{-30}
600	1.3×10^{-10} (100)	6.4×10^{-10} (20)	1.3×10^{-08}
900	9.9×10^{-03} (2)	1.6×10^{-02} (1)	2.0×10^{-02}
1200	$3.4 \times 10^{+01}$ (2)	$7.3 \times 10^{+01}$ (1)	$7.1 \times 10^{+01}$

(a) Values in parenthesis are ratios of tunneling rate calculated using Markov walk procedure to classical rate

(b) Values in parenthesis are ratio of tunneling rate calculated using Markov walk procedure to rate of tunneling on rigid equilibrium surface along minimum energy path

TABLE IX

OPEN SITE TO TOP SITE JUMP FREQUENCIES

T(K)	Classical Rate (1/s)
300	$7.1 \times 10^{+02}$
600	$6.2 \times 10^{+08}$
900	$4.6 \times 10^{+10}$
1200	$3.1 \times 10^{+11}$

VITA

Betsy Mavity Rice

Candidate for the Degree of

Doctor of Philosophy

Thesis: THEORETICAL INVESTIGATIONS OF HYDROGEN ON Si(111)

Major Field: Chemistry

Biographical:

Personal Data: Born in Lawton, Oklahoma, July 20, 1958, the daughter of John R. and Shirlene Mavity. Married to Gregory A. Rice on September 2, 1977.

Education: Graduated from Lawton High School, Lawton, Oklahoma, in May, 1976; received Bachelor of Science Degree in Chemistry from Cameron University, Lawton, Oklahoma in May, 1984; completed requirements for the Doctor of Philosophy Degree at Oklahoma State University in December, 1987.

Professional Experience: Graduate Teaching Assistant, Oklahoma State University, August, 1984-May, 1985; John W. Skinner Fellow, August, 1984; Graduate Research Assistant, June, 1985-October, 1987.

Membership in Honorary and Professional Societies: Member of Phi Lambda Upsilon, Honorary Chemical Society; member of Sigma Pi Sigma, Honorary Physics Society; member of Pi Mu Epsilon, Honorary Mathematics Society